

SEPARATION SIMULATION FOR HELICOPTER EXTERNAL STORES AND
GENERATION OF SAFE SEPARATION ENVELOPES

A THESIS SUBMITTED TO
THE GRADUATE SCHOOL OF NATURAL AND APPLIED SCIENCES
OF
MIDDLE EAST TECHNICAL UNIVERSITY

BY

ÖZGE KAPULU

IN PARTIAL FULFILLMENT OF THE REQUIREMENTS
FOR
THE DEGREE OF MASTER OF SCIENCE
IN
AEROSPACE ENGINEERING

DECEMBER 2015

Approval of the thesis:

**SEPARATION SIMULATION FOR HELICOPTER EXTERNAL STORES
AND GENERATION OF SAFE SEPARATION ENVELOPES**

submitted by **ÖZGE KAPULU** in partial fulfillment of the requirements for the degree of **Master of Science in Aerospace Engineering Department, Middle East Technical University** by,

Prof. Dr. Gülbin Dural Ünver
Director, Graduate School of **Natural and Applied Sciences** _____

Prof. Dr. Ozan Tekinalp
Head of Department, **Aerospace Engineering** _____

Prof. Dr. Ozan Tekinalp
Supervisor, **Aerospace Engineering Dept., METU** _____

Examining Committee Members:

Assoc. Prof. Dr. Oğuz Uzol
Aerospace Engineering Dept., METU _____

Prof. Dr. Ozan Tekinalp
Aerospace Engineering Dept., METU _____

Assoc. Prof. Dr. Ali Türker Kutay
Aerospace Engineering Dept., METU _____

Assoc. Prof. Dr. İlkay Yavrucuk
Aerospace Engineering Dept., METU _____

Prof. Dr. Ünver Kaynak
Mechanical Engineering Dept., TOBB University _____

Date: _____

I hereby declare that all information in this document has been obtained and presented in accordance with academic rules and ethical conduct. I also declare that, as required by these rules and conduct, I have fully cited and referenced all material and results that are not original to this work.

Name, Last name: Özge KAPULU

Signature:

ABSTRACT

SEPARATION SIMULATION FOR HELICOPTER EXTERNAL STORES AND GENERATION OF SAFE SEPARATION ENVELOPES

Kapulu, Özge

M.S., Department of Aerospace Engineering

Supervisor: Prof. Dr. Ozan Tekinalp

December 2015, 116 Pages

In many aerospace applications, simulations are used to predict the behavior of the flight vehicle and reduce the number of flight tests required. In this thesis modeling and development of separation simulation tool for helicopter external stores is carried out. Detailed explanations of mathematical modeling, procedure of store separation analysis and collision detection approach from flight dynamics point of view are presented.

The nonlinear mathematical model of armed configuration of Black Hawk helicopter is developed in FLIGHTLAB Simulation environment. 2.75-inch diameter rocket and 19-tube rocket launcher are also modeled to simulate store behavior after separation from the helicopter. A simulation code is written to trim the mathematical model at a desired flight condition; then simulate store separation at that trim point. The trajectory of helicopter and store are recorded during simulation. Store distance to critical helicopter points are calculated until the store leaves the helicopter neighborhood. Collision detection routine checks whether the store has contact with the helicopter components or exceeds the clearance margins. Using the simulation tool many points in the flight envelope are investigated to obtain safe separation and

safe jettison envelopes. These envelopes represent the maneuvers that the store separates safely without endangering the aircraft or crew. The main rotor interference on external stores is investigated using different main rotor inflow methods. The effect of launcher loading is also studied to determine the most critical launcher configuration at jettison.

The simulation tool is validated with jettison of external fuel tanks. The jettison envelope generated based on simulation results is consistent with the safe jettison limits defined by flight test data.

Keywords: Safe Separation, Jettison, Helicopter External Stores, 2.75-inch Unguided Rocket, 19-tube Rocket Pod, External Fuel Tank, UH-60A Mathematical Model.

ÖZ

HELİKOPTER HARİCİ YÜKLERİ İÇİN AYRILMA BENZETİMİ VE GÜVENLİ AYRILMA ZARFLARININ ÇIKARILMASI

Kapulu, Özge

Yüksek Lisans, Havacılık ve Uzay Mühendisliği Bölümü

Tez Yöneticisi: Prof. Dr. Ozan Tekinalp

Aralık 2015, 116 Sayfa

Bu tez helikopterlere yüklenebilen harici silahların ve taşıyıcı lançerlerin helikopterden ayrılmasının modellenmesi ve benzetim aracı geliştirilmesi için yürütülen uçuş dinamiği çalışmalarını kapsamaktadır. Harici yüklerin ana platformdan ayrıldıktan sonraki davranışı, olası bir çarpışmayı tespit etme yöntemleri ve ayrılmanın güvenli olduğu uçuş manevralarının belirlenmesi çalışmanın ana konusunu oluşturmaktadır. Çalışma kapsamında UH-60 helikopterinin silahlı varyasyonu ve bu helikopterden ateşlenebilen 2.75 inç çaplı güdümsüz roketler FLIGHTLAB benzetim ortamında modellenmiştir ve uçuş dinamiği analizleri aynı ortamda sürdürülmüştür.

Helikopter için tanımlanmış uçuş koşullarında helikopterin denge noktası bulunduktan sonra, denge anında harici yükün helikopterden ayrılma benzetimi yapılmıştır. Doğrusal olmayan ayrılma benzetimi roketler için ateşlenme ve lançerler için acil bırakma sonrasında helikopterin ve yüklerin yörüngelerinin çıkarılmasını içermektedir. Benzetim süresince, ayrılan yükün helikopterin yakınından geçerken helikopterin dış yüzeylerine, ana rotor pallerine ve diğer kanat istasyonlarına takılan silah sistemlerine olan mesafesi hesaplanmıştır. Harici yük yörüngesinin helikoptere

ve pallere kritik seviyede yakın olduđu ya da helikopterle temas ettiđi uçuş kořulları belirlenmiştir. Bu manevralar güvenli olmayan ayrılma kořulları olarak sınıflandırılmış ve helikopterin uçuş zarfı üzerinde gösterilmiştir. Çalışma kapsamında helikopter ana rotoru iç akışının modellenmesi için kullanılan farklı iç akış hesaplama yöntemlerinin harici yüklerin yörüngesi üstündeki etkisi karşılaştırılmıştır. Acil durumda lançer bırakma sırasında boş, asimetrik yüklenmiş ve dolu lançerlerin davranışları değerlendirilmiştir.

Benzetme aracının doğrulanması için harici yakıt tankları incelenmiştir. Acil bırakma benzetimi sonucunda çıkan zarf, uçuş testleriyle belirlenmiş ve uçuş el kitabına girmiş güvenli ayrılma zarfı ile örtüşmektedir. Böylece, ayrılma analizleri çıktısı olarak elde edilen güvenli ayrılma ve güvenli acil bırakma zarfları, atış ve acil bırakma testleri için başlangıç noktası olarak kullanılabilir. Analizde hesaplanan yörüngelerin güvenli öngörülen manevralarda test verisiyle doğrulanmasıyla yüksek maliyet ve çarpışma riski içeren uçuş test noktalarının sayısı azaltılabilecektir.

Anahtar kelimeler: Güvenli Ayrılma, Yük Bırakma, Harici Yük Ayrılması, 2.75-inç Güdüksüz Roket, 19'luk Roket Podu, Harici Yakıt Tankı, UH-60A Matematik Model.

to my family

ACKNOWLEDGEMENTS

I would like to express my gratitude and thanks to my supervisor Prof. Dr. Ozan Tekinalp who guided me throughout this work with his valuable comments and support. Furthermore I would like to thank my professor Assoc. Prof. Dr. İlkey Yavrucuk who inspires me to study on rotorcraft flight dynamics.

I would like to thank Kadircan Kopşa and Hakan Aydoğan for their contributions to the development of this simulation code. I am grateful to Erdem Ayan for his support on generation of aerodynamic database for external stores. Moreover I would like to express my gratitude to Sevil Avcıoğlu and Özge Polat who always encourage me to complete this study with their valuable advices. I would like to thank all my friends and aeromechanics team for their support throughout this study.

Special thanks to Bahar Güneş for her priceless friendship, for motivating me every time I am about to give up and supporting me at every step of my life. I would like to express my deepest appreciation to Emre Gülbağ who always knows how to make me happy with his love, kindness, support and patience.

Finally, I would like to thank my parents and my sister for their endless love and for their valuable guidance through my entire life.

TABLE OF CONTENTS

ABSTRACT	v
ÖZ	vii
ACKNOWLEDGEMENTS	x
TABLE OF CONTENTS	xi
LIST OF TABLES	xiv
LIST OF FIGURES	xv
LIST OF DEFINITIONS AND ABBREVIATIONS	xix
CHAPTERS	
1. INTRODUCTION	1
1.1 Requirements and Methods to Define Safe Separation.....	3
1.1.1 Flight Dynamics Simulations and Previous Studies	5
1.2 UH-60A Helicopter and 2.75-Inch Diameter Rockets	7
1.2.1 UH-60A Mathematical Modeling	9
1.3 Overview of FLIGHTLAB	10
2. MATHEMATICAL MODELING	11
2.1 Main Rotor	12
2.1.1 Blade Structure	12
2.1.2 Airloads	12
2.1.3 Induced Flow.....	13
2.1.4 Main Rotor Interference	19
2.2 Tail Rotor	22
2.3 Fuselage.....	23

2.3.1	Fuselage Interference	24
2.4	Empennage	24
2.5	Engine Model	25
2.6	Flight Control System	25
2.6.1	Stability Augmentation System.....	26
2.6.2	Stabilator Control System	26
2.7	External Stores	27
2.7.1	2.75-Inch Diameter Rocket	27
2.7.2	Rocket Launcher	29
2.7.3	External Fuel Tanks	29
3.	VALIDATION OF THE SIMULATION MODEL	31
3.1	Steady Level Flight Results.....	32
3.2	Steady Descent and Climb Results.....	37
3.3	Transient Response Results.....	42
4.	DEVELOPMENT OF STORE SEPARATION SIMULATION TOOL	45
4.1	Separation Simulation Procedure	45
4.2	Collision Detection.....	47
4.2.1	Main Rotor Clearance	51
5.	STORE SEPARATION ANALYSIS RESULTS	53
5.1	Effect of Main Rotor Downwash	53
5.1.1	2.75-Inch Rocket Launch At Hover	54
5.1.2	Rocket Launcher Jettison at Hover	58
5.2	Effect of Lanyard Release Connector	61
5.3	Effect of Launcher Loading On Jettison	63
6.	SAFE SEPARATION ENVELOPES	71
6.1	Safe Separation Envelope of 2.75-Inch Diameter Unguided Rockets	72

6.2	Safe Jettison Envelope of Rocket Launcher.....	76
6.3	Safe Jettison Envelope of External Fuel Tank	80
7.	CONCLUSIONS.....	83
	REFERENCES.....	87
APPENDICES		
A.	NONLINEAR RESPONSE ANALYSES.....	91
A.1	Response to 0.5 inch Forward Cyclic Input at Hover	91
A.2	Response to 1 inch Right Cyclic Input At Hover.....	94
A.3	Response to 1 inch Up Collective Input At Hover.....	96
A.4	Response to 1 inch Left Pedal Input At Hover	98
A.5	Response to 1 inch Aft Cyclic Input At 100 KTAS	100
A.6	Response to 0.5 inch Up Collective Input At 100 kts.....	102
A.7	Response to 1 inch Right Pedal Input At 100 kts.....	104
B.	REVIEW OF FLIGHTLAB SOLUTION PROCESS.....	107
B.1	Model Building Approach in FLIGHTLAB.....	107
B.2	Solution Process	108
B.3	Modeling External Releasable Objects	109
C.	AERODYNAMIC DATABASE OF EXTERNAL FUEL TANK	113

LIST OF TABLES

TABLES

Table 1 Choice for the Number of Inflow Radial Shape Functions.....	16
Table 2 Mass and Geometric Parameters of 2.75-inch Diameter Rocket	28
Table 3 Mass and Geometric Parameters of 19-tube Rocket Launcher	29
Table 4 Mass and Geometric Parameters of 230-Gallon Fuel Tank, Empty Configuration	30
Table 5 Maneuvers Analyzed in Separation Simulation	46
Table 6 Weight and CG of Critical Launcher Loading Configurations	65
Table 7 Legend for Different Launcher Loadings	66
Table 8 Maneuver Limitations of UH-60Q Helicopter	71
Table 9 Safe Separation Limits of Rockets Launched from UH-60 Helicopter	85
Table 10 Safe Jettison Limits of Rocket Launcher Jettisoned from UH-60 Helicopter	85
Table C 1 Variable List for Fuel Tank Aerodynamic Database Generation	113

LIST OF FIGURES

FIGURES

Figure 1 A Sea Hawk Helicopter in Maritime Mission	7
Figure 2 An Armed Variant of S-70 Helicopter equipped with STINGER and HELLFIRE Missile Systems.....	8
Figure 3 UH60A Main Rotor Blade Airfoil Section Locations	13
Figure 4 Representation of Induced Flow Field at Hover, Modeled with 15 State Inflow Method.....	17
Figure 5 Rotor Wake Representation, from Reference [11]	17
Figure 6 Representation of Induced Flow Field at Hover, Modeled with Vortex Wake	18
Figure 7 Effect of Main Rotor Induced Flow Model on Helicopter Pitch Attitude with Forward Speed	19
Figure 8 Main Rotor Aerodynamic Interference Effect on Pitch Attitude with Forward Speed	20
Figure 9 Comparison of Interference Models, Main Rotor Downwash on Horizontal Tail	21
Figure 10 Stabilator Incidence Angle Demonstration at Hover and Forward Flight (<i>Ref: www.usarmyaviation.com</i>).....	27
Figure 11 Thrust Curve for 2.75 inch Diameter Rocket, [16].....	28
Figure 12 Comparison of test data, GenHel and simulation results for Collective Stick	33
Figure 13 Comparison of test data, GenHel and simulation results for Stabilator Incidence Angle	33
Figure 14 Comparison of test data, GenHel and simulation results for Pitch Attitude	34
Figure 15 Comparison of test data, GenHel and simulation results for Roll Attitude	35

Figure 16 Comparison of test data, GenHel and simulation results for Longitudinal Cyclic	35
Figure 17 Comparison of test data, GenHel and simulation results for Lateral Cyclic	36
Figure 18 Comparison of test data, GenHel and simulation results for Pedal Position	36
Figure 19 Comparison of test data, GenHel and simulation results for Main Rotor Required Power	37
Figure 20 Comparison of test data, GenHel and simulation results at Descent and Climb, Collective Stick	38
Figure 21 Comparison of test data, GenHel and simulation results at Descent and Climb, Longitudinal Cyclic.....	39
Figure 22 Comparison of test data, GenHel and simulation results at Descent and Climb, Pitch Attitude.....	39
Figure 23 Comparison of test data, GenHel and simulation results at Descent and Climb, Lateral Cyclic	40
Figure 24 Comparison of test data, GenHel and simulation results at Descent and Climb, Pedal Position.....	40
Figure 25 Comparison of test data, GenHel and simulation results at Descent and Climb, Main Rotor Required Power	41
Figure 26 Longitudinal Axis Response to Lateral Cyclic Input, at Hover.....	43
Figure 27 The Flow Chart of Separation Analysis.....	47
Figure 28 Demonstration of Critical Helicopter Components	48
Figure 29 Helicopter Fuselage Coordinates, Top View and Side View	49
Figure 30 Representation of Rocket Launcher and 2.75-inch Diameter Rocket	50
Figure 31 Definition of a five-degree half-angle cone in MIL-STD-1289D [2].....	51
Figure 32 Demonstration of UH-60A Main Rotor Clearance for Maximum Tilted Tip Path Plane.....	52
Figure 33 Comparison of Induced Flow Distributions at Rocket Pod Waterline Level	54
Figure 34 Downwash Velocity along the Flight Path of the Rocket.....	55

Figure 35 Main Rotor Interference Effect on Rocket Pitch Attitude along the Flight Path.....	55
Figure 36 Main Rotor Interference Effect on Rocket Height above Launch Point ...	56
Figure 37 Main Rotor Interference Effect on Rocket Clearance to Main Rotor Disc	56
Figure 38 Effect of Main Rotor Interference on Rocket Trajectory, at Hover	57
Figure 39 Downwash Velocity Distribution along the Flight Path of the Launcher .	58
Figure 40 Main Rotor Interference Effect on Launcher Trajectory	59
Figure 41 Main Rotor Interference Effect on Launcher Pitch Attitude along the Flight Path.....	60
Figure 42 Main Rotor Interference Effect on Launcher Distance to Landing Gear ..	60
Figure 43 Main Rotor Interference Effect on Launcher Distance to Fuselage	61
Figure 44 Effect of Lanyard Release Connector on Empty Launcher's Pitch Attitude	63
Figure 45 Firing Sequence of 2.75-inch rockets and Loading Configurations, From Rear View.....	64
Figure 46 Behavior of Different Launcher Configurations Jettisoned at Hover.....	66
Figure 47 Behavior of Different Launcher Configurations Jettisoned at 100 knots Forward Flight.....	67
Figure 48 Behavior of Different Launcher Configurations Jettisoned at 70 knots Autorotation	68
Figure 49 Behavior of Different Launcher Configurations Jettisoned at 25 knots Lateral Flight.....	69
Figure 50 Launch Envelope of Rockets at Level Flight	73
Figure 51 Launch Envelope of Rockets at Descent and Autorotation	73
Figure 52 Demonstration of Rocket Exceeding Fuselage Safety Margin at Turn with 30°/sec and 14° Bank Angle.....	74
Figure 53 Launch Envelope of Rockets at Turn Maneuvers.....	74
Figure 54 Launch Envelope of Rockets at Pull-up and Push-over Maneuvers.....	75
Figure 55 Launch Envelope of Rockets at Flight with Roll Rate	76
Figure 56 Jettison Envelope of Rocket Launcher at Level Flight.....	77
Figure 57 Demonstration of Empty Launcher Jettison, at Pure Lateral Flight	78

Figure 58 Collision Instant of Empty Launcher, at 95 kts Airspeed with -18° Side Slip Angle.....	78
Figure 59 Jettison Envelope of Rocket Launcher at Descent and Autorotation	79
Figure 60 Recommended Emergency External Fuel Tank Jettison Envelope	80
Figure 61 Jettison Envelope of External Tanks at Level Flight.....	81
Figure 62 Jettison Envelope of External Tanks at Descent.....	82
Figure 63 Collision Instant of Empty Fuel Tank, at 100 kts Airspeed with 1250 fpm Descent Rate.....	82
Figure A 1 Comparison of test data and simulation model response to 0.5 inch Forward Cyclic Input At Hover	93
Figure A 2 Comparison of test data and simulation model response to 1 inch Right Cyclic Input At Hover	95
Figure A 3 Comparison of test data and simulation model response to 1 inch Up Collective Input At Hover	96
Figure A 4 Comparison of test data and simulation model response to 1 inch Left Pedal Input At Hover.....	98
Figure A 5 Comparison of test data and simulation model response to 1 inch Aft Cyclic Input At 100 KTAS.....	100
Figure A 6 Comparison of test data and simulation model response to 0.5 inch Up Collective Input At 100 kts	102
Figure A 7 Comparison of test data and simulation model response to 1 inch Right Pedal Input At 100 kts.....	104
Figure B 1 Relationship between Solution and Model Components	108
Figure B 2 Coordinate System of External Body, Reference [18].....	110
Figure C 1 Body Axis Axial Force Coefficient (CF_x) Variation.....	114
Figure C 2 Body Axis Side Force Coefficient (CF_y) Variation	114
Figure C 3 Body Axis Normal Force Coefficient (CF_z) Variation	115
Figure C 4 Body Axis Rolling Moment Coefficient (CM_x) Variation.....	115
Figure C 5 Body Axis Pitching Moment Coefficient (CM_y) Variation	116
Figure C 6 Body Axis Yawing Moment Coefficient (CM_z) Variation	116

LIST OF DEFINITIONS AND ABBREVIATIONS

Store: Anything that may be released deliberately from an aircraft, whether dropped under gravitational force or with ejection forces. Launched missiles, unguided rockets and their launchers, countermeasure payloads and external fuel tanks are included in store definition.

Safe Separation : The parting of a store(s) from an aircraft without exceeding the design limits of the store or the aircraft or anything carried thereon, and without damage to, contact with, or unacceptable adverse effects on the aircraft, suspension equipment, or other store(s) both released and unreleased.

Jettison: The intentional separation of stores or suspension equipment, or portions thereof (such as expended rocket pods), no longer required for the performance of the mission in which the aircraft is engaged.

Launch: The intentional separation of a self-propelled store; such as a missile, rocket, or target-drone; for purposes of employment of the store.

AEFA: Aviation Engineering Flight Activity

CFD: Computational Fluid Dynamics

CG: Center of Gravity

DOF: Degree of Freedom

GENHEL: General Helicopter Flight Dynamics Simulation

KIAS: Indicated Airspeed in knots

CHAPTER 1

INTRODUCTION

Helicopters are widely used in military forces due their numerous capabilities. In land forces helicopters are operated to transport troops, to launch anti-tank and air-to-air missiles. Hitting surface and subsurface targets are also part of helicopter missions at sea operations. All military aircrafts equipped with weapon systems have to fulfill target acquisition, stores installation and weapons separation requirements. The methods and procedures for weapon integration are explained in military standards (References [1] and [2]) and those documents are used as a reference in weapons design and integration activities,

Store is generally defined as anything (missiles, rockets and their launchers, countermeasure payloads, torpedoes, external fuel tanks) that is released from the aircraft intentionally or in emergency situation [2]. Separation term is used for situations such as release of a free-fall store or release with ejection force, launch of self-propelled missiles and rockets, fire of a gun and dispenses of chaff and flare counter measure systems. Separation is regarded as safe when the parting of the store from an aircraft without damage to or contact with the aircraft or other stores [1].

The intentional release of missile carrying launchers, rocket pods, external fuel tanks, dispensers or other equipment from the aircraft is called as jettison. With the purpose of minimizing the parasite drag or to reduce weight, pilot may decide to jettison the stores that are no longer required for the mission. This situation is known as selective jettison. However, most of the jettison cases occur in emergency conditions. The emergency procedures of rocket/missile fire failure such as hang fire situation necessitate jettison of the launcher immediately. Single engine or dual engine failure

emergency procedures also dictates to jettison all external stores and external fuel tanks as soon as possible to improve autorotational performance and to reduce the risk of damage to the helicopter on landing [17].

The techniques used for prediction of store flight characteristics released from fixed wing aircrafts are not convenient to be used in rotary wings. Although store separation from helicopters occurred in lower airspeeds compared to fixed wing aircrafts, the capability of hover, lateral and rearward maneuver capabilities makes the separation problem equally crucial. Separation at relatively low speeds has a negative impact on separation characteristics since the store may not clear the helicopter neighborhood rapidly. Main rotor induced flow is another subject to be considered in separation from helicopters since mounting locations of external stores are generally remain inside the rotor wake.

Store separation from a rotorcraft is a complicated problem because of the transient rotor induced flow field around the store. Another reason is that the missile launcher and rocket pods have dynamically unstable jettison behavior due to their geometries and low weights. Although launched rockets and missiles follow a horizontal and forward path with respect to the helicopter axes, safe separation is still a subject to concern. In dynamic maneuvers like push over and coordinated turns, the store path may be in a very close proximity to the main rotor blades and helicopter extremities such as pitot tubes. Separation simulations concern the flight dynamics of the store as far as it leaves the helicopter vicinity. Predicting unsafe separation has a major significance because a potential damage to parent helicopter and to the store itself may threaten the mission and crew safety.

Every helicopter carrying external stores and fuel tanks has a safe separation and safe jettison envelope that demonstrates the safe and critical areas in the flight envelope. These envelopes are provided to the aircrew in the flight manual. The purpose of this study is to develop a simulation tool that investigates the helicopter and store motion after separation and to detect the flight maneuvers at which separation is critical or unsafe. Safe separation and safe jettison envelopes are generated as the outcome of the simulations.

1.1 Requirements and Methods to Define Safe Separation

Flight testing is the absolute way to verify safe separation. The launch and jettison flight test procedures, purpose of the test, data requirements, test preparation, test conditions and acceptance criteria of launch and jettison tests are explained in detail in MIL-HDBK-1763 [1]. MIL-HDBK-1763 states that minor store-to-store or store-to-aircraft contact may be acceptable in emergency jettison cases. According to the same reference, the acceptance criterion for launch is that no part of the missile / rocket will strike the aircraft or adjacent stores. MIL-STD-1289 document [2] is also taken as a guideline for store installation and testing procedures. The standard provides physical clearances that are recommended to prevent any damage. Hence in this study the requirements specified in the standard are considered for safe separation determination. The allowable external store to aircraft and store to store minimum clearance is stated as 1 inches (25.4 mm). For launched stores such as missiles and rockets, the clearance measured from the trajectory of the store to the worst-case rotor plane is depicted as five-degree. These clearance limits shall be taken into account while identifying safe separation conditions.

Although the flight testing is the most reliable method to determine safe separation limits, the store may exhibit unexpected behavior in the helicopter flow field during flight trials. The unstable characteristics of the store must be analyzed before flight tests to reduce the risk of damage to helicopter and crew. Another drawback of flight testing is the high cost of flight sorties. In a similar manner, test missiles and launchers are quite expensive and they become useless once they are separated from the helicopter. Regarding all these constraints, the number of test points is limited. As an initial step of separation tests, analogy with similar shape launchers that have been already certified can be used to predict store behavior. In most of the weapon integration projects, predictive analyses specific to the store is preferable to estimations based on past experience.

Separation simulations are the appropriate way to manage the risk and cost of the flight tests. Moreover an insight about the store behavior is gained prior to tests. Wind tunnel testing, computational fluid dynamics analyses and flight mechanics

analyses are different methods used for separation simulations. Each method has advantages over other methods. Wind tunnel testing and CFD solutions are proper to simulate the highly complex flow field and aerodynamic interferences between rotor, fuselage and external store. Wind tunnel tests are performed using one-to-one or a partial scale of the helicopter and the store. Main rotor and tail rotor induced flows must be represented in wind tunnel test especially at hover and low speeds. Wind tunnels are more suitable for free drop jettison tests due to limited space. For captive trajectory wind tunnel testing, the models of helicopter and the store are supported individually with strings which enable 6 DOF motion. Aerodynamic forces and moments acting on the store are measured at each simulation time step. Equations of motions are solved numerically and the trajectory of the store at the next step is calculated. The store is placed to the new position and the procedure is repeated until the whole trajectory of the store is obtained. It is apparent that the wind tunnel testing is an expensive method requiring a special test setup.

Computational fluid dynamics (CFD) analysis is an alternative way to wind tunnel tests. CFD provides solution for store motion inside the complicated rotor wake. The aerodynamic interactions between fuselage and store can be also modeled in CFD simulations. CFD studies provide separation simulations for limited test cases because of time required to generate meshes, simulate the separation and post process the results. For this reason they are not practical for safe envelope generation that necessitates sweep of numerous flight scenarios. With the exception of the impractical sides, CFD and wind tunnel tests provides reliable data for generating store aerodynamic databases which are the crucial elements in 6 DOF flight dynamics simulations. Empirical data for including aerodynamic interference between helicopter components (main rotor, fuselage, empennage and tail rotor) may be obtained from CFD simulations as well as wind tunnel tests.

1.1.1 Flight Dynamics Simulations and Previous Studies

6DOF flight dynamics simulations offer best approach for predicting store by providing fast and inexpensive solutions. Comprehensive flight dynamics simulations compensate drawbacks of CFD and flight testing methods. In simulations, analytical methods are completed with aerodynamic data gathered from wind tunnel tests and fluid dynamics solutions. Store separation at many points in the flight envelope of helicopter may be analyzed and an initial separation envelope may be generated. This initial separation envelope is a starting point for actual flight tests. Once the critical points on the flight envelope are determined by the analysis tool, the number of flight trials would be reduced and only validation tests at certain points will be performed.

Concerning the advantages of flight dynamics simulations, all rotorcraft and weapon manufacturers develop their own simulation tools to estimate store trajectories after separation during the development phase.

The aerodynamic environment of rockets/missiles launched from helicopters and jettison behavior of missile launchers and rocket pods have been a subject of many studies. These studies are generally conducted by military sources as the operator of the armed helicopters or by companies under contract of weapon integration projects. The study of Langrebe and Egolf [3] focuses on an analytical investigation to predict the rotor wake induced flow velocities along the trajectory of 2.75-inch diameter rockets fired from AH-1G helicopter. The sensitivity of induced velocity to rotor wake model, launch attitude and launch position were also investigated. The results showed that determination of rotor wake boundary location has a strong effect on rocket trajectory; hence rotor wake geometry should be specified using a realistic method. Wasserman and Yeller have a similar work as well [4]. Their study was performed using a 6 degree of freedom trajectory program and discussed the change in downwash due to varying blade azimuth angles. The effect of varying downwash distribution resulted in a significant change in the rocket range and dispersion especially at hover.

Technical lecture series conducted by NATO-AGARD addresses the problems of integrating externally mounted weapons on helicopters and lessons learned from AH-64 Apache, RAH-66 Comanche, EH-101 and TIGER helicopters. One paper discusses a two-dimensional model built in Eurocopter Company, to gather information about trajectory in longitudinal and vertical axis and the pitch motion [5]. Empirical induced velocity and aerodynamic data from full scale wind tunnel tests were used for analysis.

As a part of integration of Hellfire Missile System into the UH-60 helicopter, jettison analyses were performed in 6 DOF computer simulations prior to tests [6]. Based on analyses, the most critical configuration in terms of collision possibility was determined as the launcher loaded with two missiles on the upper and lower inboard stations. Result of the analyses showed that the most dominant parameter that affects the movement of the store towards to the fuselage is sideslip. The separation simulation results were utilized to define the safe jettison limits with minimum number of test points. The analyses results bring about more conservative trajectory compared to actual flight jettisons in which the launcher demonstrated stable characteristics.

Another research about jettison simulations is conducted in Eurocopter by Ries and Kieseletter [7]. 6-DOF Flight Mechanical Simulation Tool is used in combination with CFD calculations. Aerodynamic coefficients of both the helicopter and the store are generated for different angle of attack and side slip angle combinations using serialization methods instead of a manual CFD calculation process. The impractical steps in CFD calculations such as coordinate transformations, interpolation between the simulated angle combinations and suitable output formatting for the flight mechanical tool are improved by the automation of the process. Moreover, a routine is developed to determine the collision energies of two bodies with the assumption of an inelastic collision. The analyses results of the jettison of Alpha Jet Tank from NH90 helicopter are validated and a good correlation is achieved.

1.2 UH-60A Helicopter and 2.75-Inch Diameter Rockets

The UH-60 Black Hawk is a medium-lift utility helicopter developed by Sikorsky Aircraft. It has been operational in the US Army since 1979 as replacement to Bell UH-1 transport helicopters. The UH-60A helicopter is the baseline version used in US Army. Modified versions and variants of Black Hawk helicopters have different capabilities and are loaded with different equipment. For example, UH-60M version has improved rotor blades and engines and it is upgraded with fly-by-wire system. UH-60Q is used for medical evacuation purposes. MH-60M helicopter is known to be designed with stealth technology and has reduced noise signature. SH-60 Seahawk is a multi-mission maritime helicopter.

S-70 helicopters are military versions of Black Hawk that are developed for export market and they have been in service in 25 nations, including Turkey for multi-mission support and military operations. By the year 2015 total number of 3600 variants of S-70, SH and UH-60 helicopters are reported to be actively operated worldwide, being the leader of the combat helicopter market with the share of %18.

In February 2014, T-70 Utility Helicopter Program Contract was signed between TAI (as Prime Contractor) and Sikorsky (as Major Subcontractor) to manufacture 109 variants of Sikorsky's S-70 Black Hawk helicopters in Turkey. T-70 helicopters will be manufactured in two different configurations for operation of Turkish Land Forces, Turkish Air Forces, Gendarmerie, Special Forces, Directorate of Security and General Directorate of Forestry.



Figure 1 A Sea Hawk Helicopter in Maritime Mission

Black Hawk helicopters are also reconfigured to meet the demands for armed reconnaissance and attack missions with weapons kit. Battle Hawk is the name of the armed multi mission variant of UH-60M. In addition to baseline configuration of UH-60M, machine guns, 7, 12 or 19 pod 2.75-inch rocket launchers, missile systems (Spike-ER, HELLFIRE, etc.) and auxiliary fuel tanks may be integrated.



Figure 2 An Armed Variant of S-70 Helicopter equipped with STINGER and HELLFIRE Missile Systems

2.75-inch diameter unguided rockets have been used in both helicopters and fixed wing platforms throughout the world. Those rockets can be fitted with various types of warheads specialized depending on the operation (anti-tank, air-to-air, anti-personnel etc...). The study of this thesis work simulates the dynamics of rockets with 2.75-inch (70 mm) diameter and MK-40 rocket motor. Four folding fins of the rocket are opened after launch and provide stabilization during flight. Effective range of 2.75-inch rocket is 8000 meters and the rocket speeds to approximately 700 m/s velocity depending on the warhead. Guidance of rocket is provided through a ballistic algorithm.

Pods are used to carry different numbers of rockets. There are 19-Tube, 12-Tube and 7-Tube 2.75" rocket launchers. Those pods can be jettisoned during mission to reduce drag or to evacuate rockets in case of hang fire.

1.2.1 UH-60A Mathematical Modeling

Since Black Hawk helicopters are operated all over the world, many studies have been conducted to generate a reliable mathematical model. The first flight dynamics simulation model was developed by Sikorsky Aircraft Company [8]. This model was based on Sikorsky General Helicopter (GenHel) Flight Dynamics Simulation and provided an engineering simulation for performance and handling quality evaluation for U.S. Army. The flight tests were performed by U.S. Army Aviation Engineering Flight Activity (AEFA) at Edwards Air Force Base to gather mathematical model verification data and assess the fidelity of the Vertical Motion Simulator (VMS) developed in NASA Ames. After validation with flight test data for steady trimmed flight and transient responses to control inputs, The Black Hawk Engineering Simulation Model was updated with some modifications in the existing simulation formulations as explained in Reference [9]. After several simulations, an upgrade of the existing systems with improved dynamic model was required. Thus, Sikorsky's GenHel model was improved by Ballin for a real-time simulator [10]. Collective servo dynamics were modified to enhance the collective response, engine and gear box models were also improved. Ballin's study presented the details of expansion of the model by NASA and comparison of real-time simulation results with existing test data and nonreal-time program on which it was based. Several upgrades and modifications have been applied on real-time UH-60A model for Vertical Motion Simulator to increase the fidelity.

Mathematical modeling of UH-60 helicopter in different simulation environments has been a part of many flight dynamics, aeroelasticity, aerodynamics, vibration and control design studies because of the accessibility of modeling parameters and availability of flight test data.

1.3 Overview of FLIGHTLAB

FLIGHTLAB is a comprehensive rotorcraft analysis and simulation program, developed by Advanced Rotorcraft Technology (ART). Although the program is specialized in rotary wing modeling and simulation, fixed wing air vehicles modeling is supported as well. FLIGHTLAB is a commercial tool which is used in many flight mechanics studies world-wide. Different tools of the program offer a complete analysis of rotorcraft system. The major tools are; FLIGHTLAB Model Editor for mathematical modeling, XANALYSIS for flight dynamics analyses, Control System Graphical Editor for control system design and Pilot Station for simulations. Several rotor configurations (tandem, co-axial, tilt rotors) with options of articulated, hingeless and teetering rotor types can be modeled in FLIGHTLAB. It is capable of performing trim, linearization, stability, performance, time and frequency response, load and handling quality analyses.

FLIGHTLAB has its own language called SCOPE which has a similar syntax structure with MATLAB. The scripts used in separation simulations of this study are written in SCOPE language.

The details of model building and solution methods are explained in Appendix B.

CHAPTER 2

MATHEMATICAL MODELING

This section describes the development and validation of UH-60A helicopter model that is used as a baseline for flight dynamics analyses conducted as a part of store separation simulation. A special emphasis is placed on mathematical modeling studies since it has an essential role in predicting the actual behavior of the helicopter.

The nonlinear mathematical model of the helicopter is generated through FLIGHTLAB Model Editor. The main features of the mathematical model and the assumptions made are explained in this chapter. Data required for modeling the helicopter is obtained from Reference [8] which is a baseline model developed by Sikorsky Aircraft Company. Since it is a baseline, many improvements carried out during validation phases as explained in References [9] and [10]. These modifications are taken into consideration as well as addition of parameters required for external stores modeling such as External Stores Support Structure attribution to total fuselage drag, change in center of gravity when external stores are loaded, etc...

In order to validate the model, the flight test data and real-time simulation of UH-60A based on GenHel mathematical model developed by Sikorsky is used. The comparison data is obtained from a very detailed study of Ballin [10].

2.1 Main Rotor

2.1.1 Blade Structure

UH-60 has an articulated rotor with four blades. It is modeled with Blade Element approach. The blade element method models the blade by segments. Each blade segments produces aerodynamic forces which are computed from local angle of attack and dynamic pressure. The total forces and moments on the rotor are calculated by integrating the airloads from each segment over the blade span. Blade element theory is widely used in helicopter aeromechanics analysis due to detailed blade loading calculations.

The articulated blade model includes feathering, flapping and lead-lag hinges. Flapping and lagging dynamics are modeled by a hinge of one rotational degree of freedom. Considering the possibility of sudden pitch-up motion of the helicopter in aggressive maneuvers, flapping of the blades is constrained. The lagging motion is limited by a lag damper model. The feathering motion is assumed to be controlled via control input.

Spanwise properties of blades such as chord distribution, twist, inertia and mass distribution, tip sweep are input to the model in table format. Actual mass and inertia distribution on the blade is estimated. A realistic distribution is generated in the mathematical model by keeping the total mass, mass moment about the hinge and inertia of the blade about the hinge values same as those of actual UH-60A blades.

2.1.2 Airloads

The blades of UH-60 Black Hawk helicopter have SC1095 and SC1094R8 airfoil sections, as shown in Figure 3. A nonuniform airfoil table that includes lift, drag and pitch moment coefficients as functions of angle of attack and Mach number is input to the model in order to calculate the airloads of blade segments. Hinge offset of blades is 1.25 ft and tip sweep of blade located at %95 span is 20 degrees.

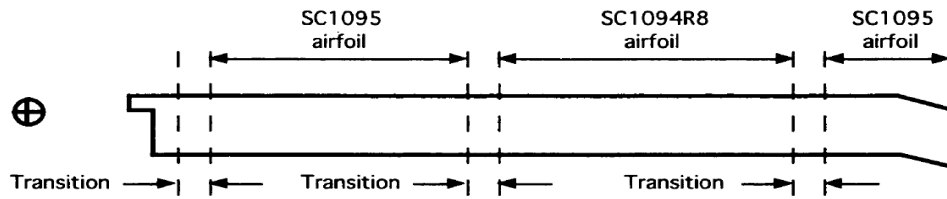


Figure 3 UH60A Main Rotor Blade Airfoil Section Locations

It is known that tip loss decreases the rotor thrust about 6% - 9% for a given collective pitch. Hence it has a significant role in estimating rotor performance. With blade element theory, blade loading near tips cannot be calculated correctly. In the mathematical model of Black Hawk helicopter, the tip loss factor of 0.97 is set with the purpose of preventing the overestimation of the rotor thrust and make a good correlation with flight data.

2.1.3 Induced Flow

Modeling the inflow correctly is an important and challenging part of mathematical modeling since it has a dominating effect on helicopter behavior in all aspects. Helicopter performance, flight dynamics, stability and vibration are strongly influenced by rotor wake. Predicting the rotor wake characteristics has been a subject of a number of studies over the years. Dynamic wake and vortex wake inflow models have been developed so far in order to improve the estimation of rotor downwash effects on helicopter flight dynamics. Dynamic inflow models are represented by set of first order equations and corresponding inflow states. Hence they can be extensively used in flight simulation due to their reliability and inexpensive computational costs. However the structure of wake geometry is modeled based on assumptions in dynamic wake models. Vortex wake method has advantage of modeling wake geometry and structure more accurately but it does not include effects of time variations in inflow. The drawback of vortex wake model formulation is the difficulty of integration into flight dynamics simulations that requires numerical solutions with states.

FLIGHTLAB has different solution options for induced flow. Each inflow model has specific advantages and disadvantages over other methods. In all models an empirical inflow correction factor as a function of wake skew angle can be added in order to account for the additional losses of the actual rotor.

These models are explained briefly in following subsections.

2.1.3.1 Uniform Inflow Model

Uniform model is the simplest form of dynamic inflow models. This method computes the inflow over the main rotor using momentum theory. It is a simple model limited with assumption of linear distribution of inflow along the blade radius.

The structure of wake geometry is assumed to be undistorted and skewed with forward speed. With these simplifications, it doesn't provide realistic simulation results. Nevertheless, uniform model can be adequate for initial design studies.

2.1.3.2 Finite State Model

Finite state dynamic inflow model is developed by Peters and He ([12] and [13]). Finite state model computes the unsteady rotor induced flow in three dimensions. Inflow distribution is modeled in terms of radial variation and harmonic variation of inflow over azimuth. That means radial and azimuth position of blade elements are taken into account in calculations. Hence, drawback of uniform inflow model is improved by using higher order polynomials and generating a more general distribution of pressure along rotor disc. Tip losses and skewed wake effects are also included in the model. Another advantage of the finite state model over uniform model is that tip vortex distortion effect caused by hub rotation is included. Off- axis response characteristics can be improved in this way. The finite state model has the sophistication of the vortex wake method with more efficient computational capability. Therefore finite state model can be utilized in both steady and dynamic maneuvers.

The finite state dynamic wake model is formulated in state-space form with finite number of states. Describing the inflow in terms of explicit state variables makes the mathematical model more applicable for rotor aeroelasticity, aeromechanical and control system design studies and can be used in real-time simulations.

The details of the theory and formulation are explained in Reference [14]. In this section, only the summary of the formulation is given to comprehend the background information of determining state numbers.

Formulation of theory is developed from fluid mechanics equations for incompressible potential flow with skewed cylindrical wake. The induced inflow distribution at the rotor disk is expressed in terms of a set of harmonic and radial shape functions with expansion coefficients as inflow states, α_j^r and β_j^r . The formulation of generalized dynamic wake is represented in FLIGHTLAB Theory Manual [18] as;

$$\omega_i(\hat{x}, \psi, t) = \sum_{r=0}^N \sum_{j=r+1, r+3, \dots}^{2S_r+r-1} \phi_j^r(\hat{x}) [\alpha_j^r(t) \cos(r\psi) + \beta_j^r(t) \sin(r\psi)] \quad (1)$$

With radial shape function;

$$\phi_j^r(\hat{x}) = \sqrt{(2j+1)H_j^r} \sum_{q=r, r+2, \dots}^{j-1} \hat{x}^q \frac{(-1)^{\frac{q-r}{2}} (j+q)!!}{(q-r)!!(q+r)!!(j-q-1)!!} \quad (2)$$

And factorial ratios,

$$H_j^r = \frac{(j+r-1)!!(j-r-1)!!}{(j+r)!!(j-r)!!} \quad (3)$$

where \hat{x} is radial coordinate, ψ is the azimuth position and t is time, r is harmonic number and j is polynomial number.

Using this representation induced flow can be truncated at desired harmonic number in azimuth direction, N and for each harmonic, specific number of radial shape function, S_r is chosen.

The total inflow states are determined according to Table 1 depending on number of harmonics and radial shape functions. Numbers of harmonics are related with the blade numbers and same highest order of radial variation corresponding to each harmonic is selected. For $m=0$ only one inflow state is modeled, and for $m \neq 0$ two inflow states that correspond sine and cosine terms are modeled. For example according to Table 1, Peters-He 3 state model consists of uniform inflow component, sine and cosine inflow components.

FLIGHTLAB has individual modeling options for 3 State, 6 State and Finite State models. In Finite State option, the number of harmonics and shape functions can be determined. For four-blade UH-60A helicopter, Finite State (4x4) modeling is selected. Hence total number of states are calculated as $3+2(2+2+1+1)=15$.

Vector field representation of dynamic wake around Black Hawk helicopter at hover is generated with 15 State (4x4) Induced Velocity method and is shown in Figure 4.

Table 1 Choice for the Number of Inflow Radial Shape Functions

Highest Power of \hat{x}	m (harmonic value)													Total Inflow States
	0	1	2	3	4	5	6	7	8	9	10	11	12	
0	1													1
1	1	1												3
2	2	1	1											6
3	2	2	1	1										10
4	3	2	2	1	1									15
5	3	3	2	2	1	1								21
6	4	3	3	2	2	1	1							28
7	4	4	3	3	2	2	1	1						36
8	5	4	4	3	3	2	2	1	1					45
9	5	5	4	4	3	3	2	2	1	1				55
10	6	5	5	4	4	3	3	2	2	1	1			66
11	6	6	5	5	4	4	3	3	2	2	1	1		78
12	7	6	6	5	5	4	4	3	3	2	2	1	1	91

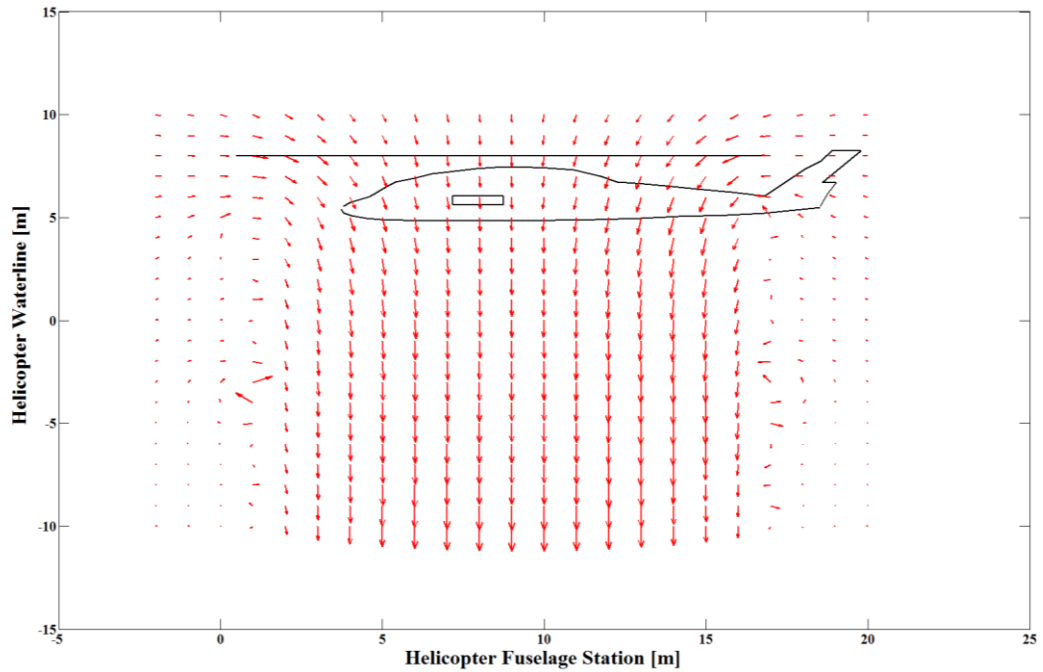


Figure 4 Representation of Induced Flow Field at Hover, Modeled with 15 State Inflow Method

2.1.3.3 Vortex Wake Models

Vortex theory calculates the rotor wake and predicts the induced velocity distribution at the rotor disk using vortex elements. The geometry of the wake is modeled with blade tip vortices and inboard vortex sheet. The induced velocity is calculated as a combination of these vortices. Vortex sheet consists of two components; shed vorticity which is oriented parallel to the blade span and trailed vorticity which is perpendicular to the blade span (Figure 5).

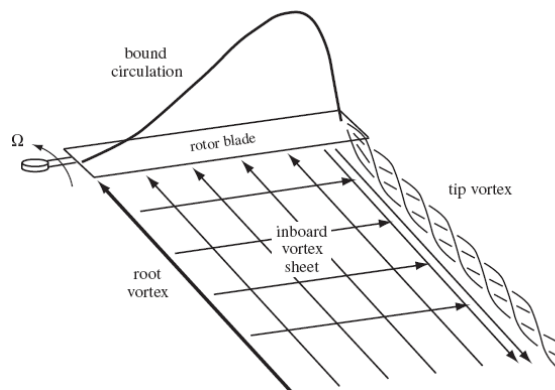


Figure 5 Rotor Wake Representation, from Reference [11]

Vortex wake methods require iterative computations. Although in theory, vortex wake method is more realistic than other inflow models, the complexity of the wake geometry makes it time consuming and difficult to be solved numerically. Another disadvantage is that the inflow is not represented by first order equations; hence there are no states linked with inflow. Consequently, vortex wake models are not suitable for flight dynamics analyses that require linearized models and dynamic maneuvers. Generally vortex wake methods are implemented for non-real time steady-state analyses.

In FLIGHTLAB, vortex modeling method has Prescribed Wake and Free Wake options. The knowledge of the wake structure (vortex peak model, inboard wake model, vortex element model, wake element strength variation, etc...) is required to model the wake accurately. Prescribed Wake models the geometry of vortex elements and only the strength of the wake is updated as blade loading changes. On the other hand, in free wake model tip vortex is allowed to distort due to flight condition and change in blade loading. Inboard wake is still prescribed.

Vector field representation of vortex wake around Black Hawk helicopter at hover is generated and shown in Figure 6. The formation of tip vortices is apparent and the magnitude of induced velocity decreases as wake moves away from the rotor disc.

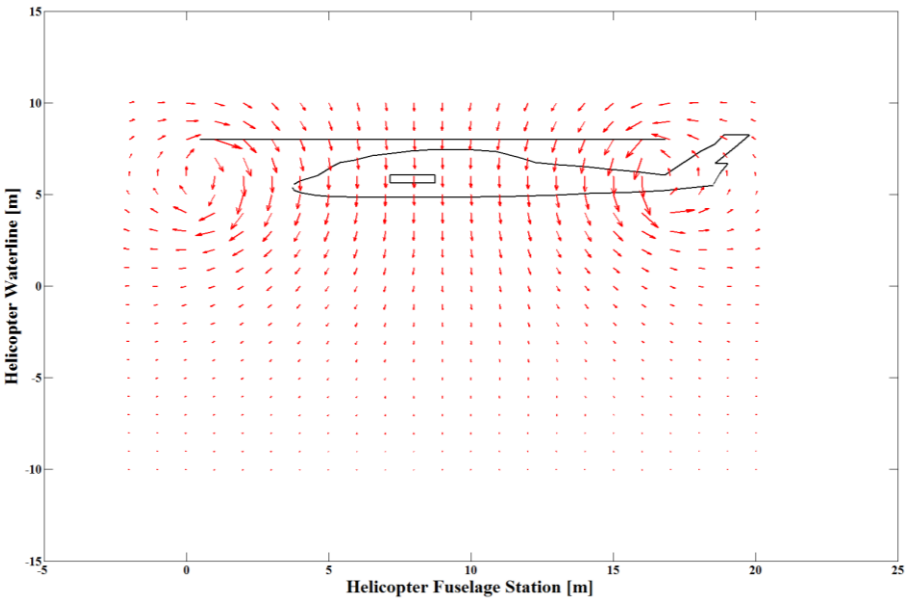


Figure 6 Representation of Induced Flow Field at Hover, Modeled with Vortex Wake

2.1.3.4 Inflow Model used in Model Validation

Neglecting rotor downwash causes under prediction of pitch attitude at hover and low speeds as expected (Figure 7). Trim results of mathematical models with different inflow models are compared during mathematical model validation study. Regarding its advantages Peters-He 15 state inflow model is considered quite adequate for mathematical model validation. The mathematical model validation study is explained in CHAPTER 3.

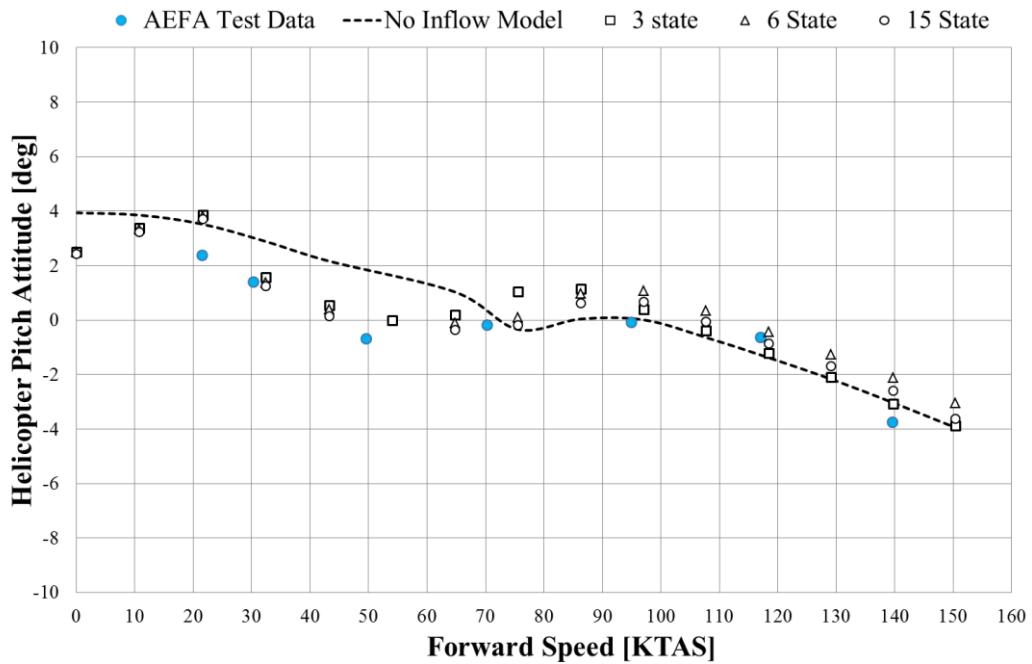


Figure 7 Effect of Main Rotor Induced Flow Model on Helicopter Pitch Attitude with Forward Speed

2.1.4 Main Rotor Interference

Another important concept in mathematical modeling and flight dynamics analyses is to predict aerodynamic interference between helicopter components because aerodynamic interferences have significant effect on helicopter flight characteristics and control. In the separation simulation model main rotor to tail rotor, main rotor to fuselage and main rotor to empennage influences are included through the use of empirical formulas.

A main rotor induced velocity effect (k_{xr}, k_{yr}, k_{zr}) as a function of the wake skew angle, χ , and the longitudinal tip path plane angle, α_{1f} is obtained through look-up table in the model. The total interference of main rotor is computed as;

$$\begin{bmatrix} v_x \\ v_y \\ v_z \end{bmatrix} = \lambda_r \Omega_r R_r \begin{bmatrix} k_{xr} \\ k_{yr} \\ k_{zr} \end{bmatrix} \quad (4)$$

where $\lambda_r \Omega_r R_r$ is uniform component of main rotor induced velocity.

The empirical data as functions of wake skew angle and longitudinal tip path plane angle is obtained from Reference [8].

Addition of main rotor interference on fuselage and lifting surfaces has a significant outcome on helicopter pitch attitude at trim. On Figure 8 pitch angle in level flight are compared for mathematical models with and without aerodynamic interference of main rotor. First, the main rotor interference on fuselage is added to the model. It is observed that helicopter nose-down behavior increases at all speeds. When the impingement of main rotor downwash on empennage is added, the change in pitch attitude trend is remarkable, particularly at lower speeds. Main rotor interference on tail rotor has negligible effect on trim results.

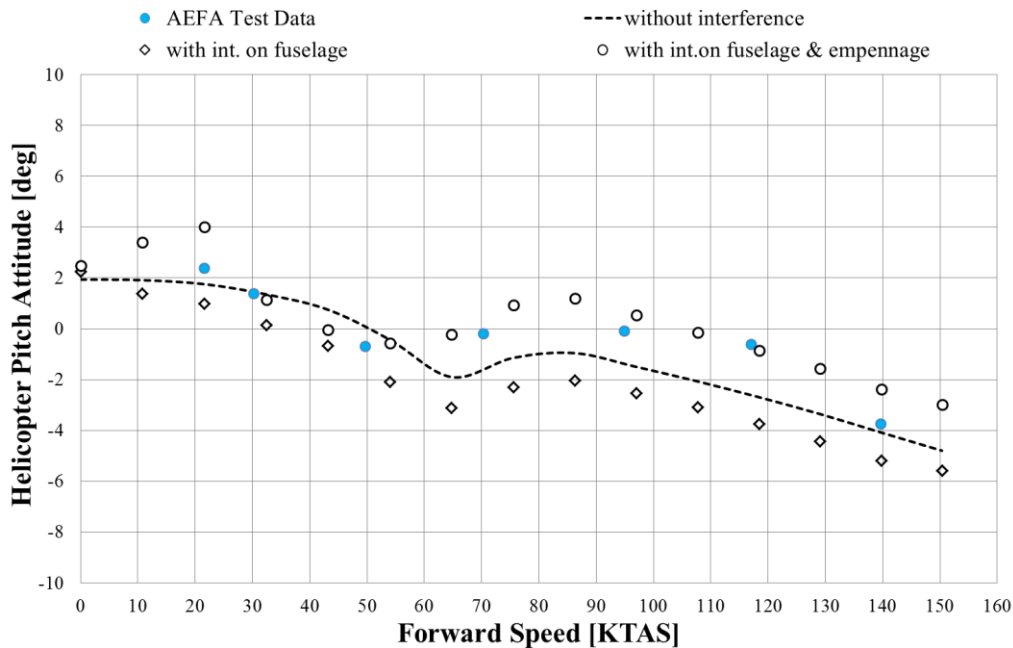


Figure 8 Main Rotor Aerodynamic Interference Effect on Pitch Attitude with Forward Speed

In order to determine which interference method gives more realistic results, the main rotor downwash at horizontal tail with different solution methods is compared against empirical data. It is seen in Figure 9 that dynamic interference methods provides more consistent results with empirical data at all speeds.

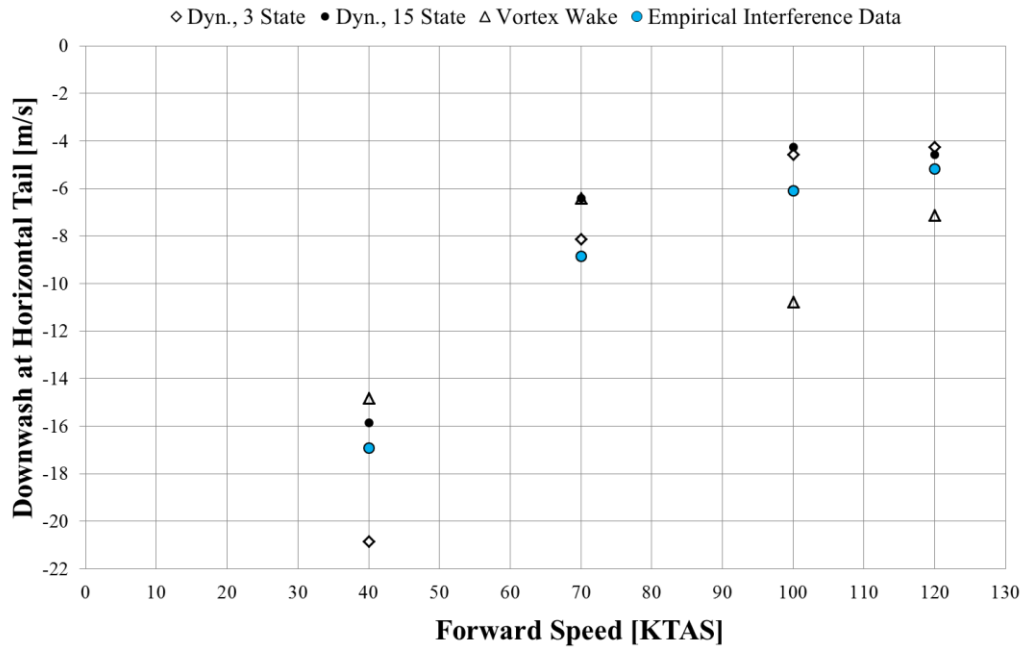


Figure 9 Comparison of Interference Models, Main Rotor Downwash on Horizontal Tail

2.1.4.1 Rotor Interference on External Stores

Armed versions of Black Hawk helicopters are capable of carrying external fuel tanks, anti-tank guided missiles, air to air missiles and rockets. These stores are directly subject to aerodynamic effect of main rotor wake due to their mounting positions. While simulating the trajectory of a launched rocket or a jettisoned launcher, rotor wake interference should be included in order to increase the level of accuracy.

FLIGHTLAB is not capable of integrating induced flow on the external stores; therefore a script is generated to model the inflow effects on the store. This script is embedded to the main separation simulation code. First, the model is trimmed at desired flight condition and induced velocity components over the flow field are generated. Second, separation of the store is simulated without any interference on

store and trajectory of the store is recorded. In the third step, the instantaneous induced velocity components at each point along the path of jettisoned launcher / launched rocket are calculated in the model using the geometric relationship between the rotor and trajectory points. Finally, separation is simulated once again, but this time induced velocity is added to the store equations of motion as a wind input.

An accurate inflow model should be selected for the simulation to predict the trajectory of the store after separation more precisely. Hence a set of studies are conducted to determine the sensitivity of the separation behavior to flow field around the rocket pod and launched rocket. The analyses are performed at hover to better understand the downwash effects of 3 State, 6 State, 15 State dynamic inflow and vortex wake inflow models. The results of this study are given in Section 5.1. It is decided to use 15 State inflow method to compute the interference on external stores in safe separation envelope generation.

2.2 Tail Rotor

UH-60A helicopter has a four blade, canted tail rotor mounted on the right side of the vertical fin. Tail rotor hub has teetering configuration with 11 ft. diameter. With the shaft tilt of 20 degrees upward, tail rotor provides approximately %2.5 of the total lifting force as the clearance with the vertical fin increases.

Similar to main rotor blades, tail rotor blades has SC1095 airfoil sections. Blade twist is linear and chord is constant along the span.

In this study, tail rotor model is similar but simpler than the main rotor model. Tail rotor of helicopter is modeled using Bailey Rotor method. There is only collective pitch input that means only thrust is calculated. Since there is no cyclic input, flapping motion is ignored. Bailey rotor model calculates tail rotor torque and thrust by integrating the airloads over the blade span and averaging them over azimuth angle.

The inflow over tail rotor disk is assumed uniform. Main rotor downwash and fuselage sidewash effects are also considered to modify airflow through the tail rotor disk.

At hover and low speeds, aerodynamic interactions due to proximity of the vertical fin have impact on yaw characteristics of the helicopter as a result of reduction in the tail rotor efficiency. This correction in overall thrust calculation is implemented in the model by using empirically determined blockage effect factor.

2.3 Fuselage

The UH-60 fuselage is modeled as rigid fuselage with six degrees of freedom. The total weight, center of gravity and corresponding moment of inertia values of the analyzed configuration of helicopter are input to the model excluding the mass properties of external stores. The mass, cg and moment of inertia of the external stores are defined separately at External Body subsystem and their effect on helicopter trim and dynamic response are taken into consideration during simulation.

In mathematical modeling and model validation studies, fuselage aerodynamic characteristics have an important role on estimation of helicopter behavior at forward flight. In FLIGHTLAB, fuselage is modeled using aerodynamic relations in which force and moment coefficients of fuselage vary with angle of attack and sideslip angle. Aerodynamic characteristics used in the mathematical modeling study are specific to Black Hawk helicopter which are directly derived from wind tunnel tests as stated in Reference [8]. Drag, lift and side force and roll, pitch, yaw moment coefficients of fuselage at varying angle of attack and sideslip angles are obtained from the look-up table.

The interaction of main rotor wake with fuselage is an important phenomenon that influences helicopter attitude in an obvious manner. The effect of main rotor interference around fuselage flow field is modeled using empirical data obtained in Reference [8]. Rotor interference induced velocity components are expressed as functions of rotor wake skew angle and tip path plane tilt angle arguments.

2.3.1 Fuselage Interference

A similar formulation with main rotor interference computation (Section 2.1.4) is used for fuselage interactions. First, the dynamic pressure reduction effect is calculated as a function of fuselage sideslip angle and angle of attack.

$$k_{qdyn} = f_{qdyn}(\beta, \alpha) \quad (5)$$

Fuselage downwash λ_{fz} and sidewash λ_{fy} effects on Tail Rotor and Lifting Surfaces are evaluated via empirical look-up tables.

The total interference velocity is computed as;

$$\begin{bmatrix} v_x \\ v_y \\ v_z \end{bmatrix} = \lambda_r \Omega_r R_r \begin{bmatrix} k_{xr} \\ k_{yr} \\ k_{zr} \end{bmatrix} + (k_{qdyn} - 1) \begin{bmatrix} v_p(1) \\ v_p(2) \\ v_p(3) \end{bmatrix} - v_p(1) \begin{bmatrix} 0 \\ k_{qdyn} \lambda_{fy} \\ k_{qdyn} \lambda_{fz} \end{bmatrix} \quad (6)$$

where v_p is the velocity vector computed from the fuselage motion and wind vector.

2.4 Empennage

Total velocity on the aerodynamic surfaces has contributions from main rotor wash, fuselage downwash and sidewash. The components of main rotor downwash acting on horizontal and vertical tail are expressed as functions of rotor wake skew angle and longitudinal tip path plane angle arguments. The sidewash and downwash effects of fuselage on these aerodynamic surfaces are computed based on dynamic pressure correction using the wind tunnel test data given in Reference [8].

Horizontal tail of a helicopter has a role of improving longitudinal stability. Horizontal stabilator of UH-60 helicopter was designed with a variable incidence angle mechanism. The purpose is to eliminate undesired high pitch-up behavior of the helicopter at hover and low speeds produced by main rotor downwash on horizontal stabilator. By Black Hawk Stabilator Control System, the incidence is optimized to align the horizontal tail surface with the rotor flow. The control system operates with feedbacks from flight speed, collective stick position, pitch rate and lateral acceleration. The incidence angle ranges from 39 degrees (at hover) to -8

degrees (at high speeds). The control system also allows for a fixed incidence angle that can be specified by the pilot. The airfoil section of horizontal stabilator is NACA 0014 [8].

The vertical fin of UH60 improves the yaw stability and provides anti torque force at forward flight, with NACA 0021 airfoil and constant sweep angle of 41 degrees [8]. Lift and drag force coefficients as well as moment coefficients of aerodynamic surfaces are tabulated with varying angle of attack and Mach number values.

2.5 Engine Model

UH-60A helicopter is powered by two T700-GE-700 turbo shaft engines with a maximum take-off power rating of 3086 HP and continuous rating of 2800 hp.

In order to model the propulsion system, Ideal Engine model of FLIGHTLAB is used. In Ideal Engine model, rpm is constant and drive train is not included. Engine available power and fuel consumption data with varying altitude, temperature and flight speed arguments is provided to the mathematical model. The sophistication level of ideal engine model is regarded adequate for the separation simulations.

2.6 Flight Control System

Black Hawk helicopter is equipped with Mechanical Control System and Automatic Flight Control System (AFCS). AFCS consists of Stability Augmentation System (SAS), Stabilator, Pitch Bias Actuator (PBA) and Flight Path Stabilization (FPS) to ease the pilot workload and to enhance stability and handling qualities. Sensors, mechanical controls such as actuators, mixing unit, trim system are the basic elements of flight control system of Black Hawk.

The detailed architecture of control systems in terms of block diagrams with gains and transfer functions are presented in Reference [8]. The control system models of UH-60A are incorporated to simulation model.

2.6.1 Stability Augmentation System

UH-60A helicopter has a Stability Augmentation System designed to provide short term rate damping in pitch, roll and yaw axes. SAS is a dual system with digital and analog SAS channels at three axes. The control authority of each is 5% to restrict the total control travel. Hence total 10% authority is provided to mechanical limits of SAS actuators. If digital or analog SAS fails, the total control authority of that channel is reduced to 5% but gain on the on channel is doubled to compensate for the failed SAS. Signals from the sensors are filtered before being shaped by SAS.

2.6.2 Stabilator Control System

Stabilator incidence angle is controlled by Stabilator Control System to enhance the longitudinal control. The logic of stabilator uses velocity, collective stick position, lateral acceleration and pitch rate feedback and outputs the signal through horizontal tail servo to adjust the incidence angle. Without stabilator control system, helicopter may experience high nose-up behavior due to main rotor interference on horizontal stabilator. Stabilator aligns the main rotor downwash by adjusting the incidence angle, so pitch-up attitude is minimized. At hover and low speeds incidence is in its maximum value, 39 degrees. As the speed increases, the incidence decreases gradually to be aligned with air stream. Therefore, the static stability of the helicopter is improved. Another function of Stabilator is to provide pitch rate feedback to improve dynamic stability. Stabilator control can be disabled and incidence angle can be fixed to a certain value by the pilot [8].

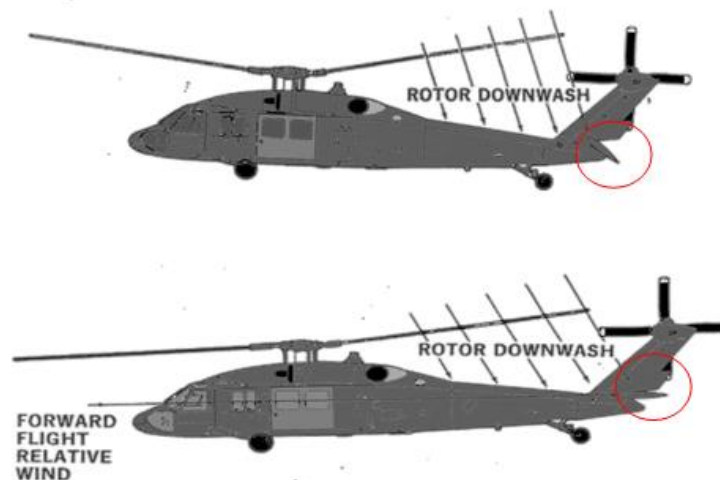


Figure 10 Stabilator Incidence Angle Demonstration at Hover and Forward Flight (Ref: www.usarmyaviation.com)

2.7 External Stores

FLIGHTLAB External Stores model has two options: Simple Body and Jettison Body. For launch analyses rockets are modeled using Simple Body model which accounts for propulsional thrust level, fuel burning rate, mass and inertia change during flight. Target position and controller gain modeling options are also available but performance of a rocket or missile after it clears the helicopter is not in the scope of separation simulations considered in this study. Jettison Body models the gravity dropped stores and deals with their behavior after being jettisoned.

Both models necessitate store location and its orientation with respect to helicopter in order to calculate the air loads and moments acting on the store. For separation simulations, full aerodynamic database of the rocket and jettisoned launcher are required to calculate the trajectory after the store begins its free flight.

2.7.1 2.75-Inch Diameter Rocket

In separation simulations 2.75-inch Mk-40 rockets are modeled. The parameters required to simulate the rocket motion after separation and geometric parameters to

investigate collision possibility are tabulated in Table 2. The thrust-time curve of the rocket is provided in Reference [16] for temperatures of -65 F and 165 F; hence the data is interpolated in the code to the temperature of the simulated flight condition as shown in Figure 11.

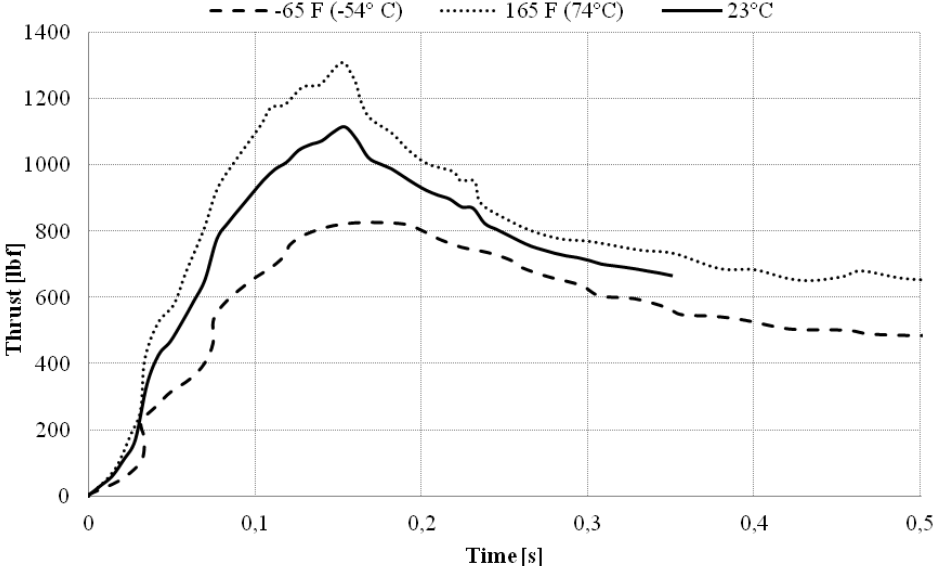


Figure 11 Thrust Curve for 2.75 inch Diameter Rocket, [16]

Table 2 Mass and Geometric Parameters of 2.75-inch Diameter Rocket

Initial Mass [kg]	9.3
Initial Inertia [kgm ²] (Ixx,Iyy,Izz)	(0.006, 1.353, 1.353)
Initial CG from nose [mm]	550
Mass at propellant burn-out [kg]	8.85
Inertia at propellant burn-out [kgm ²] (Ixx,Iyy,Izz)	(0.0057, 1.285, 1.285)
CG from nose at propellant burn-out [mm]	450
Length [mm]	1150
Diameter [mm]	70
Wing Span (with open fins) [mm]	400

2.7.2 Rocket Launcher

Launchers carry multiple rockets and provide a platform to fire the rockets. In this study, jettison of LAU-61C/A is analyzed. LAU-61C/A is a launcher that can carry 19 unguided 2.75-inch diameter rockets.

The parameters required for simulating the launcher motion after jettison and geometric parameters to investigate collision possibility are listed in Table 3.

Table 3 Mass and Geometric Parameters of 19-tube Rocket Launcher

	Empty Launcher	Fully Loaded Launcher
Weight [kg]	57	234
CG from nose [mm]	836	667
Moment of Inertia (Ixx, Iyy, Izz) [kg.m ²]	(1.32, 12.45, 12.45)	(4.68, 41.96, 41.96)
Length [mm]	1587.5	1620.5
Width [mm]	430	430
Height [mm]	430	430

The aerodynamic database of launcher used in the analyses includes force and moment coefficients at angle of attack and sideslip angle values varying from -90 to 90 degrees and -180 to 180 degrees respectively.

2.7.3 External Fuel Tanks

External Extended Range Fuel system kit configuration of UH-60 helicopters is utilized with 230 gallon fuel tanks. According to the Operators Manual [17] the external fuel tanks can be installed on outboard store pylons and the jettison of external tanks is allowed only at emergency conditions. The external fuel tanks are modeled in scope of this study to generate jettison envelopes. These envelopes are

verified with recommended emergency jettison envelope of external fuel tanks given in Reference [17].

The aerodynamic database of the external tank is generated using Missile Datcom method. The USAF Missile Datcom is a design tool used for the prediction of aerodynamic parameters of variety of missile configurations [19]. Since external fuel tank has an elliptical shaped body similar to missiles, this tool is considered to be adequate to estimate force and moment coefficients of the fuel tank. The program computes the aerodynamic coefficients as a function of angle of attack and sideslip angles. The aerodynamic database of external fuel tank used in the analyses includes body axis force and moment coefficients at angle of attack and sideslip angle values varying from -90 to 90 degrees and -180 to 180 degrees respectively. The aerodynamic coefficients of fuel tanks are given in Appendix C.

The physical parameters of the tank are listed in Table 4 . Fuel tank is approximated by cylindrical body shape for the calculation of moment of inertia value. In Reference [20] it is stated that the external fuel tanks are mounted on the ejector racks of the external support system pylons with 4° nose-up angle with reference to the helicopter waterline level. Therefore, the tanks are modeled with 4° orientation.

Table 4 Mass and Geometric Parameters of 230-Gallon Fuel Tank, Empty Configuration

Weight [kg]	70
CG from nose [mm]	1800
Moment of Inertia (Ixx, Iyy, Izz) [kg.m ²]	(7.12, 91, 91)
Length [mm]	3874
Width [mm]	663
Height [mm]	628
Reference Area [m ²]	0.159
Reference Length [m]	0.225

CHAPTER 3

VALIDATION OF THE SIMULATION MODEL

The object of this section is to see how well the mathematical model generated for separation analyses simulates the actual helicopter behavior during steady flights and when disturbed by pilot inputs. First, static conditions such as level flight, descent and climb are investigated. Store separation is simulated at the instant helicopter reaches a trim flight condition for the prescribed maneuver. Therefore, verification of static trim results, particularly helicopter attitudes should demonstrate a good agreement with test data.

In the second part, transient responses to step, pulse and doublet inputs at each control axis is tested. Hover and forward flight conditions are analyzed with disabled Stability Augmentation System.

Sikorsky Aircraft Company used flight test data for the validation of the UH-60 helicopter simulator as explained in Reference [9]. These tests were conducted by Army Aviation Engineering Flight Activity (AEFA) and data is available in open literature (References [9] and [10]). For the validation of the simulation model used in this study, flight test data is obtained from Reference [9]. The simulation results of GenHel model developed at AMES [10] is also given in the comparison plots in order to gain a better insight for the accuracy level of GenHel and simulation models.

Trim analyses are performed at the same gross weight of the test helicopter, longitudinal and lateral center of gravity locations and density altitude. The horizontal stabilizer incidence angle is allowed to be determined by the Stabilator Control System.

3.1 Steady Level Flight Results

Steady trimmed flight results of simulation model are compared to the flight test data and Sikorsky GenHel simulation results. In the simulation model, Peters-He 3 state and 15 state inflow models are applied. The results of two different inflow models are also plotted to decide which method represents the actual helicopter better. Validation parameters are cockpit control positions, helicopter attitudes, stabilator incidence angle and main rotor power. Validation parameters are obtained at trim conditions of airspeeds from hover to 160 knots with 10 knots increments. Comparison of test data, GenHel and simulation results for the steady flight at various forward speeds are presented in Figure 12-Figure 19. In these figures a pretty good agreement of the simulation results with the test results is observed.

Among all these parameters, collective stick position accuracy is most significant because it is linked with other mechanical control systems. Stabilator Control System is also a function of collective position. Hence a difference in collective stick position may degrade the simulation validation fidelity directly. Figure 12 shows that collective stick positions are estimated well in both simulations but more accurate results are obtained with 15 state inflow model.

The second important parameter to be checked is the stabilator incidence angle since it directly affects the helicopter pitch attitude. It is seen that stabilator incidence angle results of simulations and GenHel results slightly differ from test data. Although at low speed tests incidence is almost 45 degrees, in Reference [9] it is declared that stabilator angle never exceeded 40 degrees at the tests conducted at Sikorsky. It was concluded in Reference [9] that flight test data is in error. As explained at earlier sections the main purpose of the adjustable stabilator angle is to balance the pitch attitude of the helicopter.

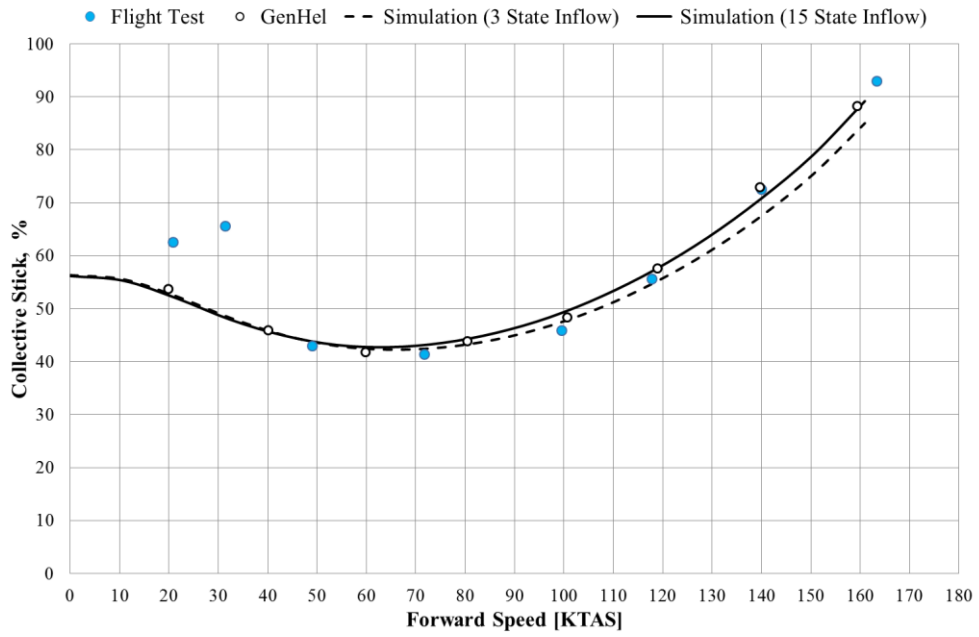


Figure 12 Comparison of test data, GenHel and simulation results for Collective Stick

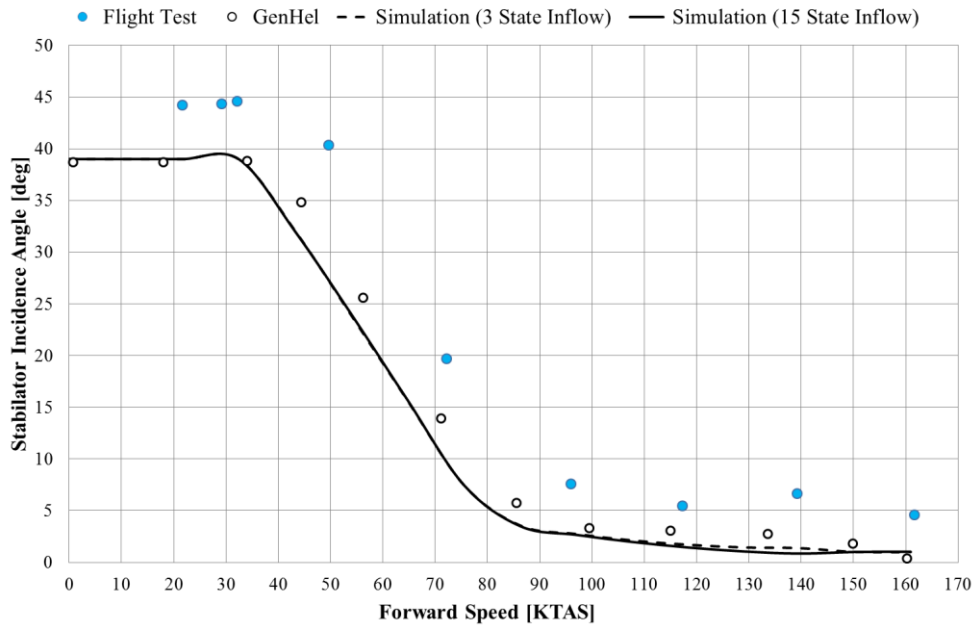


Figure 13 Comparison of test data, GenHel and simulation results for Stabilator Incidence Angle

When pitch attitude results are compared (Figure 14), good agreement with the test data is obtained particularly at speeds below 120 knots. At higher speeds it is observed that 3 State model predicts pitch attitudes better than 15 state model. However at 160 knots the difference of pitch angle between flight test data and 15 state model is 3 degrees which is considered as satisfactory. Since the pitch attitude results are consistent with the test data, the difference in stabilator angle can be neglected.

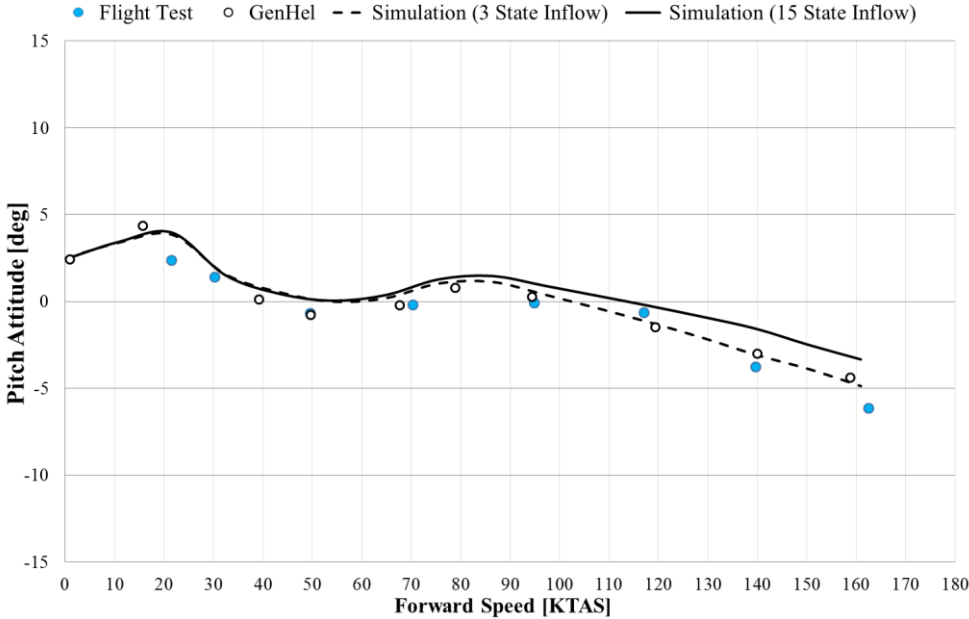


Figure 14 Comparison of test data, GenHel and simulation results for Pitch Attitude

As seen in Figure 15, the trim roll attitudes obtained from simulation model agrees very well with the test data and GenHel simulation at varying forward speeds.

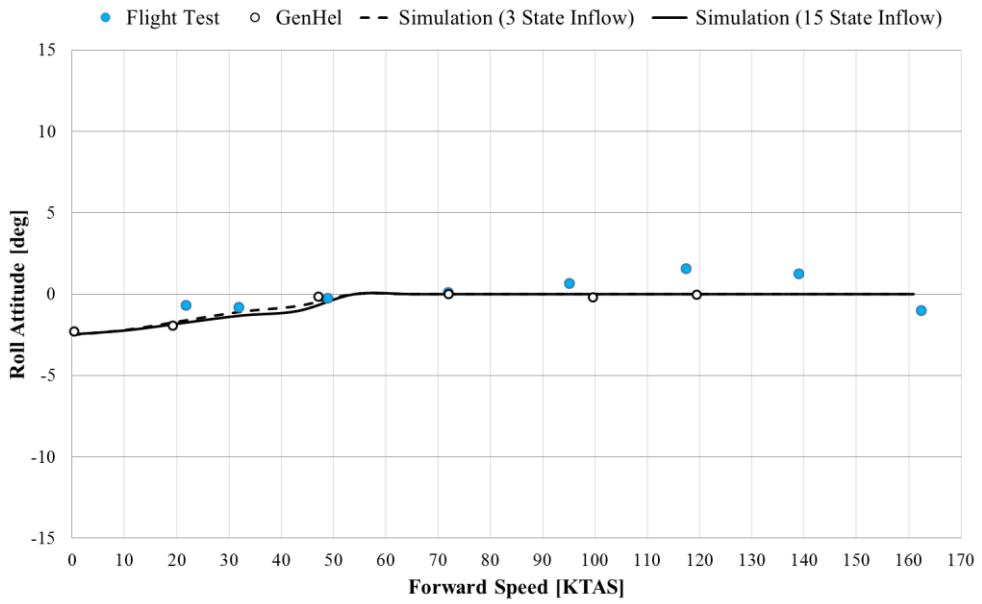


Figure 15 Comparison of test data, GenHel and simulation results for Roll Attitude

The longitudinal and lateral cyclic positions are shown in Figure 16 and Figure 17. At most of test points, cyclic stick position estimations are realistic in simulations. At higher speeds, longitudinal cyclic positions are improved by finite state model. At 160 knots 7% difference from test data is observed.

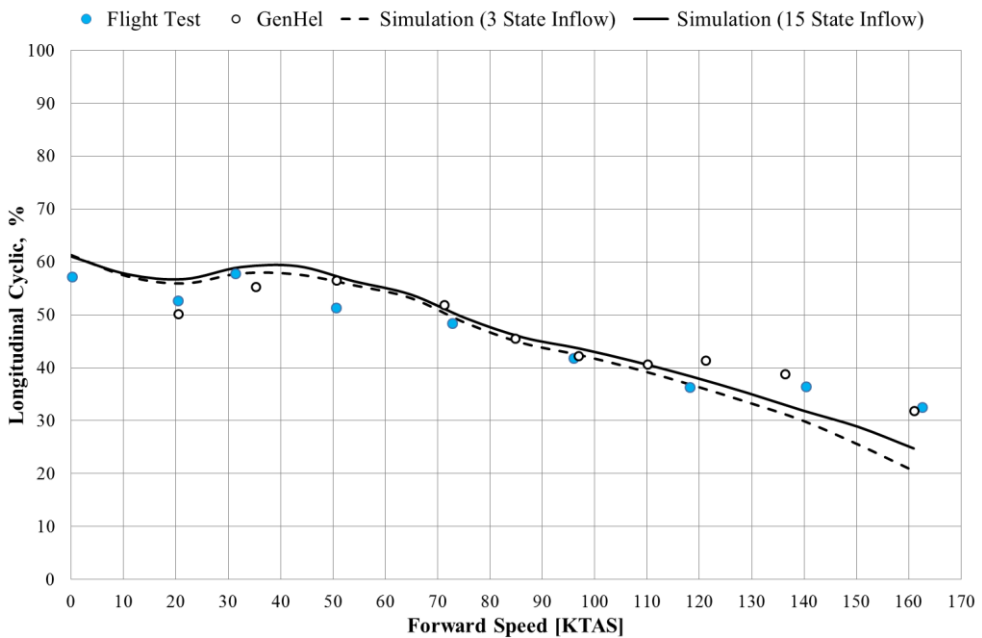


Figure 16 Comparison of test data, GenHel and simulation results for Longitudinal Cyclic

The lateral cyclic position results are almost overlapped with test data (Figure 17) and better agreement is obtained when compared to GenHel simulation results are low speeds.

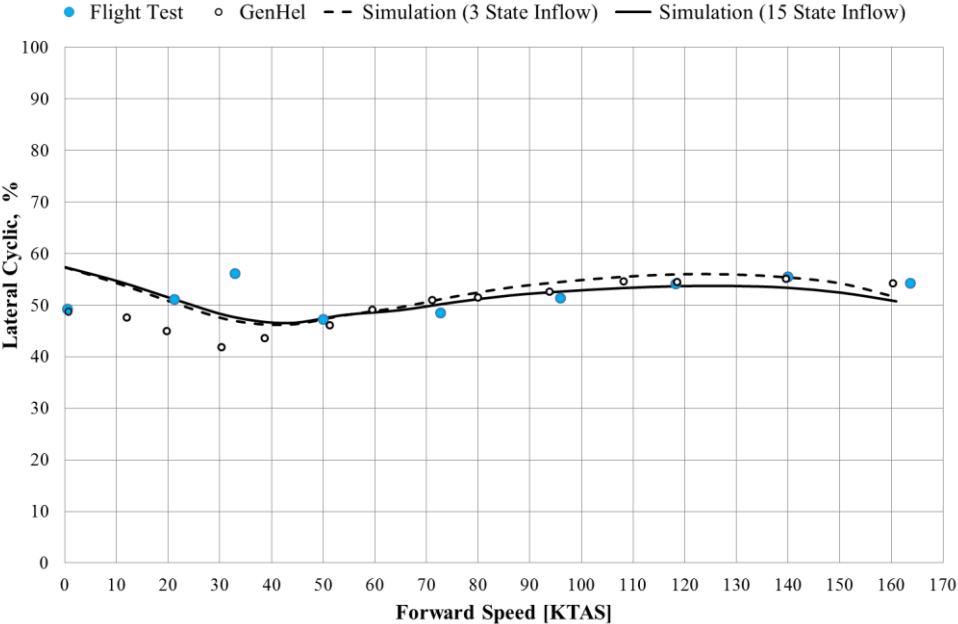


Figure 17 Comparison of test data, GenHel and simulation results for Lateral Cyclic

Pedal positions at trim flight are shown in Figure 18. Simulation results are consistent with test data especially above flight speed of 50 knots.

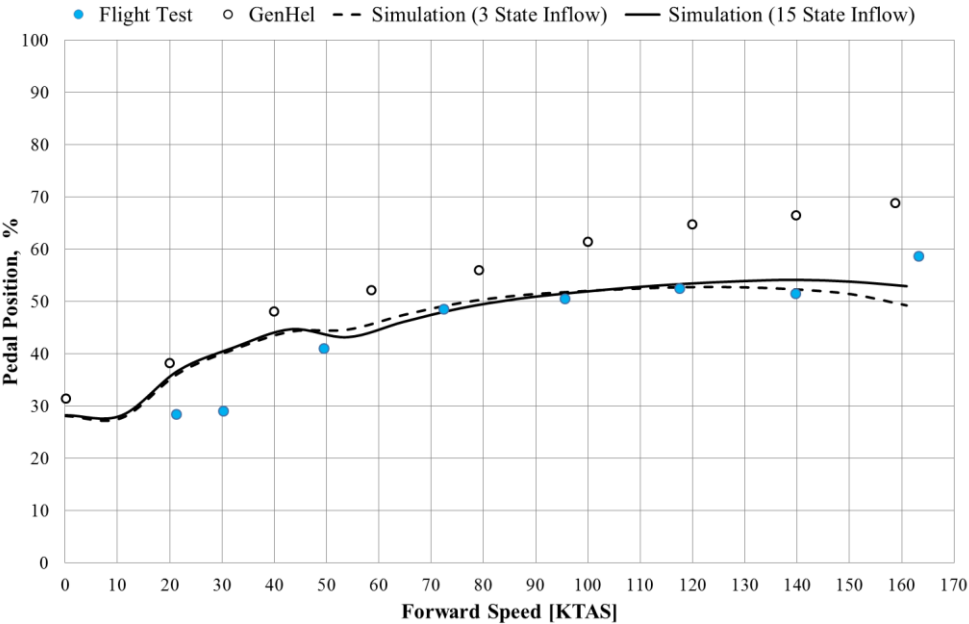


Figure 18 Comparison of test data, GenHel and simulation results for Pedal Position

Required main rotor power results are given in Figure 19. Although simulation modeled with 3 State inflow method over predicts the main rotor required power, 15 state inflow model results are consistent with test data as in collective stick position results.

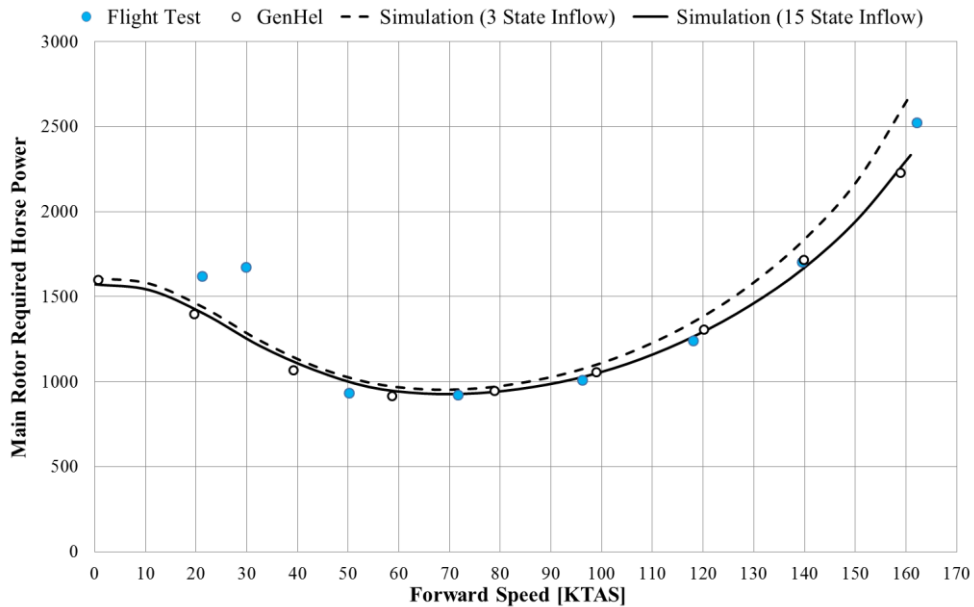


Figure 19 Comparison of test data, GenHel and simulation results for Main Rotor Required Power

As a conclusion, good agreement with test data is obtained in trim results of level flight. 15 state inflow model predicts collective stick and longitudinal cyclic positions more accurate than 3 state inflow model. The effect of aerodynamic interference of main rotor on fuselage and stabilator are calculated extensively in 15 state method.

3.2 Steady Descent and Climb Results

Another important aspect in model validation is to investigate the climb and descent maneuvers. Safe jettison of launchers is needed during emergency descent and autorotation conditions hence consistency with test data is necessary. Steady climb and descent comparisons at 100 knots forward speed are performed. It should be

noted that in flight test and GenHel simulation results, the stabilator angle is fixed at the corresponding trim value of 100 knots.

Collective stick positions are almost same with test data except at zero rate of climb flight (Figure 20). 10 % difference is similar that of observed in collective stick comparison in low speed level flight in Figure 12.

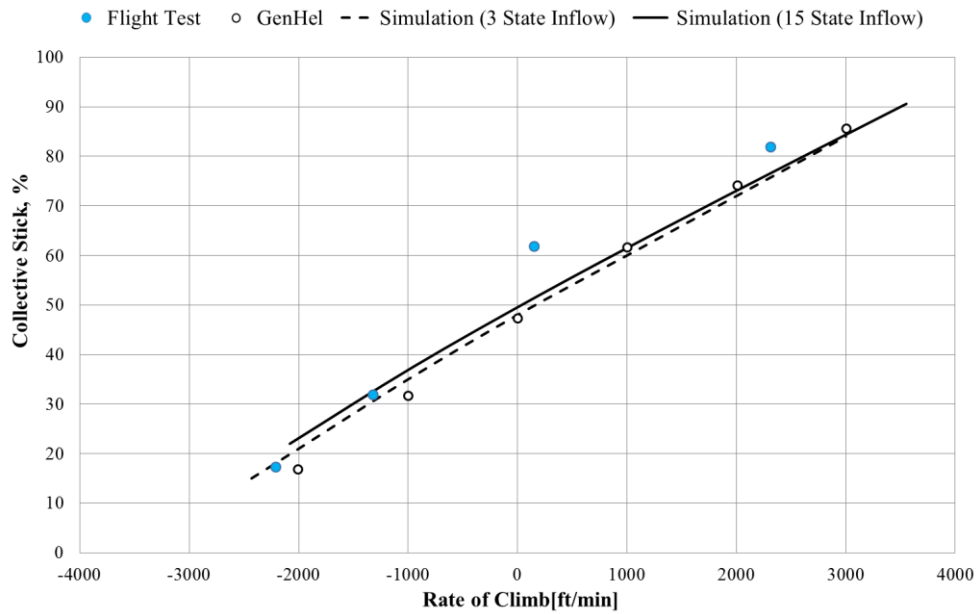


Figure 20 Comparison of test data, GenHel and simulation results at Descent and Climb, Collective Stick

When longitudinal cyclic positions are investigated, simulation results are very reliable in descents. However in climb with 2300 ft/min climb rate, simulation estimates the forward cyclic positions 6% smaller than test data which can be regarded as an acceptable error. Although longitudinal cyclic values differ from test data at climb, good consistency is observed in pitch attitudes (Figure 22).

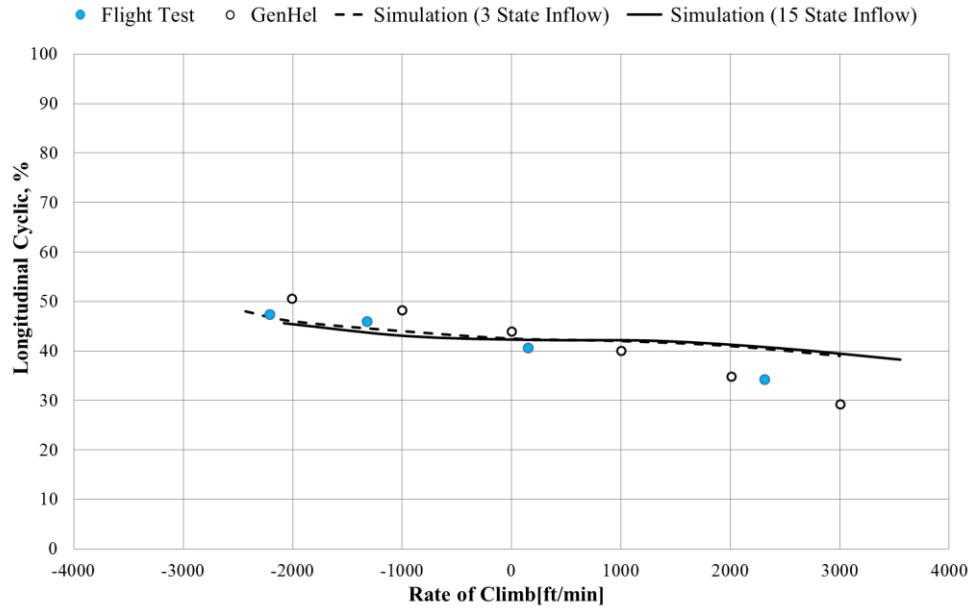


Figure 21 Comparison of test data, GenHel and simulation results at Descent and Climb, Longitudinal Cyclic

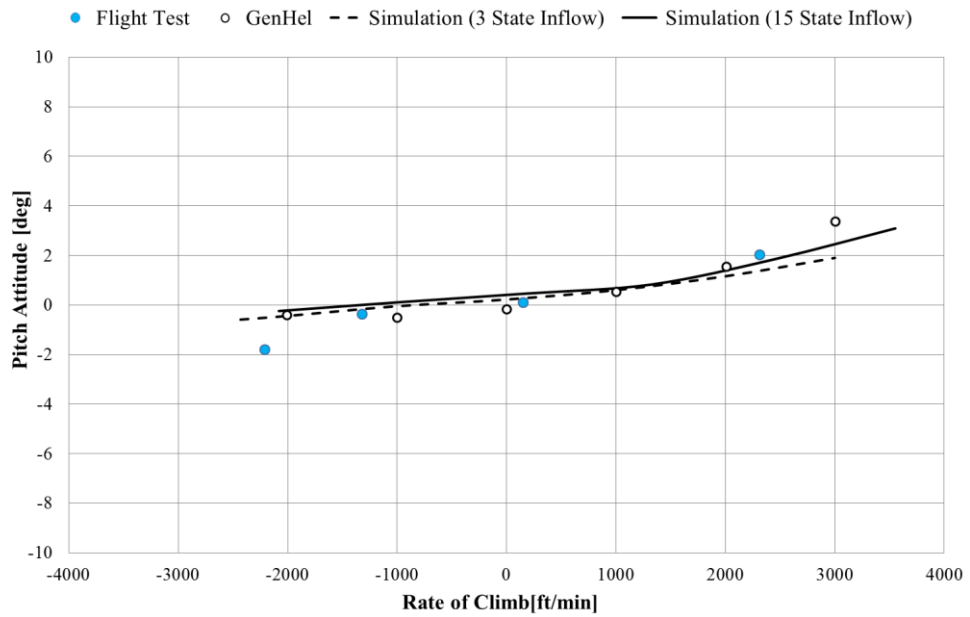


Figure 22 Comparison of test data, GenHel and simulation results at Descent and Climb, Pitch Attitude

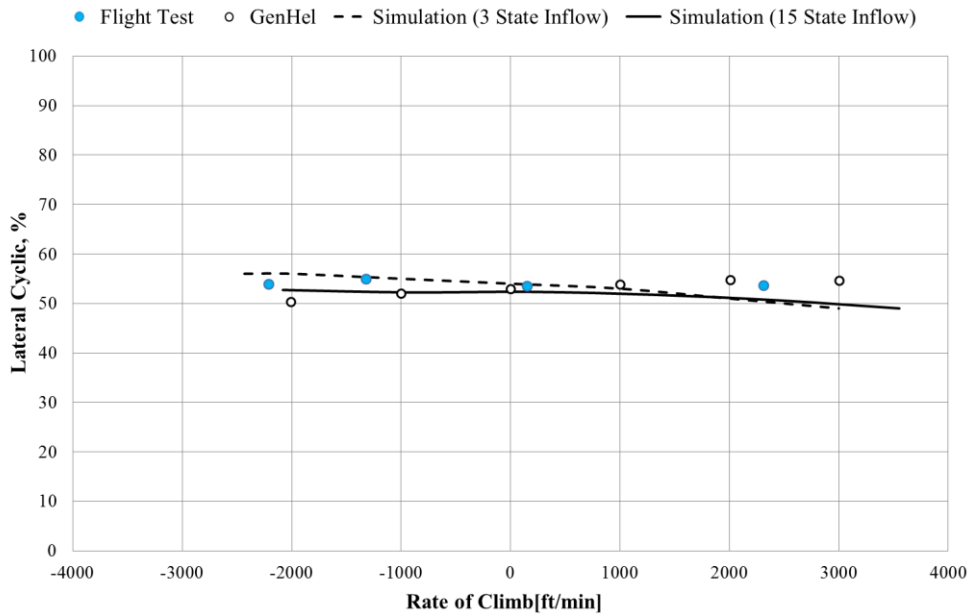


Figure 23 Comparison of test data, GenHel and simulation results at Descent and Climb, Lateral Cyclic

Although a good agreement is achieved in simulation model results of lateral cyclic positions (Figure 23), there is a discrepancy in pedal positions. As seen in Figure 24, the deviation from test data at descent is higher than 10%. Although descent results are not satisfactory, pedal positions at climbs are adequate.

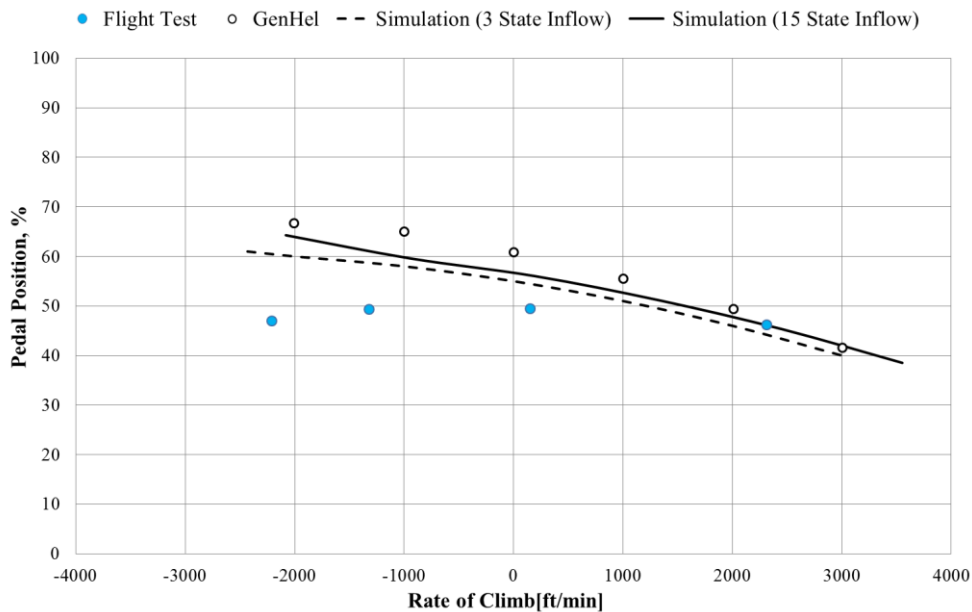


Figure 24 Comparison of test data, GenHel and simulation results at Descent and Climb, Pedal Position

Main rotor required power curve obtained by simulations are consistent with test data as expected (Figure 25).

Results for steady descent and climb maneuvers are regarded acceptable for separation simulation where helicopter trim attitudes have more powerful influence in trajectory of the store as an initial point. The effect of induced velocity models are not dominant in flight with climb rates, thus both models are adequate to be used in separation simulations

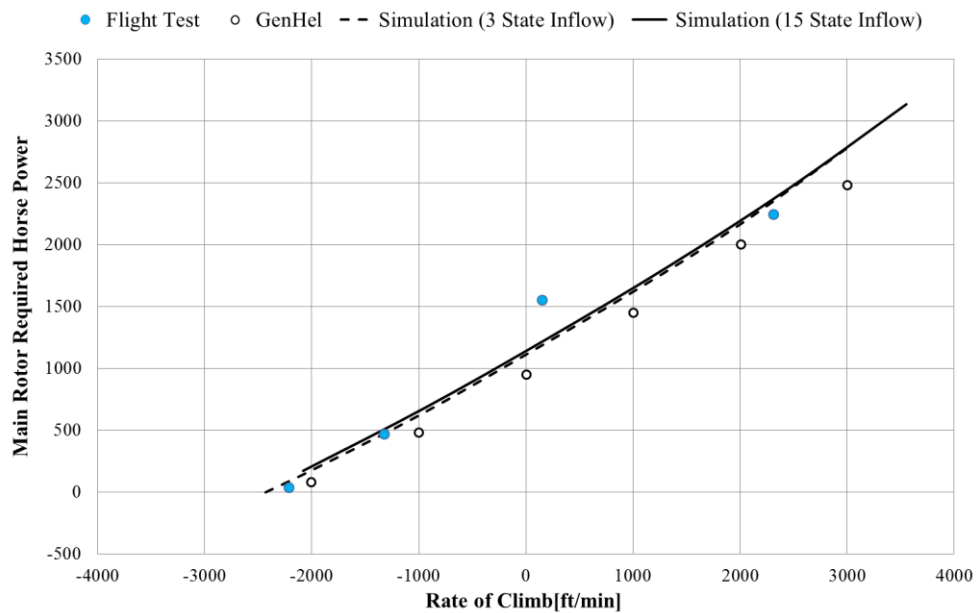


Figure 25 Comparison of test data, GenHel and simulation results at Descent and Climb, Main Rotor Required Power

3.3 Transient Response Results

Mathematical model responses to control inputs are also compared with flight test data and GenHel simulation results. The analyses are performed in the test conditions stated in Reference [10] and with SAS Off. The validation cases are listed below and their results are given in Appendix A.

- Response to longitudinal stick input
 - 0.5 inch forward cyclic input at hover
 - 1 inch aft cyclic input at 100 KTAS
- Response to lateral stick input
 - 1 inch right cyclic input at hover
- Response to collective input
 - 1 inch up collective input at hover
 - 0.5 inch up collective input at 100 KTAS
- Response to pedal input
 - 1 inch left pedal input at hover
 - 1 inch right pedal input at 100 KTAS

In order to perform transient response analyses of the helicopter, initially 3 State Inflow model is used. On axis responses are consistent with test and GenHel simulation results; however adverse responses are observed in off-axis results. Cross-coupling effects should be modeled in the model to improve off-axis responses; hence 15 State model is implemented to the mathematical model instead of 3 State model which neglects tip vortex distortions. In Figure 26, an example case of 1 inch right cyclic step input results are given to show the improvement in pitch response to lateral cyclic input at hover. After selecting the induced flow model as 15 State, the next step is to decide whether to use empirical data or Finite State Interference model to take account of main rotor interference on fuselage, empennage and tail rotor. According to Figure 26, Finite State interference modeling fits better with test data and more accuracy is achieved in off-axis responses.

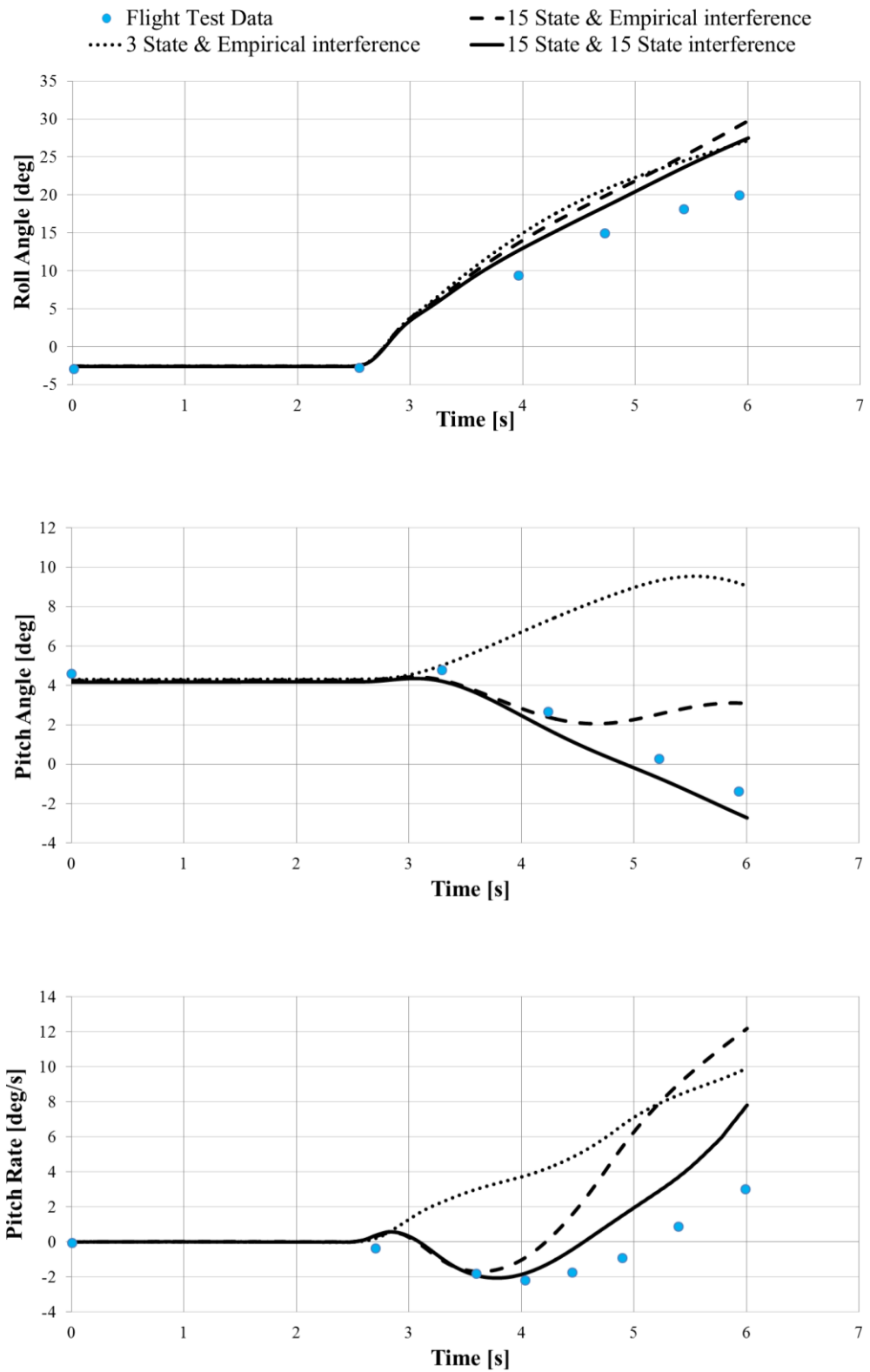


Figure 26 Longitudinal Axis Response to Lateral Cyclic Input, at Hover

The results of all transient validation cases listed are presented in Appendix A. The results show that general characteristics of responses are satisfactory. At some cases higher roll and yaw angles are observed which propagate from sudden increases in angular rates. These large responses in the simulation are attributed to flight control system dynamics modeled as simplified second order system. Since comparative cases are performed at SAS-Off conditions, these differences in angular rates are considered as acceptable. However improvement is required particularly in directional characteristics. Another remarkable result is adverse response in pitching motion when pedal input is applied at hover. At 100 knots compensating coupling of pitch response in the model is evident to be stronger than the actual helicopter. Hence nose-down pitching is smaller in the simulation.

The transient response comparisons with SAS disengaged demonstrate that simulation model is adequate to be used in separation simulations. Moreover, separation simulations are performed with SAS engaged and they don't include control inputs. Therefore model fidelity would be higher in separation simulations.

CHAPTER 4

DEVELOPMENT OF STORE SEPARATION SIMULATION TOOL

Separation simulation is performed in FLIGHTLAB environment. The procedure after developing a reliable mathematical model is explained in this chapter. In order to generate an envelope, wide range of maneuvers should be swept. Hence, a routine for successive analyses is developed to ease the workload.

4.1 Separation Simulation Procedure

First, the maneuvers to be analyzed are determined. The test points are selected considering the operational flight envelope of the helicopter and launch envelope of the store. The total flight speed, horizontal and vertical flight path angle, in / out of ground effect flag, SAS on/off flag, trim variables and targets suitable for each test condition are written in separate input files. Those identification files are called successively and fed to the next simulation. The pressure altitude and temperature conditions are also inputs to the code.

Store geometric parameters are defined for collision detection. CG location with respect to geometric center of the store, the length, width and height of the launcher, length and wing span of the rocket are required to calculate the clearance to the helicopter.

Table 5 Maneuvers Analyzed in Separation Simulation

Rocket Separation	Launcher Jettison
<ul style="list-style-type: none"> • Forward Flight • Flight with Sideslip • Descent • Autorotation • Coordinated Turn • Pull-up, Push-over • Flight with Roll Rate 	<ul style="list-style-type: none"> • Forward Flight • Flight with Sideslip • Descent • Autorotation

After defining input parameters, the main simulation code is executed. The steps of the simulation procedure are as follows;

- Load test conditions and maneuver identification file.
- Trim the mathematical model at specified flight condition
- Trigger the separation signal and start simulation
- Calculate and record the trajectory of helicopter and store separately, neglecting the main rotor interference on the store.
- Calculate the main rotor induced flow field through the recorded store path.
- Repeat the simulation and add calculated induced velocities to the store velocity at each time interval.
- Record the updated store trajectory
- Run collision detection routine to detect whether the separation is safe or not. Details of the collision detection routine are explained in Section 4.2.
- Repeat the procedure for the next test point.
- Write the summary of the analyses results to an output file. The output file includes list of unsuccessful trim points, unsafe test conditions and the helicopter component that store collides.
- Generate the safe separation envelope by combining the results of all test conditions

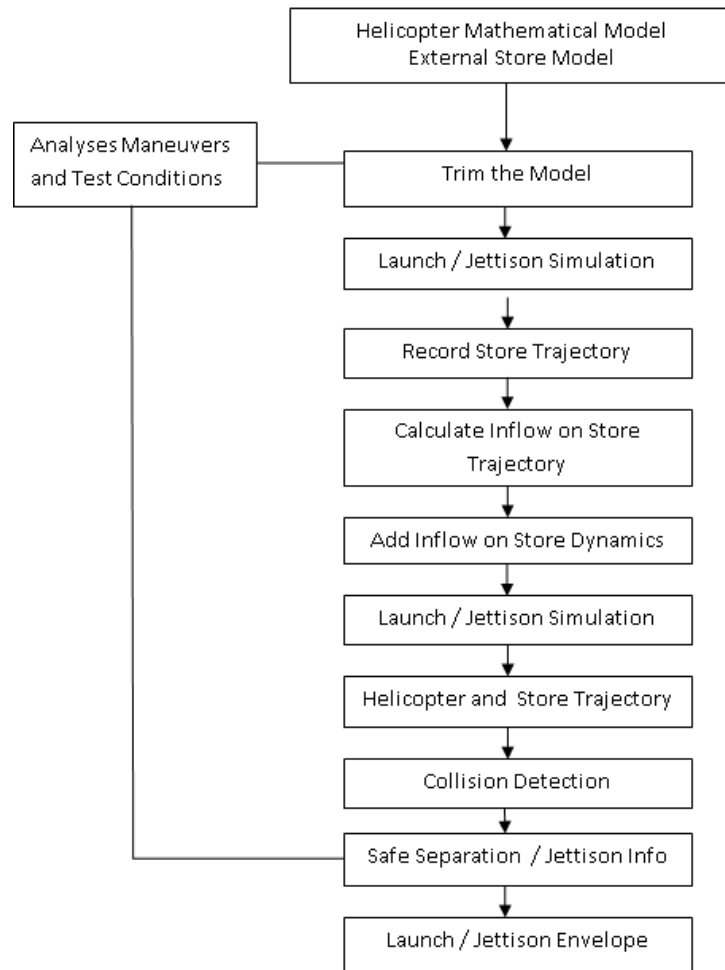


Figure 27 The Flow Chart of Separation Analysis

4.2 Collision Detection

Since Black Hawk is a utility helicopter, there are several extremities in the fuselage. The collision detection script is based on introducing the helicopter extremities and parts as rectangular volumes which cover the whole volume of that component (Figure 28). The components of the helicopter that are defined as rectangular volumes are:

1. Landing gear struts
2. Front wheels
3. Rear wheels
4. Fuel tanks loaded at the outboard stations of the stub wing

5. Cockpit steps
6. Cabin door
7. Counter measure dispensers
8. Horizontal tail
9. Tail rotor

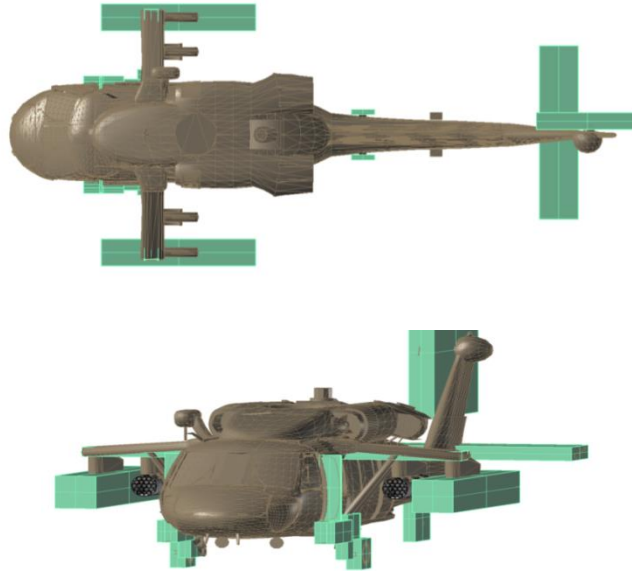


Figure 28 Demonstration of Critical Helicopter Components

Apart from rectangular components, fuselage limits and struts of External Store Support Structure are described in the collision detection routine. The points on the fuselage coordinates are given in the routine in a tabulated format. The fuselage is divided into 4 regions as upper-left, upper-right, lower-left and lower-right.

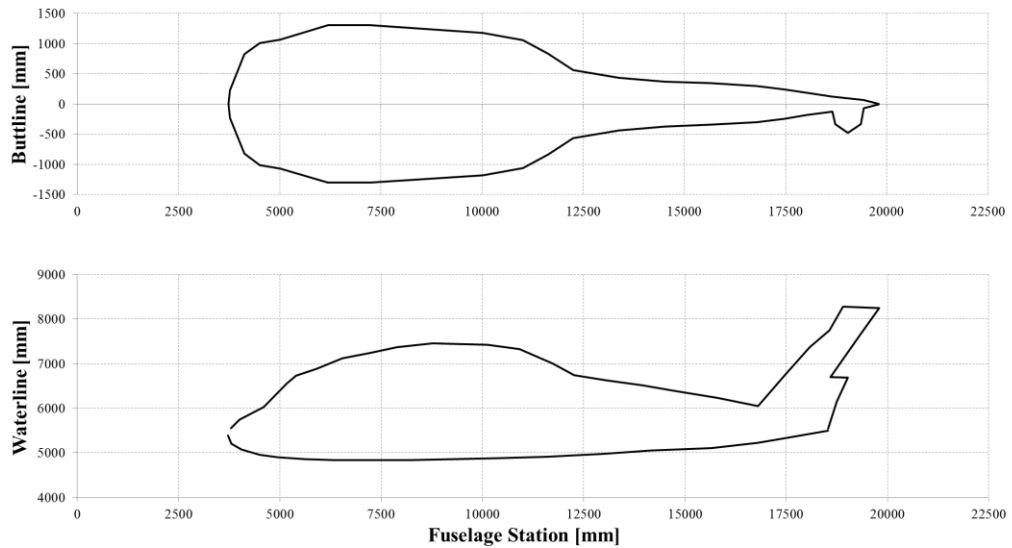


Figure 29 Helicopter Fuselage Coordinates, Top View and Side View

Uppermost and lowermost limits of the stub wing struts are embedded in the routine. The routine checks if the store position is in stub wing strut limits in vertical direction, if so, lateral limit of the strut at corresponding vertical position is calculated using linear interpolation method. Interaction is investigated while store passes near the struts.

The separation simulation outputs helicopter and store trajectory only at the prescribed center of gravity locations. Hence a routine is developed to calculate the trajectory at many points on the helicopter and the store. The maximum and minimum coordinates of boxes when helicopter is in neutral position are embedded to the code. According to store coordinates which region of the fuselage should be considered during separation simulation is determined. As helicopter attitudes change during simulation, the coordinates of the boxes are re-positioned using direction cosine matrix of helicopter body attitudes and helicopter CG distance to the box points. Hence the instantaneous helicopter orientation is obtained at each time step of simulation.

In the simulation, the store motion is calculated as a point at the center of gravity. However, store volume is required for collision investigation. Hence the geometry of external stores analyzed in the separation simulation tool is modeled using points. To describe the jettisoned store, a rectangular volume is constructed with 12 points, 8

points at the corners of the rectangular volume and 4 points aligned to the center of gravity. At each time interval of the simulation, position of those points is recalculated with the changing store attitudes.

Similarly, the rocket motion is characterized with the points at center of gravity, nose and tip of the rocket position. Moreover, modeling fins of the rockets are more crucial for separation analyses. Therefore, the wing span of 40 cm is included in the rocket diameter.

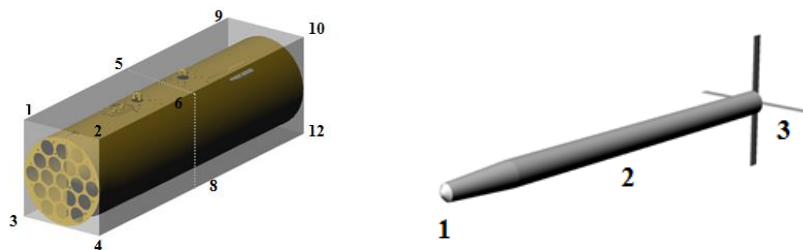


Figure 30 Representation of Rocket Launcher and 2.75-inch Diameter Rocket

A similar approach is carried out to calculate store orientation with respect to the helicopter frame. First the oriented store points with respect to the store center of gravity are computed, and then store position according to helicopter body motion is determined.

When the box coordinates and store points are updated, the next step is determination of collision. All points on the store are analyzed individually whether to coincide the boundary of each helicopter component volume.

As a penalty of this bounding box approach in collision detection step in separation simulation, dummy gaps may be included in component volumes, hence volumes checked for interactions are larger than the actual geometry. A test condition is treated as unsafe if a point on the store interferes with even a small gap. That method results in a more conservative envelope and dummy gaps may be interpreted as safety margins. However applying different safety distance margins for different helicopter components is not an objective approach. For this reason, after running 6-DOF flight mechanics simulation on FLIGHTLAB, another collision detection method is applied using the actual geometry of the helicopter and jettisoned store in

Blender software. The purpose is to re-analyze the unsafe cases and to check whether the actual bodies are in contact with each other.

Blender is a free software product used for creating 3-D computer graphics for animated films, video games and simulations. 3-D geometries of both helicopter and store are used in collision detection in Blender. A script is generated that visualizes the trajectory of the helicopter and store using separation simulation data. As the actual geometries are taken into account, the reliability of the analysis is improved.

4.2.1 Main Rotor Clearance

As noted in military standards, in rocket launch the main rotor clearance is the most important parameter to be checked. According to MIL-STD-1289D [2], propeller and rotor disk clearance shall be five-degree which is measured from the trajectory of the outermost surface of the weapon to the worst-case rotor plane or aircraft structure, Figure 31.

Regarding the clearance requirement, a five degree cone is drawn between rocket launcher and the worst case tip path plane position of the UH-60 helicopter as shown in Figure 32 . The distance to the most deflected rotor plane is measured as 586 mm and that value is embedded to the collision detection routine as main rotor safety margin.

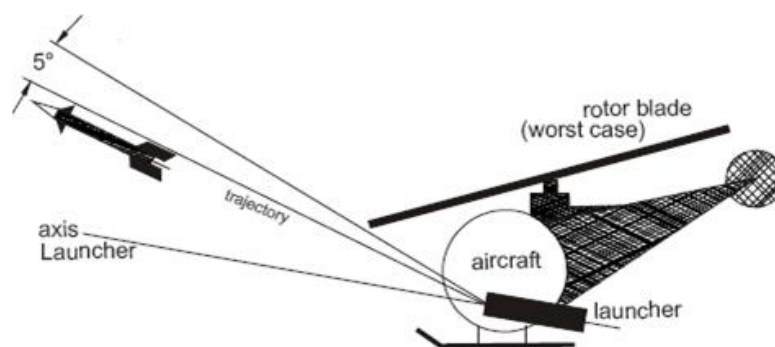


Figure 31 Definition of a five-degree half-angle cone in MIL-STD-1289D [2]

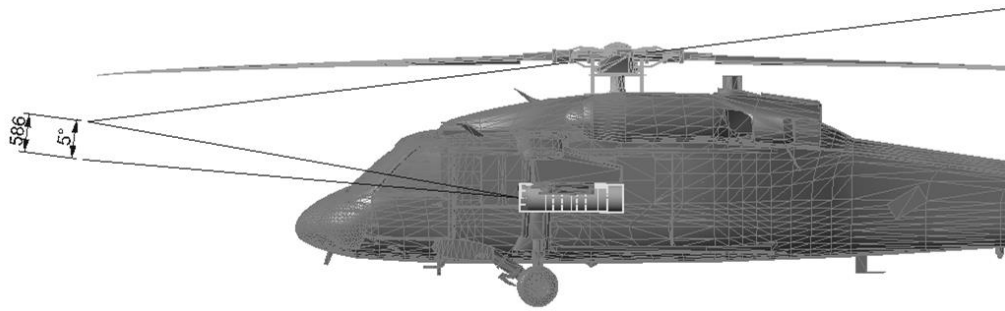


Figure 32 Demonstration of UH-60A Main Rotor Clearance for Maximum Tilted Tip Path Plane

CHAPTER 5

STORE SEPARATION ANALYSIS RESULTS

The parameters that may affect the store behavior after being released from the parent helicopter are investigated in this chapter. Main rotor interference on the external stores and the impulse applied by lanyard released connector at jettison instant are the major parameters that must be included in the simulations. Jettison of the launchers loaded with different number of rockets is also analyzed to determine the most critical configuration.

5.1 Effect of Main Rotor Downwash

The most dominant parameter affecting behavior of stores after separation is main rotor induced flow. Consequently it must be introduced during simulation studies accurately and worst case scenarios must be simulated to prevent any collision during actual flights. With this purpose, different inflow models are implemented in sequence and their influence on store behavior are compared.

The normal induced flow distribution to UH-60A longitudinal axis at rocket pod waterline level is generated for different solution methods (Figure 33). As it is explained at Section 2.1.3, as the number of states used in the dynamic wake method increases, the distribution becomes more accurate and the effect of tip losses is observed. It is clearly seen that vortex wake method results in different radial distribution due to incorporation of wake contradiction. The drastic increase is observed at points aligned with blade tip region where rolled-up vortex is formed. A sudden change from downwash to upwash at rotor wake boundaries is observed for

all methods due to blade tip vortex distortions. This can be explained as inside rotor wake contributions of tip vortex and inboard wake are added while they become contradictory outside the wake.

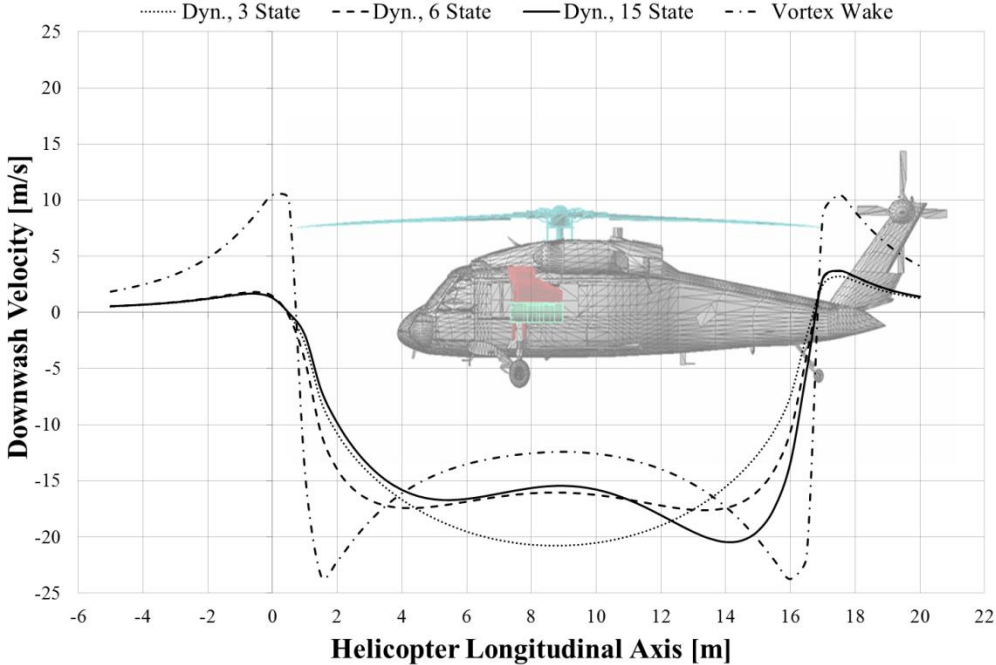


Figure 33 Comparison of Induced Flow Distributions at Rocket Pod Waterline Level

5.1.1 2.75-Inch Diameter Rocket Launch at Hover

Peters-He 3 State, 6 State, 15 State (4x4) and Prescribed Vortex inflow models are tested at hover and their influences on rocket trajectory are compared.

The distribution of induced flow components along rocket trajectory is plotted in Figure 34. It is clearly seen that rocket passes the rotor wake boundary in the first 0.1 seconds of the simulation. It should be noted that simulation starts at the instant rocket leaves the launcher and begins its free flight. Simulation ends when rocket travels approximately 20 meters away from the helicopter.

As an anticipated result, the downwash velocity leads to an angle of attack in the store and consequently the store encounters a nose-up pitch motion (Figure 35). After

rocket escapes from the rotor wake, pitch attitude slope is reversed due to up-wash occurred outside the wake.

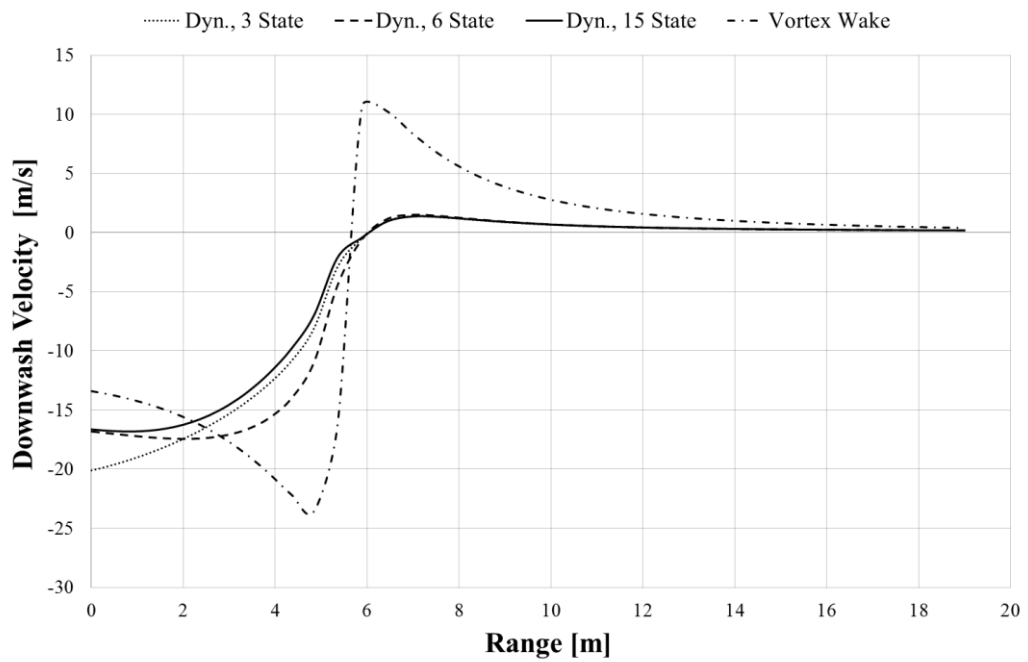


Figure 34 Downwash Velocity along the Flight Path of the Rocket

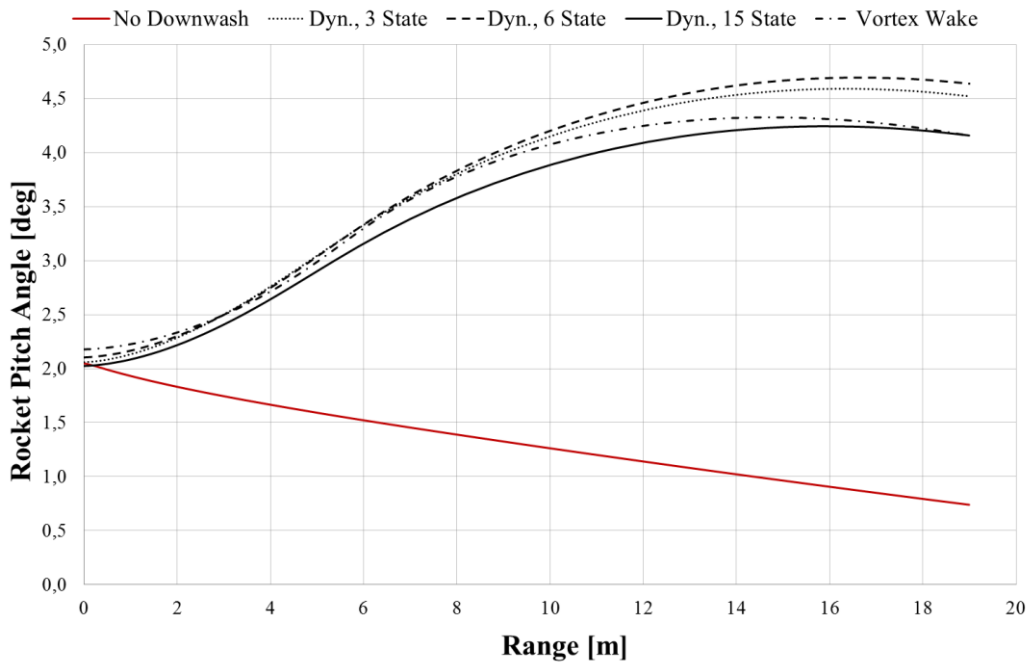


Figure 35 Main Rotor Interference Effect on Rocket Pitch Attitude along the Flight Path

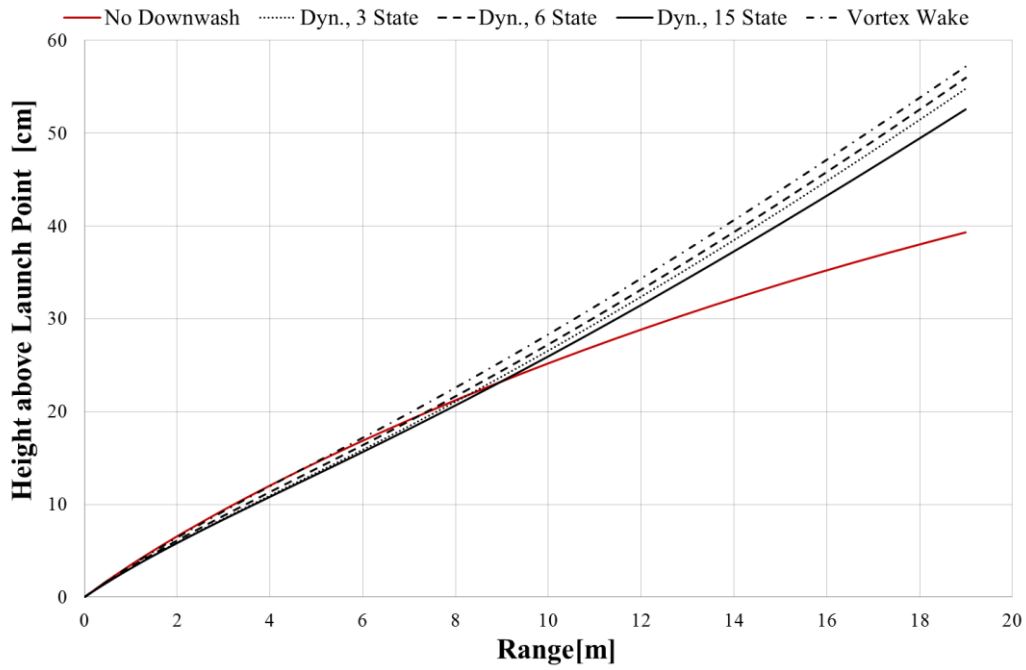


Figure 36 Main Rotor Interference Effect on Rocket Height above Launch Point

The most important phenomenon in rocket launch is to maintain the permissible distance with main rotor tip path plane. The distance to main rotor tip path plane is plotted in Figure 37.

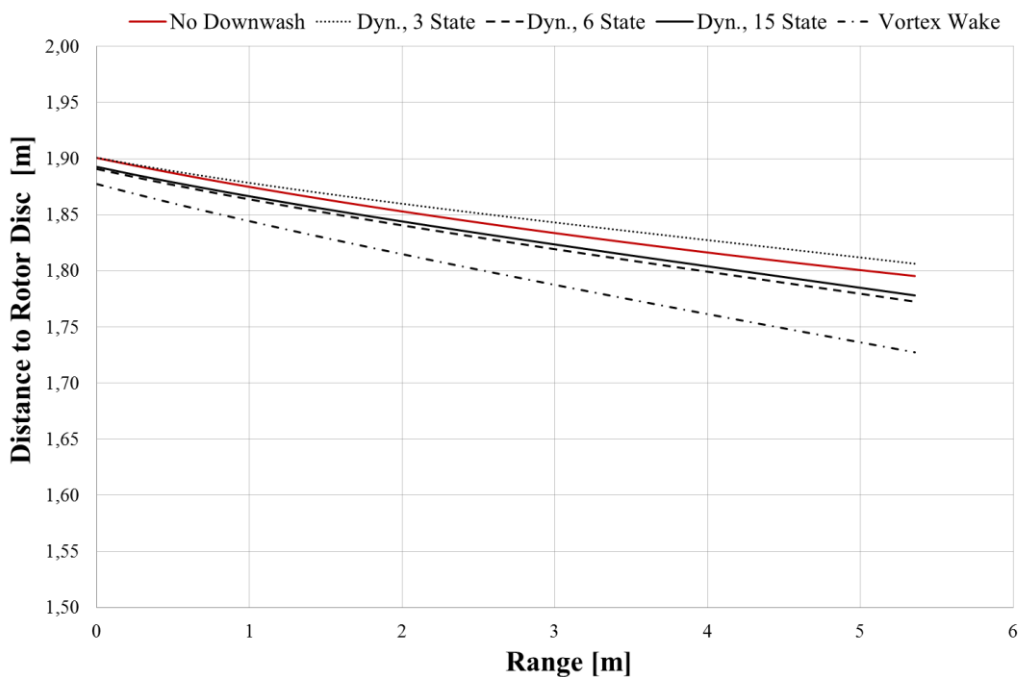


Figure 37 Main Rotor Interference Effect on Rocket Clearance to Main Rotor Disc

The change in roll and yaw attitudes of rocket are negligible in all simulations. It is concluded that downwash effects don't have an influence on lateral dynamics of 2.75-inch diameter of rocket at hover.

Although, the safe separation behavior is not severely affected by the method used to model main rotor interference on rockets, the performance of unguided rockets depends on the downwash distribution. As an example, the trajectory of a 2.75 inch diameter unguided rocket is plotted in Figure 38. In this simulation, the elevation angle of the rocket is considered to be 1 degree with respect to helicopter body axis at launch point. Modeling of main rotor interference with finite state models extends the rocket range 388 meters due to increasing angle of attack caused by downwash velocity. When vortex wake model is used for main rotor interference the increase in range is only 146 meters. It is seen that validation of the unguided rocket trajectory with flight testing is essential to decide which method should be used to calculate rocket performance accurately.

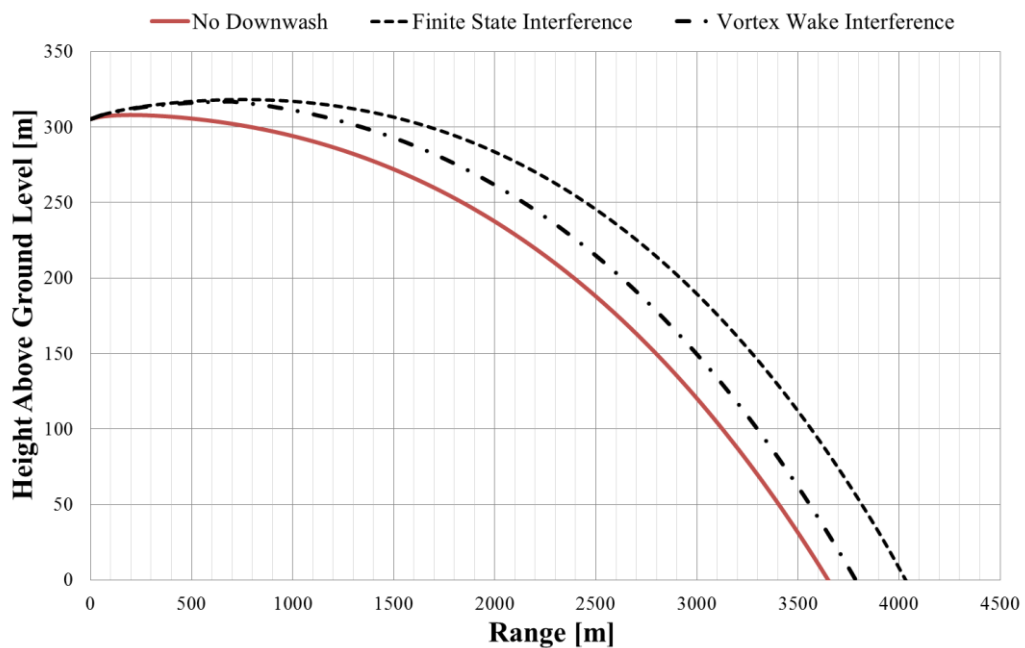


Figure 38 Effect of Main Rotor Interference on Rocket Trajectory, at Hover

5.1.2 Rocket Launcher Jettison at Hover

The effect of main rotor inflow on 19-tube rocket launcher during jettison is also analyzed. Different inflow solutions are compared to determine the sensitivity of the jettison behavior to flow field around the rocket pod. The rocket launcher is jettisoned from inner store station of right pylon of the Black Hawk helicopter. Empty configuration of the launcher is selected regarding that it would be more sensitive to aerodynamic interferences due to its low weight and inertia values. Since launchers are not ejected, the gravitational and aerodynamic forces are dominant on the store attitudes.

The vertical component of induced velocity impinged on the launcher during its downward motion after jettison is compared for different solution methods (Figure 39). The results are compatible with Figure 4, Figure 6 and Figure 33 . Peters-He 3 State predicts larger downwash magnitudes. Another expected result is increasing downwash velocity under the main rotor plane due to accelerated flow approach used in dynamic wake models. In vortex wake solution, induced velocity is reduced at far wake region. The comparative plots show the effect of downwash on translational motion and attitudes of jettisoned rocket pod.

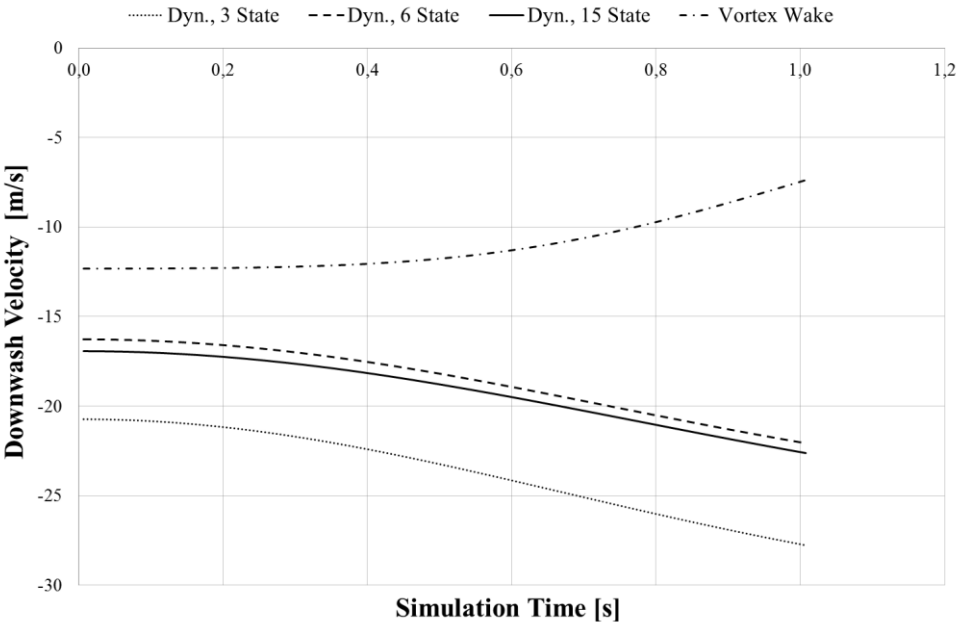


Figure 39 Downwash Velocity Distribution along the Flight Path of the Launcher

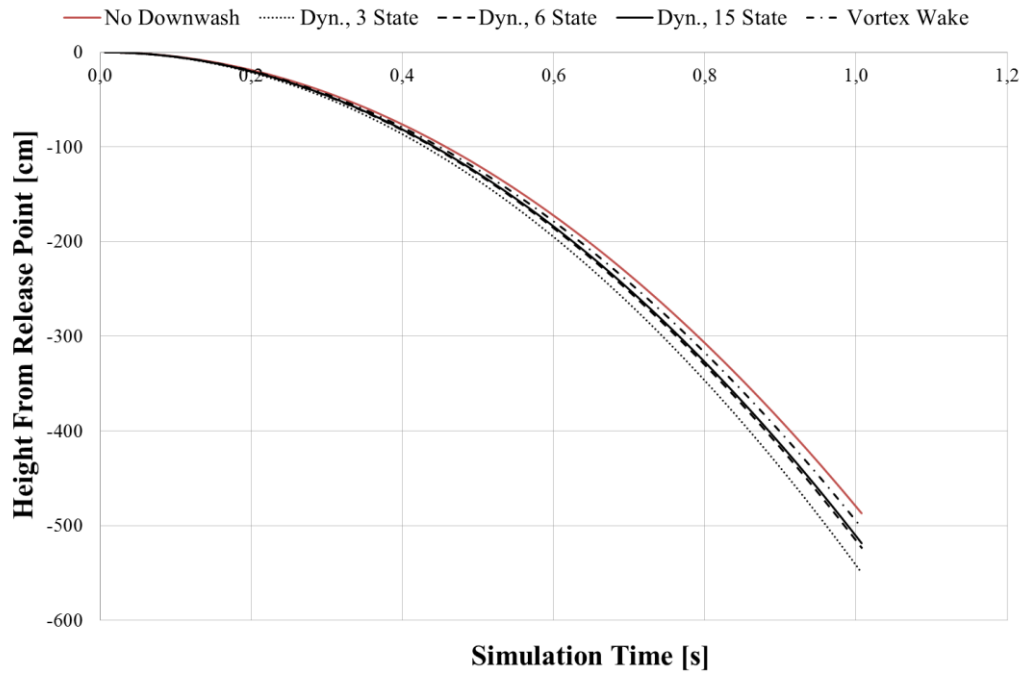


Figure 40 Main Rotor Interference Effect on Launcher Trajectory

The difference in magnitude of inflow velocity at Peters-He 3 State solution results in larger pitch up behavior in the launcher (Figure 41). Hence launcher is considered to be most sensitive to the inflow modeling with Peters-He 3 State dynamic wake approach. Although comparative results for jettison at hover show that store attitudes are more sensitive to 3-State inflow modeling, the difference among inflow models are around 1 degree at the instant store clears the helicopter vicinity. Figure 42 and Figure 43 show the distance of launcher to helicopter landing wheels and fuselage respectively. Approximately 5 cm difference is observed between trajectories obtained by vortex wake and finite state interference methods.

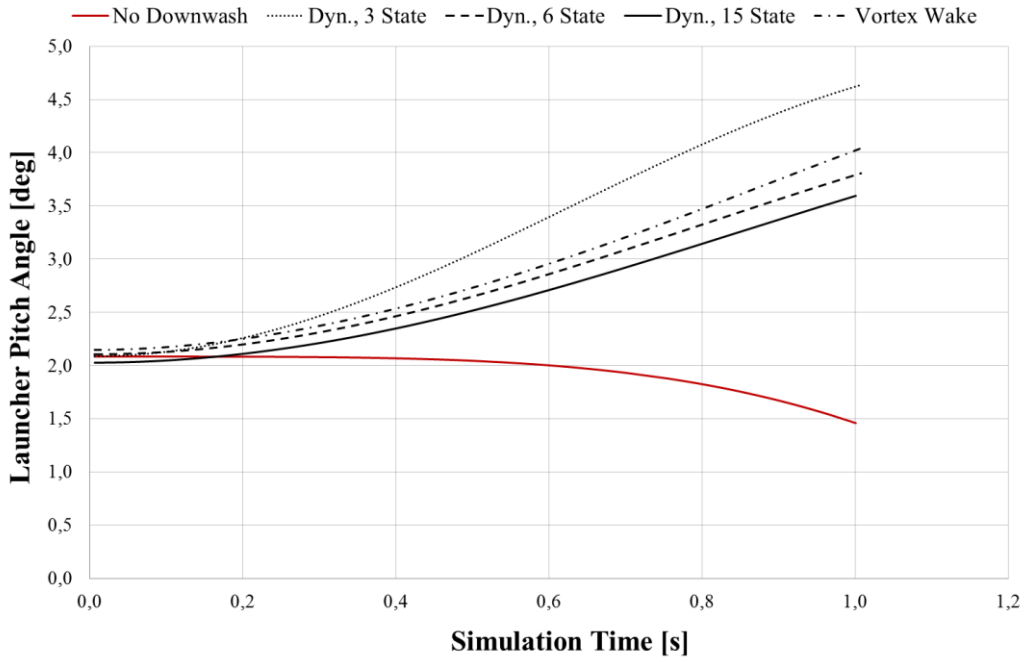


Figure 41 Main Rotor Interference Effect on Launcher Pitch Attitude along the Flight Path

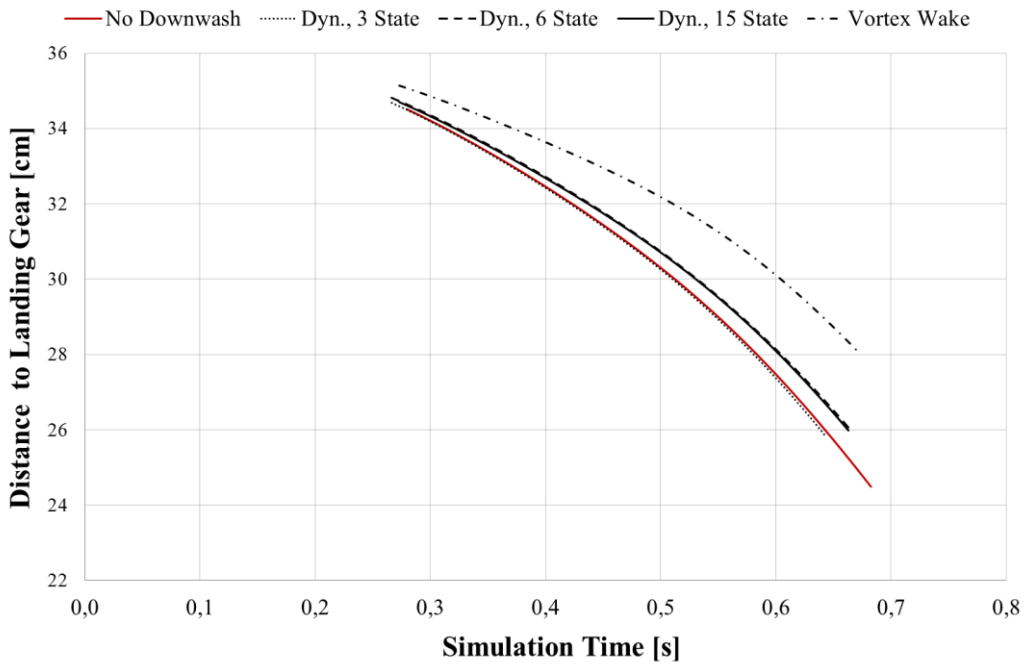


Figure 42 Main Rotor Interference Effect on Launcher Distance to Landing Gear

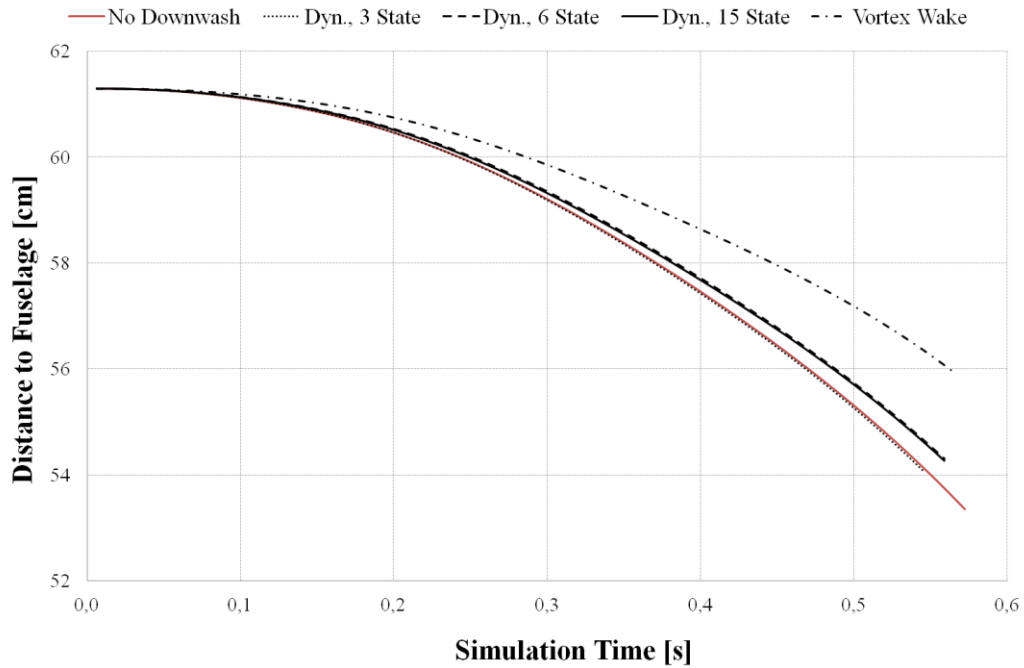


Figure 43 Main Rotor Interference Effect on Launcher Distance to Fuselage

In the envelope generation simulations, 15 State inflow model is selected since it provides more reliable results in as mathematical model validation at level flight and dynamic response analyses (Figure 7 and Figure 26). The reason of choosing dynamic wake model to the vortex wake model is that the launcher moves closer to helicopter landing gear and fuselage when finite state interference method is applied.

5.2 Effect of Lanyard Release Connector

The electrical communication between the helicopter and the launchers are provided through umbilical cables and connectors. They are also used as mechanical safety devices to prevent undesired disconnection of the launcher during flight. In case of a jettison necessity, connector allows disconnection of the connector plug and receptacle with an axial pull force on the lanyard. Connector simply disengages from the receptacle on the launcher as the required axial pull force is applied on the lanyard. Hence launcher would be free to separate from the wing pylon. Connectors are designed with different sizes, lanyard lengths and disengagement forces based on requirements stated in MIL-STD-1760 Interface Standard for Aircraft/ Store

Electrical Interconnection System. Hence, the effects of lanyard length and pull up forces on the launcher behavior after jettison must be investigated in order to select an appropriate connector type.

In the jettison simulation tool, connector location on the launcher, maximum disconnection force of the connector and lanyard length are inputs. After jettison signal is triggered, the launcher starts its free fall and pre-determined pull up force is applied when launcher drops to the point that the lanyard cable is fully stretched. Hence connector detaching instant is simulated. When selecting lanyard length, it is crucial that the launcher is accelerated enough to overcome the disconnection force at the instant lanyard reaches its maximum stretch. Otherwise although launcher is released from the suspension lugs, the connector will not be disengaged. Such a situation may cause launcher to sling and crash to the helicopter fuselage. To check the force exerted on the connector for a certain lanyard length, governing equation of the free body when the lanyard is fully stretched can be written as

$$T = m \left(g + \frac{\sqrt{2gl}}{t_d} \right) \quad (7)$$

where, T is the force exerted on the connector,

m is the mass of the store,

g is the gravitational acceleration,

l is the free fall distance of the store before the lanyard is fully stretched (i.e. lanyard length),

t_d is the detach time elapsed from the instant the lanyard is fully stretched to the instant the connector detaches from the store.

The jettison analyses are conducted for 10 and 25 cm lanyard length and 100N and 200N lanyard pull forces to observe the effect of an axial release force. The results are compared in Figure 44 for empty rocket pod configuration at the hover condition. As expected, the pull force generates a nose-up pitch moment on the launcher.

In the jettison envelope generation simulations, 10 cm lanyard length and 100N (22 lbf) disconnection force is applied on the launcher dynamics.

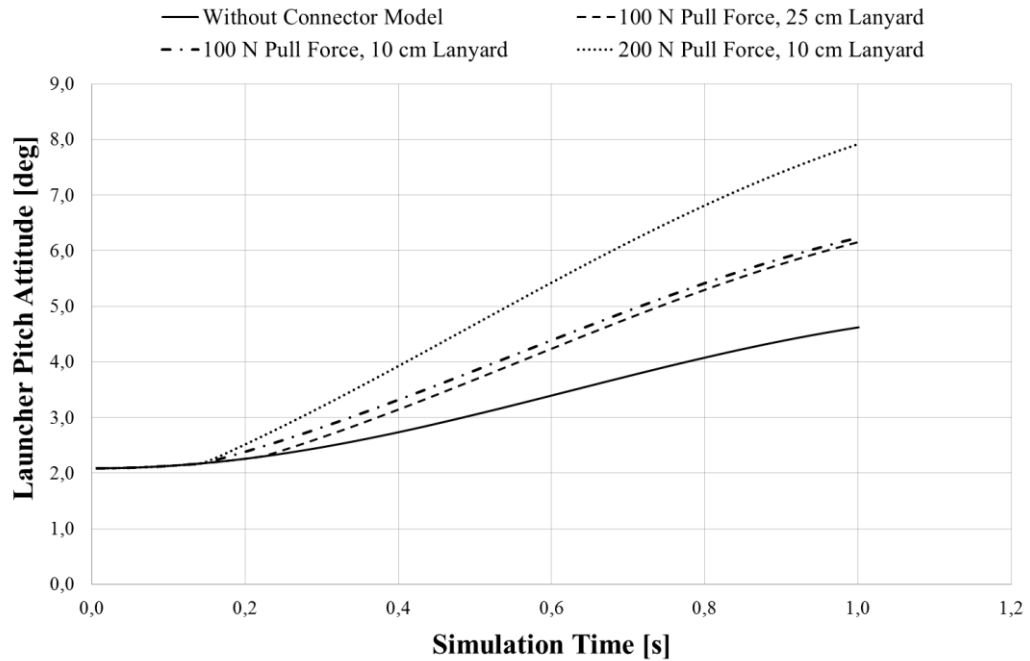


Figure 44 Effect of Lanyard Release Connector on Empty Launcher's Pitch Attitude

5.3 Effect of Launcher Loading On Jettison

As noted previously, there are two jettison types; selective and emergency jettison. In selective jettison, the main intention is to reduce total weight and drag of the aircraft. Mostly the launchers are released after all rockets / missiles are fired since they are not any longer required for the mission. Other situations that necessitate jettison are emergency conditions like engine failures and hang fire of a missile in the launcher. In emergency the launcher must be dropped immediately without spending time to launch the remaining rockets. Hence the launcher may be in any loading configuration at the instant of jettison. That is why all launcher loading possibilities must be covered for determination of the flight conditions that allows a safe jettison. The most critical launcher loading configurations in terms of collision possibility are selected based on weight (empty and fully loaded launchers) and center of gravity offset from the centerline (asymmetric configurations). The launcher with lightest weight and inertia has the tendency to be influenced more by the aerodynamic

interferences. Similarly, the fully loaded launcher remains in the helicopter vicinity for the longest time due to its lower velocity during jettison.

Center of gravity location has a major role in roll and pitch motion of the launcher. The possible asymmetrical loadings are determined regarding the firing sequence of the rockets. The firing sequence of the 2.75-inch rockets loaded on 19-tube launcher is demonstrated in Figure 45. It is seen that firing order is settled in such a way that the center of gravity is almost always kept balanced. In order to find the configuration with largest offset from the center, center of gravity of the launcher is updated regarding the fire order. The configurations after 7th rocket is fired (12 rockets remaining) and 18th rocket is fired (1 rocket remaining) are determined to be the most critical rocket loadings.

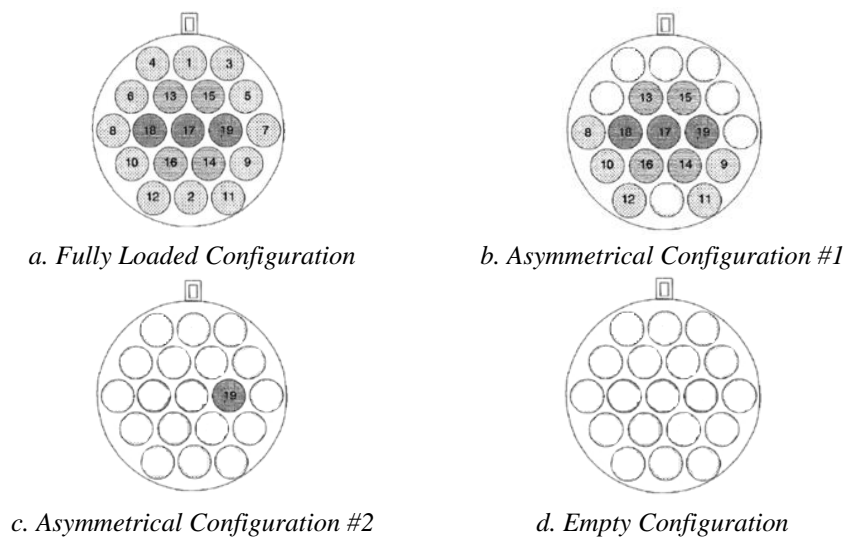


Figure 45 Firing Sequence of 2.75-inch rockets and Loading Configurations, From Rear View

Table 6 Weight and CG of Critical Launcher Loading Configurations

Launcher Loading Configurations	Remaining rockets	Weight [kg]	CG offset from launcher geometrical center		
			X _{cg} [mm] (+ forward)	Y _{cg} [mm] (+ to right)	Z _{cg} [mm] (+downward)
Full	19	234	113	0	0
Asymmetrical #1	12	169	91	-10	24
Asymmetrical #2	1	66	-27	12	0
Empty	0	57	-42	0	0

Separation simulations are performed for four configurations jettisoned from both starboard (right side with respect to pilot) and port (left side with respect to pilot) inboard stations with the purpose to include all possible worst-case scenarios in terms of collision possibility. The representative flight conditions are selected as hover, 100 knots forward flight and autorotative descent at 70 knots. The simulation results of the four different launcher configurations are visualized together to establish a better understanding about the behavior after jettison.

Table 7 Legend for Different Launcher Loadings

	Full configuration
	Asymmetrical #1 configuration
	Asymmetrical #2 configuration
	Empty configuration

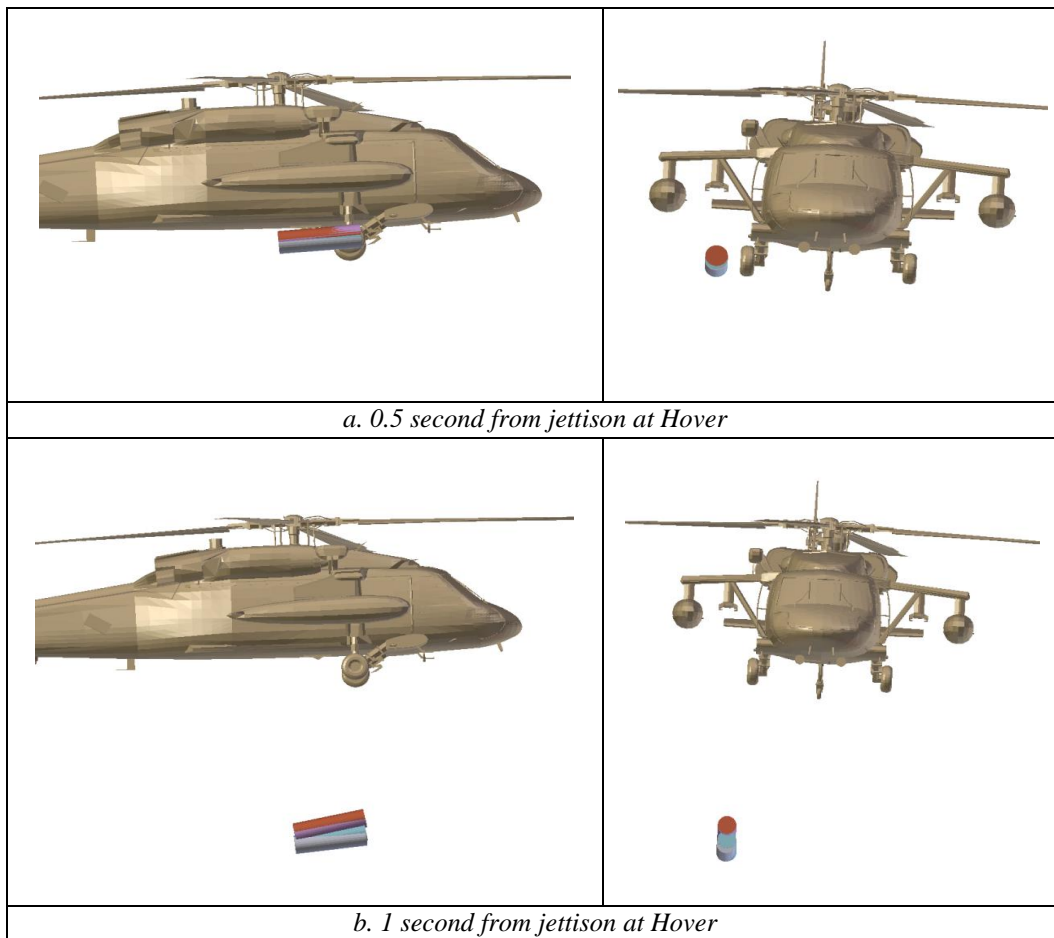


Figure 46 Behavior of Different Launcher Configurations Jettisoned at Hover

At hover, rocket launchers with lower weight, namely empty and asymmetrical #2 configurations reach higher jettison velocities compared to heavier launchers because of perceivable effect of main rotor downwash. Therefore the heavy launcher spends more time in the proximity of the helicopter which makes it critical from safe separation point of view. Figure 46 shows that the attitudes of all configurations remain same for a certain time which is enough to clear the main wheel.

As the forward velocity increases, the effect of parasite drag around the launcher rises. Drag force acts dominantly in the lightest launcher due to lower inertia values (Figure 47). The asymmetrically loaded launcher also encounters yaw and roll moments due to center of gravity offset in lateral direction.

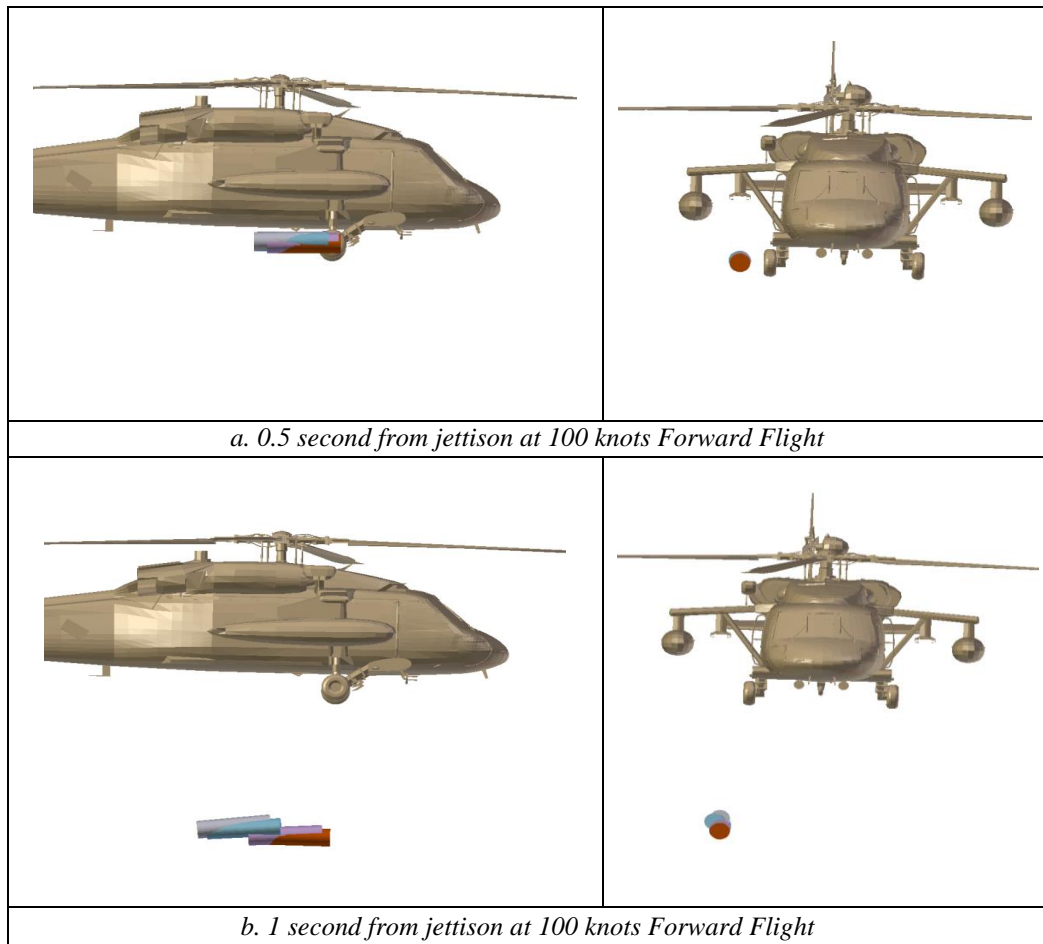


Figure 47 Behavior of Different Launcher Configurations Jettisoned at 100 knots Forward Flight

As noted previously, most of the jettison cases occur with the purpose to prevent a hazardous landing by removing weapons away from the helicopter. Hence jettison at autorotative descent is one of the most critical flight conditions that should be examined well before flight tests. Figure 48 represents the jettisoned store motion when exposed to high angle of attack during descent phase of autorotation. As expected the empty launcher is influenced mostly by the upward flow and encounters an obvious nose-up pitch motion compared to heavier launchers.

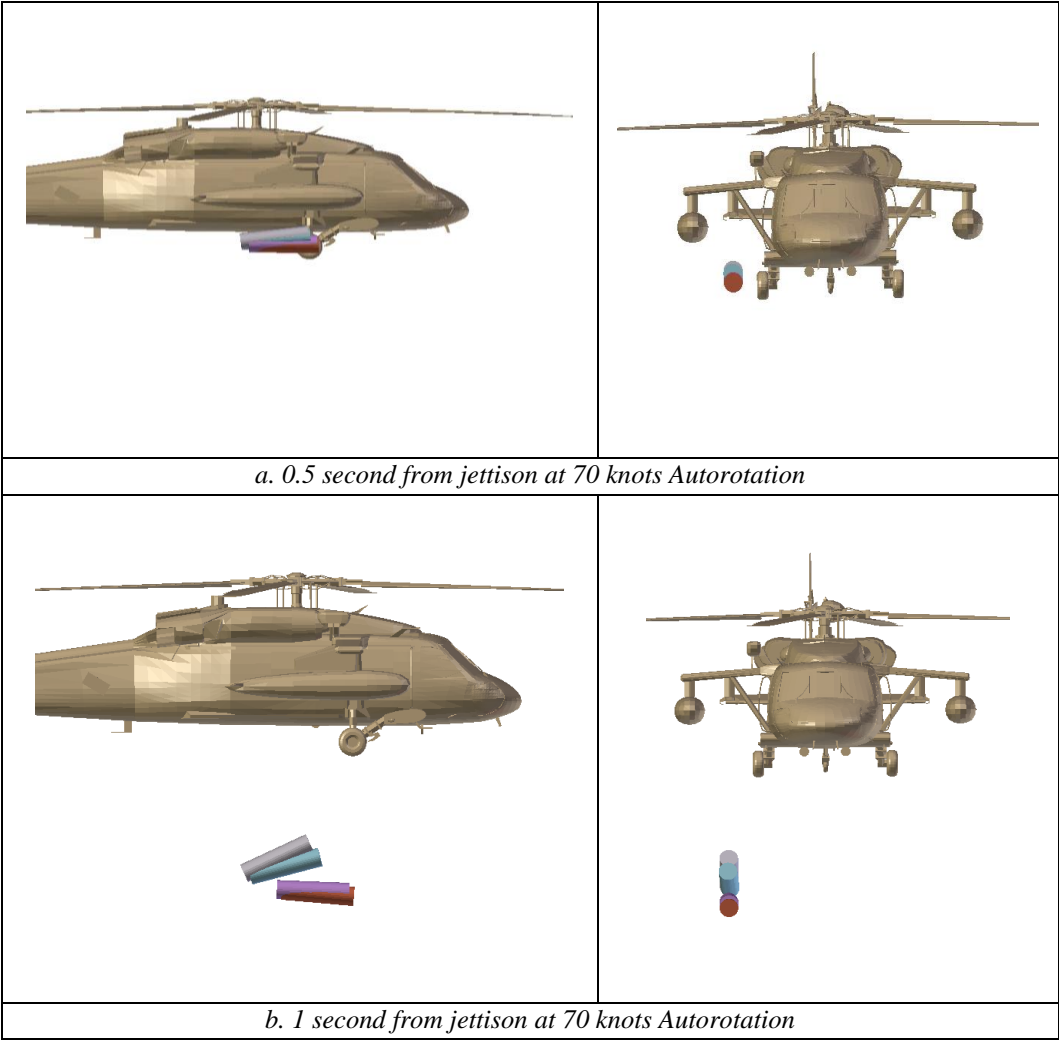


Figure 48 Behavior of Different Launcher Configurations Jettisoned at 70 knots Autorotation

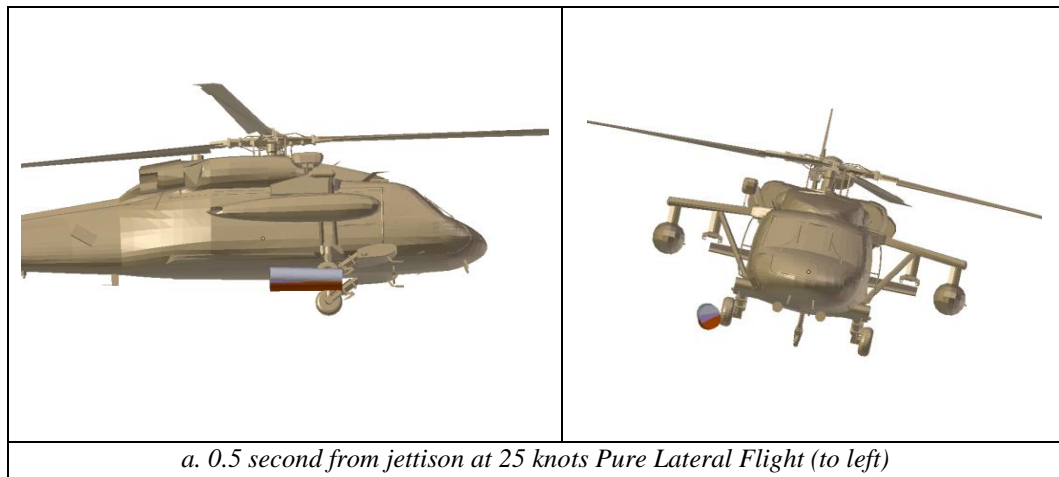


Figure 49 Behavior of Different Launcher Configurations Jettisoned at 25 knots Lateral Flight

The results of jettison at lateral flight are shown in Figure 49. In this flight maneuver, the launchers have an initial lateral speed and move towards to the helicopter landing gear. Consequently, the contact to landing gear is encountered for all configurations. Another outcome is that fully loaded launcher accelerates more than lighter launchers.

Comparative analysis results point out that weight has a significant effect on launcher behavior at all flight maneuvers. Particularly the motion of the launchers with low weight and moment of inertia are affected more by large aerodynamic loads. A small disturbance during free flight generates large deviations in the store attitudes. Moreover loaded launchers may be critical as well since they fly in the neighborhood of the helicopter for a longer time and they fall without change in their attitudes. The roll and yaw tendency of the asymmetrically loaded launchers also require to be analyzed in scope of safe separation studies.

Regarding these outcomes of the comparative study, jettison simulations of all four configurations listed in Table 6 are performed individually to obtain a safe jettison envelope that covers all possible worst-case conditions.

CHAPTER 6

SAFE SEPARATION ENVELOPES

In the simulations, the separation throughout the helicopter flight envelope is investigated and flight maneuvers at which separation is regarded as unsafe are detected. The critical and unsafe launch and jettison points are recorded. This combined envelope is called as safe separation or safe jettison envelope. It consists of;

- safe region for store separation
- unsafe region where store distance to helicopter exceeds the limits or the collision is expected

The flight speed and maneuver limitations stated in the UH-60Q Operators Manual [17], are taken into account in definition of analysis conditions.

Table 8 Maneuver Limitations of UH-60Q Helicopter

Maximum airspeed for autorotation	130 KIAS
Sideward/rearward flight limit with fuel tanks	35 knots
Descent at level flight	> 40 KIAS
Hovering turn	30° /sec
High Speed Yaw Maneuver limitation	80 KIAS

The analyses are conducted at gross weight of 16000 lbs. and center of gravity in which the mathematical model is validated. The connector detach force is assumed as 100 N and lanyard cable length is 10 cm.

In the analyses 15 State Inflow model is used to include the main rotor interference on the store as it predicts the inflow better than 3 and 6 State models. In addition it is more convenient to analyze set of dynamic maneuvers successively with more efficient computational capability of dynamic wake model compared to vortex wake methods.

In the envelopes, the safe and unsafe flight conditions are distinguished with different markers. The cross markers are used to show the conditions at which mathematical model is not capable to be trimmed. The results of simulation at untrimmed points are excluded in the envelopes since they may not give reliable information about store motion after separation.

In the forward and lateral flight envelopes, positive lateral speeds represent the sideward motion of the helicopter with positive sideslip angles. Sideslip angle is defined to the right of the helicopter nose direction.

6.1 Safe Separation Envelope of 2.75-Inch Diameter Unguided Rockets

Separation simulation of rockets is performed to determine the maneuvers at which the rocket trajectory is critically close to the helicopter fuselage or main rotor tip path plane. Trajectory of the rockets launched from the innermost station and from the uppermost stations of the launcher have the smallest clearance to the fuselage and main rotor blades respectively. The safe separation simulation investigates most of the firing scenarios. Rocket launch from launchers located at right and left inboard stations are analyzed and safe separation results are combined to generate an envelope.

The results of the analyses show that launch at forward flight, lateral flight (Figure 50) and descent maneuvers (Figure 51) don't contain any risk of contact with any part of the helicopter

At military operations, unguided 2.75 inch diameter Mk-40 rockets are fired at hover and level flight conditions to provide a better accuracy to hit the target. Thus Figure 50 constitutes a basis for safe separation envelope of this weapon system.

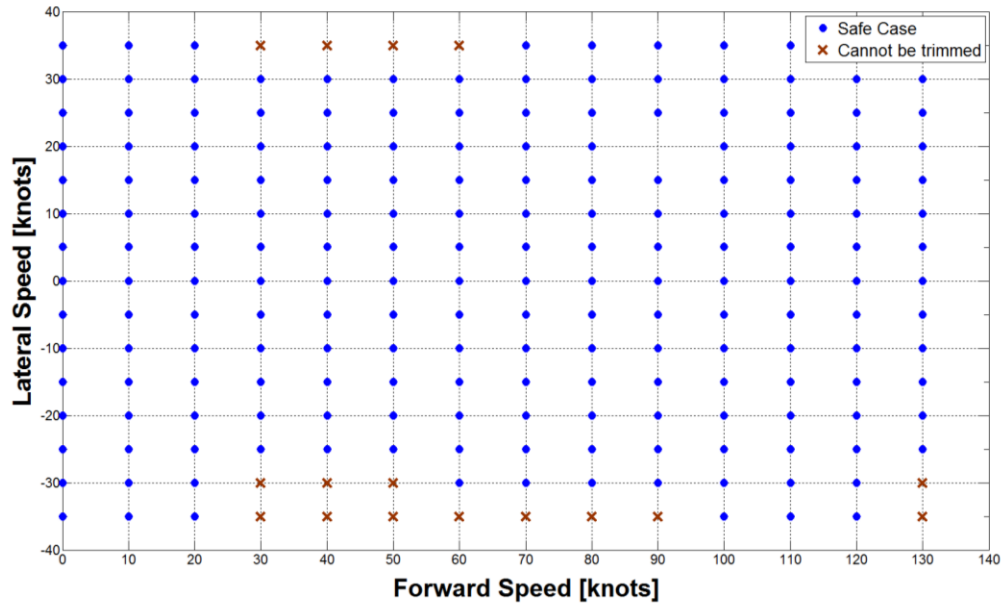


Figure 50 Launch Envelope of Rockets at Level Flight

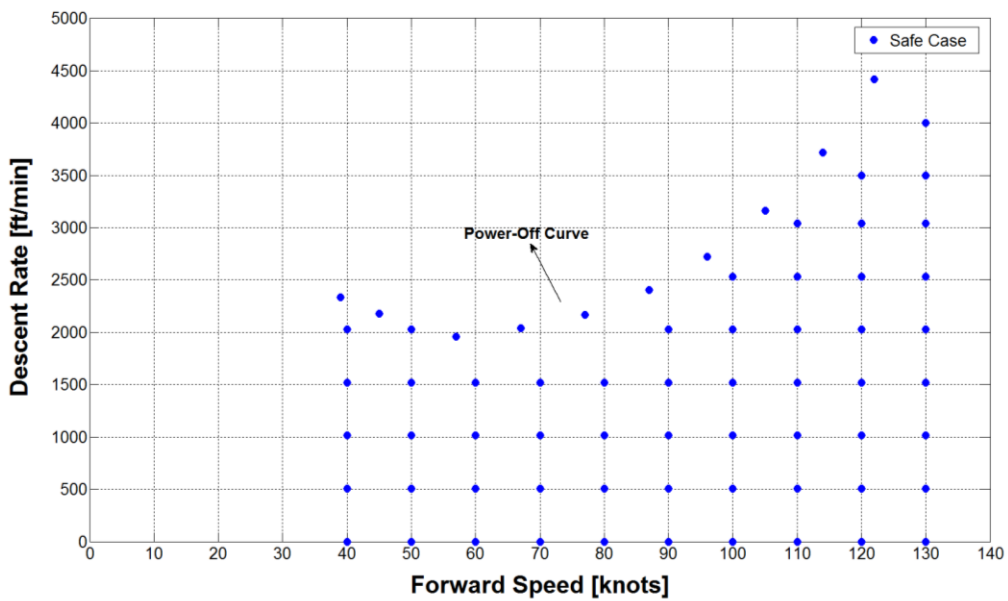


Figure 51 Launch Envelope of Rockets at Descent and Autorotation

The flight maneuvers with constant angular rate are also investigated in this study to determine the safe limits at dynamic maneuvers. On the contrary to level flight and descent maneuvers, rocket separation at coordinated turn maneuver is restricted to ± 20 deg/s yaw rate as seen in Figure 53. At turn maneuvers rocket trajectory passes through a distance that exceeds allowable safety margin of fuselage which is 9 cm. This margin is measured from the outermost points on the fuselage regarding the clearance definition stated in MIL-STD-1289D [2]. One of the maneuvers at which rocket launch must be avoided is demonstrated in Figure 52. At this instant, rocket fins are closest to the fuselage, exceeding 9 cm safety margin.

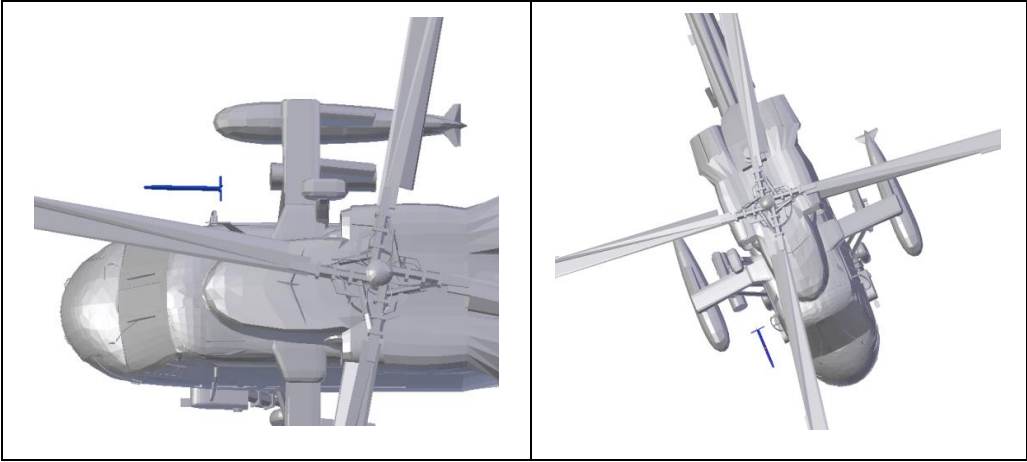


Figure 52 Demonstration of Rocket Exceeding Fuselage Safety Margin at Turn with 30°/sec and 14° Bank Angle

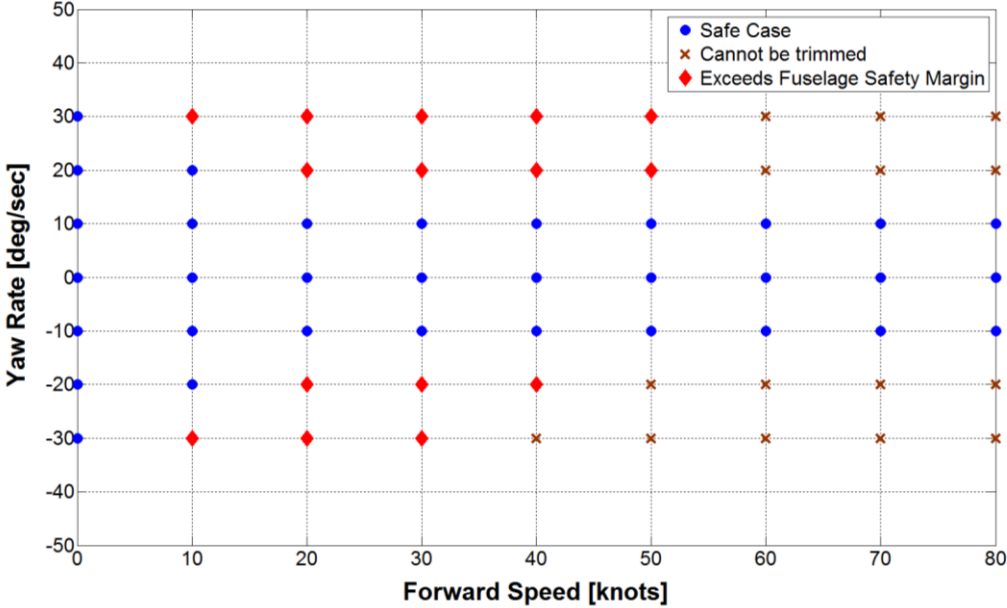


Figure 53 Launch Envelope of Rockets at Turn Maneuvers

Similarly at push-over maneuver pilot reduces the helicopter angle of attack with constant negative pitch rate; therefore the rocket path may coincide with five-angle cone determined for the most deflected main rotor plane (Figure 31). The conditions that must be avoided are shown in Figure 54. At pull-up maneuvers launch is safe because the main rotor disc moves away from the rocket trajectory with increasing pitch-up motion.

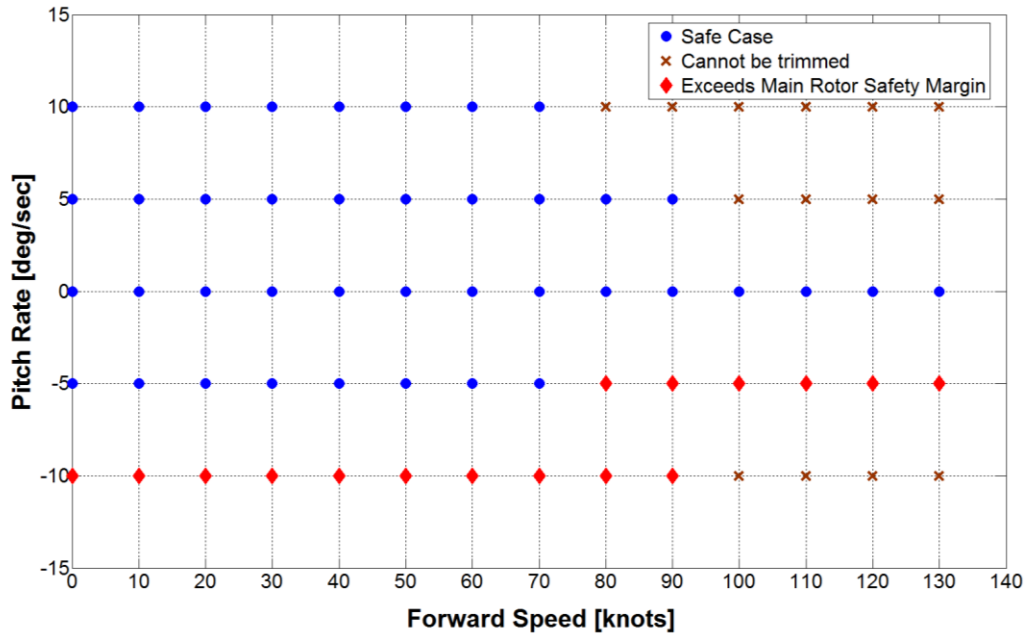


Figure 54 Launch Envelope of Rockets at Pull-up and Push-over Maneuvers

At maneuvers with roll rate, separation is safe until roll rate is increased to ± 30 deg/sec (Figure 55). At this rate, helicopter rolls very rapidly so the rocket trajectory may pass through five-angle cone margin of main rotor.

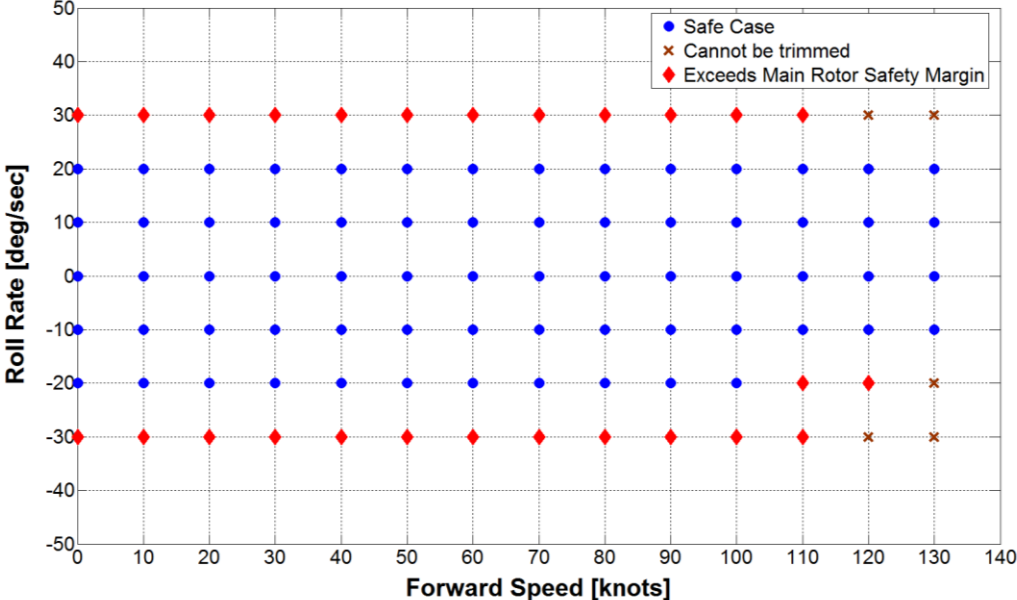


Figure 55 Launch Envelope of Rockets at Flight with Roll Rate

6.2 Safe Jettison Envelope of Rocket Launcher

The jettison analyses of 19-tube rocket pod are performed. All possible launcher loadings are covered in the analyses by investigating the jettison characteristics of fully loaded (19 rockets), 12 rockets loaded, 1 rocket loaded and empty launchers. Jettison analyses are conducted from both right and left wings and inboard stations which are considered to be more critical due to short distance to fuselage and landing gear. Jettison is simulated considering the fuel tanks are loaded at the outboard stations to investigate store to store collision possibility. Forward flight, lateral flight, flight with constant sideslip angles, descent and autorotation conditions are analyzed for jettison.

The unsafe conditions obtained based on collision detection routine in separation simulation are revised by visualizing the simulation using actual geometries of the

helicopter and the launcher. It is seen that at some points the launcher does not have any contact although it passes by the landing gear with a small clearance. Jettisons at these points are determined as safe.

The safe separation information obtained from the simulation of each launcher configuration is combined and a unified jettison envelope is given in Figure 56. The safe jettison envelope is limited to 20 knots lateral speed at all forward speeds.

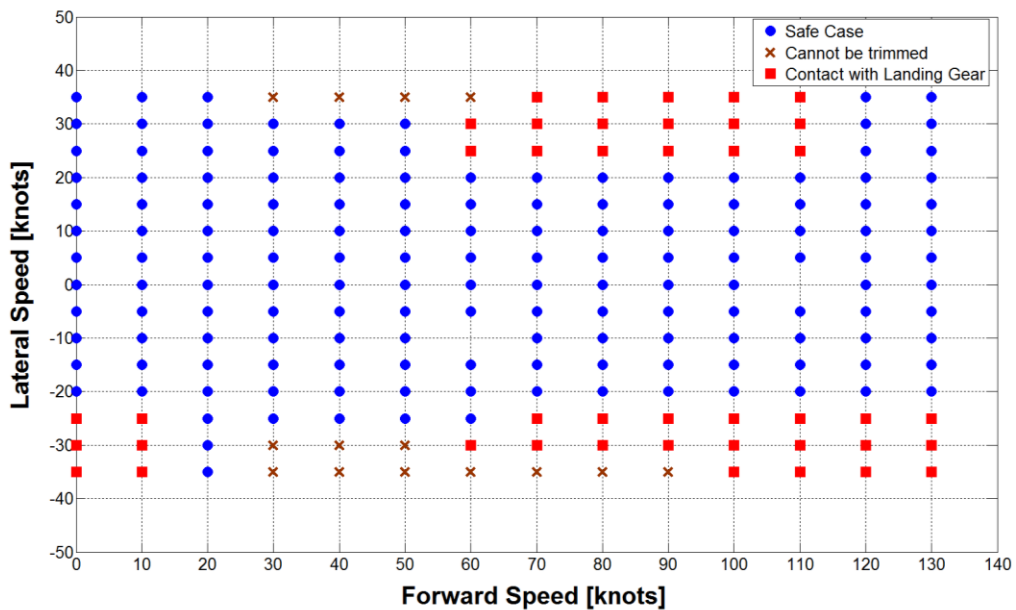


Figure 56 Jettison Envelope of Rocket Launcher at Level Flight

According to the jettison simulations, empty launchers jettisoned from both left and right inboard stations are the most critical configurations since they contact with the landing gear at high air speeds when lateral speed is more than 20 knots. As seen in Figure 56, lateral flight to the left (negative sideslip angles) is more critical in terms of collision to landing gear. This asymmetrical distribution of the unsafe points on the envelope is due to higher negative roll attitude of the helicopter when it slides to the left side. As helicopter rolls towards left, the right landing gear approaches to the store which is jettisoned from right wing. Jettisons at same lateral speed but to different sides are illustrated in Figure 57. Although sideslip to right side is performed with 10 degrees roll angle, -17 degrees roll attitude is required to slide to

the left side with the same lateral speed. Contact with landing gear is observed for jettison at right inboard station.

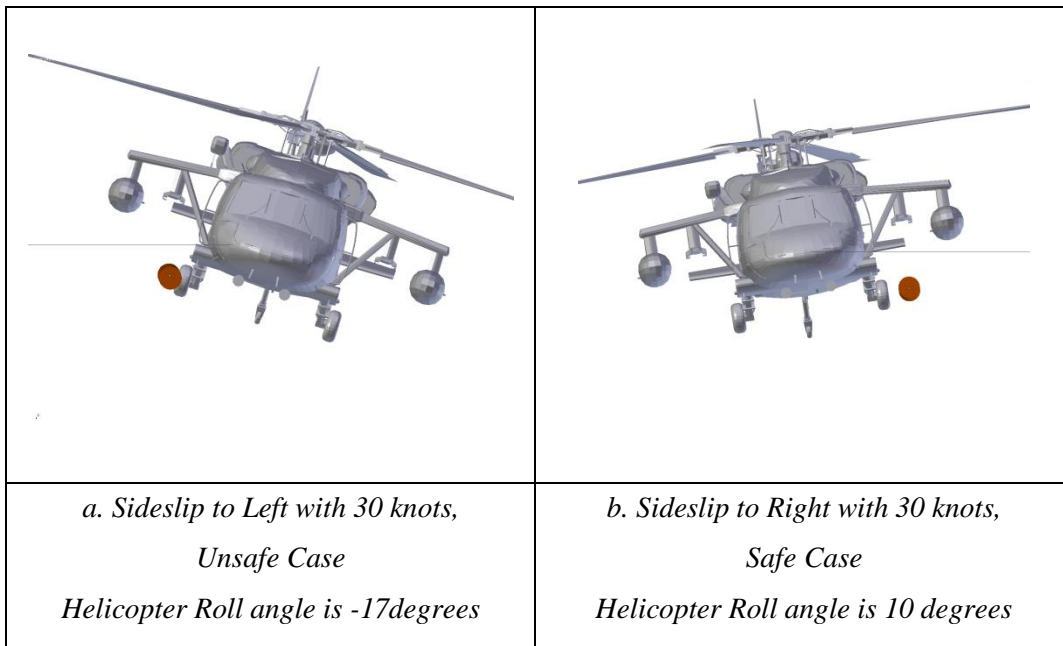


Figure 57 Demonstration of Empty Launcher Jettison, at Pure Lateral Flight

On the contrary to pure or low speed lateral flights, at higher speeds launchers jettisoned from right (left) wings have contact with landing gear when helicopter flies with positive (negative) sideslip angle, which means to right (left) side. Figure 58 shows the collision instant when store is jettisoned from left wing while helicopter sideslips to the left. The launcher moves towards the landing gear under the influence of sideward airflow.

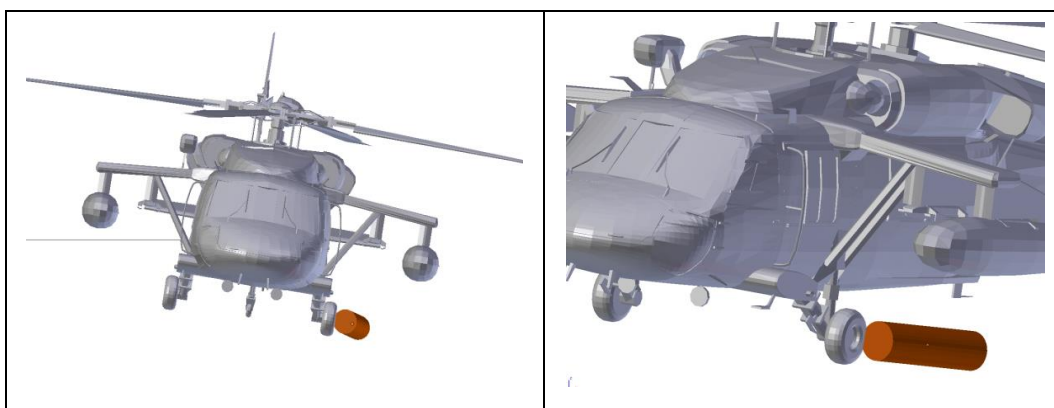


Figure 58 Collision Instant of Empty Launcher, at 95 kts Airspeed with -18° Side Slip Angle

The most important flight maneuver for emergency jettison is autorotation. When single or dual engine failure is encountered, the weapons should be released to maintain helicopter safety at landing. Thus descent and autorotation conditions are investigated from safe jettison point of view. The simulation results show that launchers can be jettisoned safely at all points in helicopter descent envelope in emergency situations.

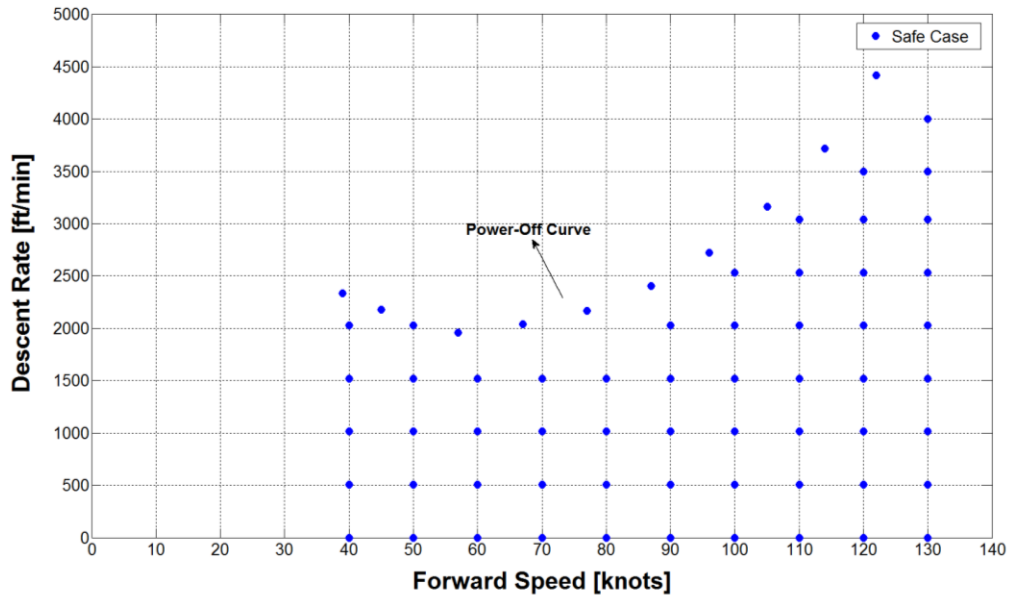


Figure 59 Jettison Envelope of Rocket Launcher at Descent and Autorotation

6.3 Safe Jettison Envelope of External Fuel Tank

The 230-gallon jettisonable fuel tanks are carried on the outboard pylons of UH-60 helicopter. The recommended jettison envelope of the auxiliary tanks which is given in Operator’s Manual, [17] is shown in Figure 60.

RECOMMENDED EMERGENCY JETTISON ENVELOPE							
LEVEL FLIGHT	AIRSPEED KIAS						
	0 TO 120					120 TO Vh	
	SLIP INDICATOR DISPLACED NO MORE THAN ONE BALL WIDTH LEFT OR RIGHT					NO SIDESLIP BALL CENTERED	
DESCENT	*JETTISON BELOW 80 KIAS NOT RECOMMENDED	AIRSPEED KIAS					*JETTISON ABOVE 120 KIAS NOT RECOMMENDED
		80	90	100	110	120	
		1000	875	750	625	500	
MAX RATE OF DESCENT FT/MIN							
*Not recommended because safe jettison at these conditions has not been verified by tests.							

Figure 60 Recommended Emergency External Fuel Tank Jettison Envelope

The jettison simulations of empty tank and tank loaded with 230-gallon of JP-4 fuel are performed using the separation simulation code. Analyses are conducted for tanks jettisoned from both right and left outboard pylons of the helicopter. The simulation results of all configurations are combined and the unified jettison envelopes are generated. The jettison simulations at level flight conditions show that there is no contact to any of the helicopter parts. The jettison envelope at level flight is given in Figure 61.

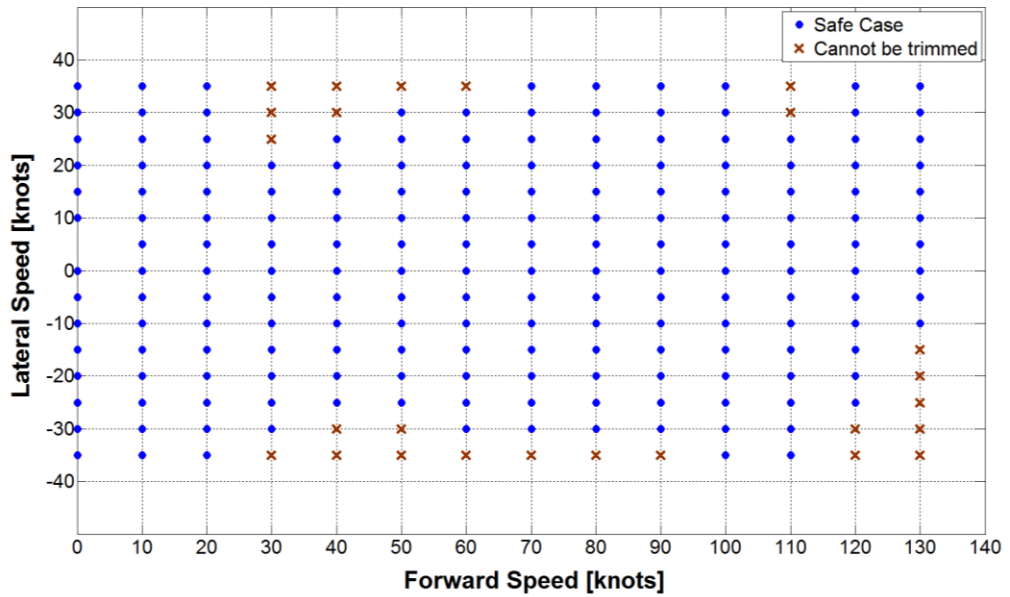


Figure 61 Jettison Envelope of External Tanks at Level Flight

The simulation results of jettison at descent maneuvers are unified and shown in Figure 62. The recommended jettison maneuver limits (Figure 60) given in Operators Flight Manual of UH-60Q Helicopters [17], are also plotted. When tanks are jettisoned at the maneuvers marked with “Contact with Store Pylons”, it is observed that the empty tank encounters a nose-up pitch motion immediately after jettison and hits to the store pylon as demonstrated in Figure 63. Therefore jettison at these cases is determined as unsafe and they should be excluded from the jettison envelope. When the safe jettison envelopes obtained by simulation and flight tests are compared, it is seen that simulation results are agreeable with the test data. During the maneuvers at the boundary of the simulated jettison envelope, although the empty tank approaches to the pylons critically, it doesn't have any contact. Hence, the recommended jettison envelope limits are specified considering a safety margin to prevent any collision during jettison tests of external fuel tanks.

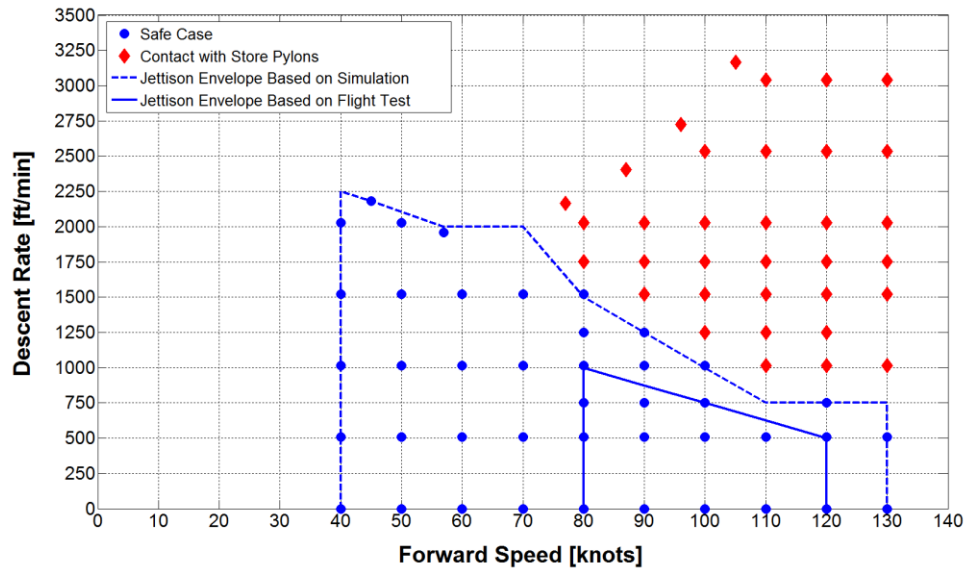


Figure 62 Jettison Envelope of External Tanks at Descent

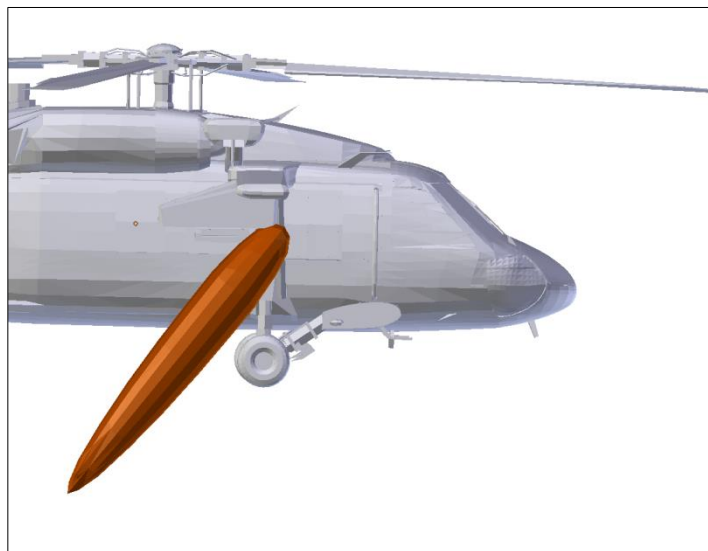


Figure 63 Collision Instant of Empty Fuel Tank, at 100 kts Airspeed with 1250 fpm Descent Rate

CHAPTER 7

CONCLUSIONS

Store separation from an aircraft is a vital problem that should be analyzed and tested to ensure that separated store clears the aircraft safely without endangering the aircraft or crew. Flight tests provide most reliable data for determination of store behavior after separation. However, high costs and risk factors limit the number of test points. Hence a methodology is developed to predict the store characteristics and to determine the unsafe flight conditions for store separation issues. This thesis work handles the store separation problem from flight dynamics point of view. A store separation simulation tool is developed to study characteristics of launch of 2.75-inch diameter rockets and jettison of the 19-tube rocket launchers and external fuel tanks from armed Black Hawk helicopter.

The mathematical model of the UH-60A helicopter and external stores is developed to simulate the separation. The modeling of main rotor inflow and its interference on the fuselage, horizontal tail and external stores is a challenging part of the mathematical modeling study. Hence, Peters-He 3 State and 15 State inflow methods are applied in the model and they are compared with the flight test data. The mathematical model validation analyses are carried out at steady level flight, descent, climb conditions and transient response cases. It is seen that 15 State inflow solution method simulates the actual helicopter behavior better than 3 State inflow approach.

The parameters that may have influence on the store trajectory are also investigated in scope of thesis. Main rotor induced flow contribution has one of the most dominant effect on the store behavior after separation. Dynamic wake (Peters-He 3 State, 6 State, 15 State) and vortex wake inflow calculation approaches are

implemented on separation simulation to distinguish to which method store motion is more sensitive. Comparative results of store trajectory and attitudes indicate that inflow distribution computed by Peters-He 3 State has the most significant effect on longitudinal dynamics of store due to higher magnitude downwash velocity. However the attitudes and trajectory of the store have small differences when different methods are implemented to the mathematical model. Regarding the reliability of the Peters-He 15 State method in model validation study and its advantages over other methods, the main rotor interference on external stores is modeled with Peters-He 15 State approach.

The comparison of different launcher loading configurations show that special consideration must be given to decide the most critical loading. Generally empty launchers and fuel tanks are aerodynamically unstable due low weight and moment of inertia values. As expected, the orientation of lighter launcher is more sensitive to airflow around it. At hover and low speed flight with addition of downwash empty launchers fall more rapidly than heavier launchers. Although fully loaded launchers demonstrate more stable motion after jettison, they leave the helicopter neighborhood later than lower weight launchers at hover. This situation makes full launcher even critical since the collision possibility is evident for longer period of time. Partially loaded launchers also demonstrate critical roll and yaw motions since the total center of gravity is located at a certain offset. Yaw tendency of asymmetrically loaded launchers towards the helicopter fuselage is encountered during flights with sideslip angle.

Safe separation and safe jettison envelopes are generated as an outcome of separation simulations at wide range of maneuvers. These envelopes represent the flight conditions and maneuvers that store separate safely. The launch and jettison limits obtained based on simulations are summarized at Table 9 and Table 10 respectively.

Table 9 Safe Separation Limits of Rockets Launched from UH-60 Helicopter

Maneuver	Safe Separation Limit
Flight with Sideslip	No limit
Descent and Autorotation	No limit
Coordinated Turn	Yaw Rate $\leq 10^\circ/\text{sec}$ and Speed < 80 knots
Push-over	Pitch Rate $\leq 5^\circ/\text{sec}$ and Speed < 80 knots
Flight with Roll Rate	Yaw Rate $< 30^\circ/\text{sec}$

Table 10 Safe Jettison Limits of Rocket Launcher Jettisoned from UH-60 Helicopter

Maneuver	Safe Jettison Limit
Flight with Sideslip	Lateral Speed ≤ 20 knots
Descent and Autorotation	No limit

The allowable jettison limits of the 230-gallon external fuel tank are given in Operator's Manual of UH-60Q Helicopter [17]. The recommended jettison envelope given in the Operator's Manual is used to verify the accuracy of the simulation code developed in this thesis work. The simulation results show that the safe jettison limits determined based on analysis are consistent with the envelope verified with flight tests. Hence it is concluded that the simulation code provides fast and reliable results for the definition of safe separation envelopes of helicopter external stores.

Envelopes obtained by separation analysis constitute the initial step for flight tests in weapon integration projects. Store trajectory information at safe conditions according to the analysis will be used to determine the first flight test points. Once the simulation is validated at these points, the number of flight tests will be reduced to test only corner points of the envelopes.

REFERENCES

- [1] U.S. Department of Defense, “MIL-HDBK-1763 Aircraft / Stores Compability: Systems Engineering Data Requirements and Test Procedures”, 1998.
- [2] U.S. Department of Defense, MIL-STD-1289D Airborne Stores Ground Fit and Compability, Requirements, 2003.
- [3] Landgrebe A., Egolf, T.A., “Rotorwake Induced Flow Along Helicopter Rocket Trajectories”, *Proceeding of Conference on the Effects of Helicopter Downwash on Free Projectiles, US Army Aviation Systems Command, August 1978.*
- [4] Wasserman, S., Yeller, R., “Preliminary Analysis of the Effect of Calculated Downwash Distributions on the Flight Performance of the 2.75 inch Rocket”, *Proceeding of Conference on the Effects of Helicopter Downwash on Free Projectiles, US Army Aviation Systems Command, August 1978.*
- [5] Wennekers, R., “Helicopter Weapon System Integration Session 4: Case Histories TIGER”, *AGARD Lecture Series 209, Helicopter / Weapon System Integration*
- [6] Roberts, D., Capezutto, R., “Development, Test and Integration of the AGM-114 Hellfire Missile System and FLIR/LASER on the H-60 Aircraft”
- [7] Ries, T., Kiesewetter, U., Jettisoning Simulation Improvements, Process, Modeling and Validation with Flight Test Results, *European Rotorcraft Forum 2013*
- [8] Howlett, J.J., “UH-60A Black Hawk Engineering Simulation Program – Volume I- Mathematical Model,” NASA CR-166309, Dec. 1981.

- [9] Kaplita, T. T.: "UH-60A Black Hawk Engineering Simulation Model Validation and Proposed Modifications." Tech. Rep. SER-70982, United Technologies Sikorsky Aircraft, 1984.
- [10] Ballin, M. G., "Validation of a Real-Time Engineering Simulation of the UH-60A Helicopter," NASA TM-88360, 1987.
- [11] Johnson, W., "Rotorcraft Aeromechanics", Cambridge University Press.
- [12] He, C.J., "Development and Application of Generalized Dynamic Wake Theory of Lifting Rotors".
- [13] Peters, D.A. and He, C.J., "A Closed form unsteady Aerodynamic Theory of Lifting Rotor in Hover and Forward Flight".
- [14] Peters, D.A., and He, C.J., "Finite State Induced Flow Models Part II: Three-Dimensional Rotor Disk".
- [15] Howlett, J.J., "UH60A Black Hawk Engineering Simulation Program: Volume II- Background Report", NASA CR-166309, Dec. 1981.
- [16] "Rocket Motor, 2.75 inch Rocket, Mark 40 and Mods, Mark 4 and Mods, Loading, Assembling and Packing", MIL-R-609954, 1992
- [17] Technical Manual, Operator's Manual For UH-60Q Helicopter, TM 1-1520-253-10
- [18] FLIGHTLAB Theory Manual, Advanced Rotorcraft Technology
- [19] Missile Datcom User's Manual, U.S. Army Aviation & Missile Research, Development and Engineering Center, AFRL-RB-WP-TR-2011-3071, March 2011

[20] Marshall, A.R., Oliver, R.G., Buckanin, R.M., Adler, R.S.,“Preliminary Airworthiness Evaluation of the UH-60A Configured with the ESSS, Final Report ”, USAAEFA Project No. 82-14, March 1983

APPENDIX A

NONLINEAR RESPONSE ANALYSIS

The results of response analysis performed for mathematical model validation with flight test data are provided. The tests are conducted when SAS is disabled and to be consistent with test data analyses are performed with SAS-Off condition as well.

A.1 Response to 0.5 inch Forward Cyclic Input at Hover

Forward longitudinal cyclic input results are given in this section. Higher and positive pitch rate values generated in the simulation model results in difference in pitch angle. Off-axis responses as roll angle and roll rates are overlapped with test data. However, yaw axis response needs improvement.

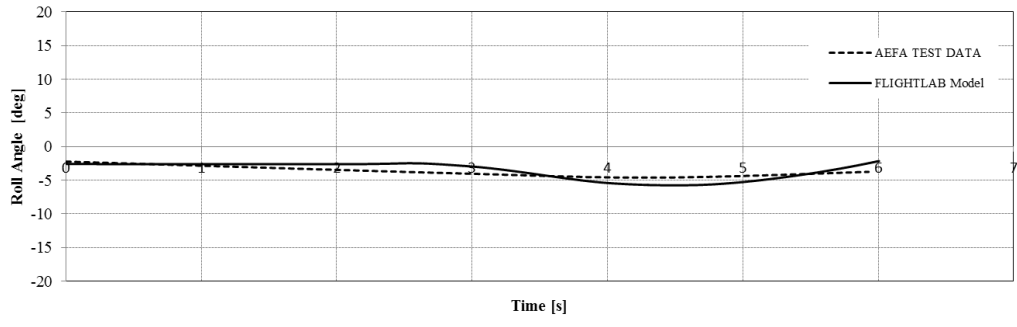
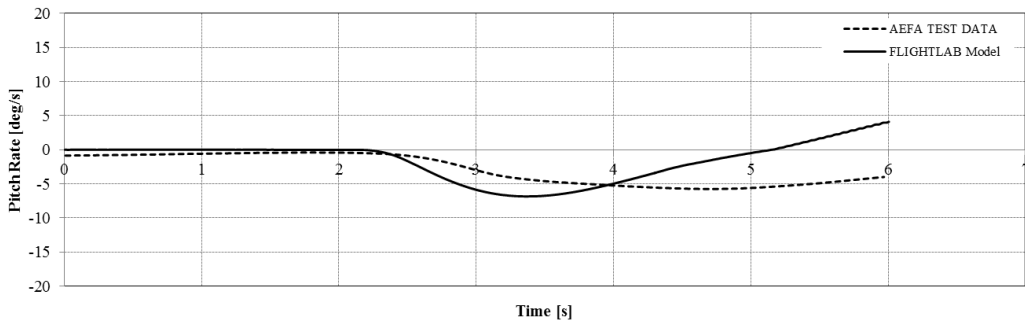
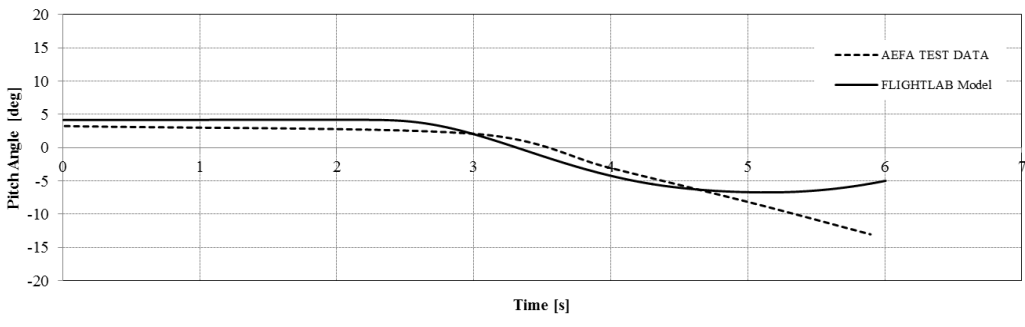
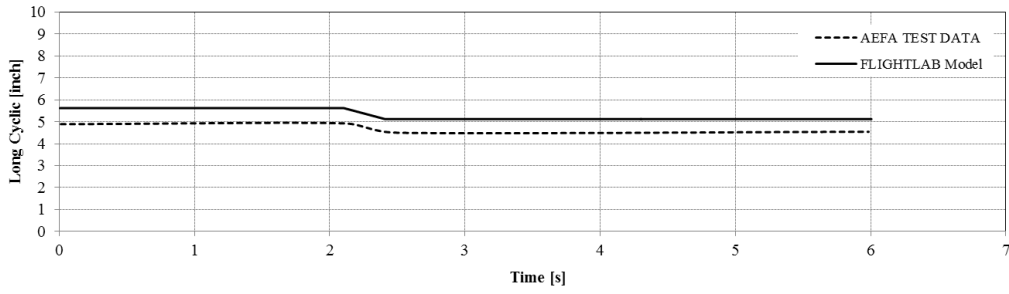


Figure A 1 Comparison of test data and simulation model response to 0.5 inch Forward Cyclic Input At Hover

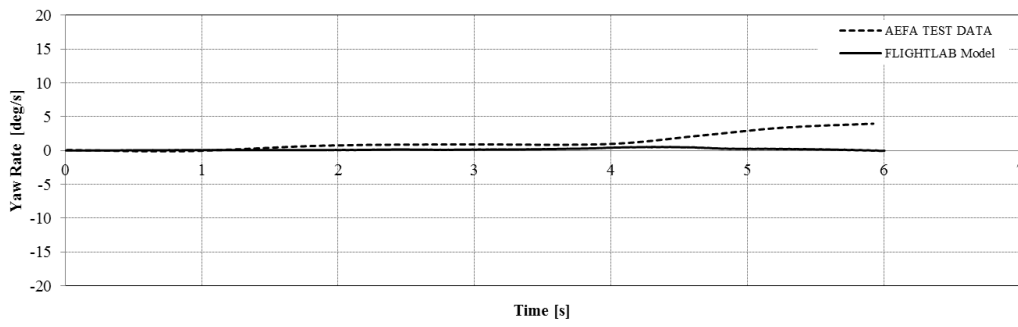
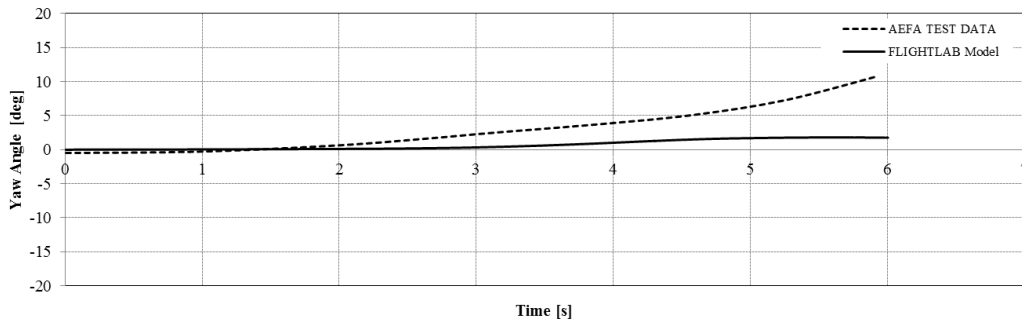
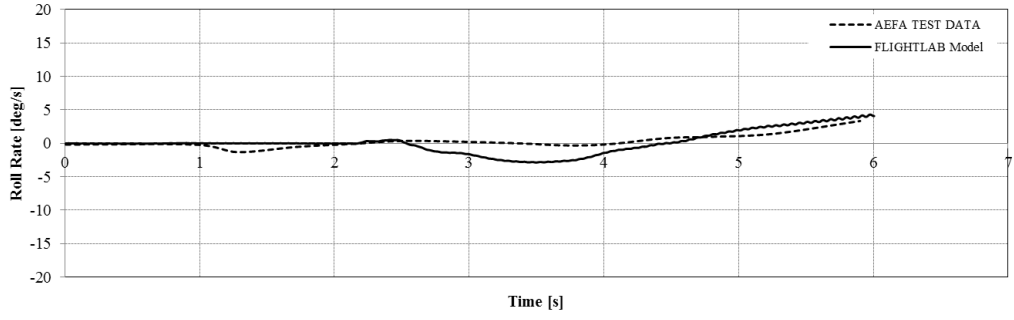


Figure A 1 (continued)

A.2 Response to 1 inch Right Cyclic Input At Hover

When simulation model is disturbed by lateral cyclic input at hover, very good agreement is achieved with test data in on-axis and off-axis responses.

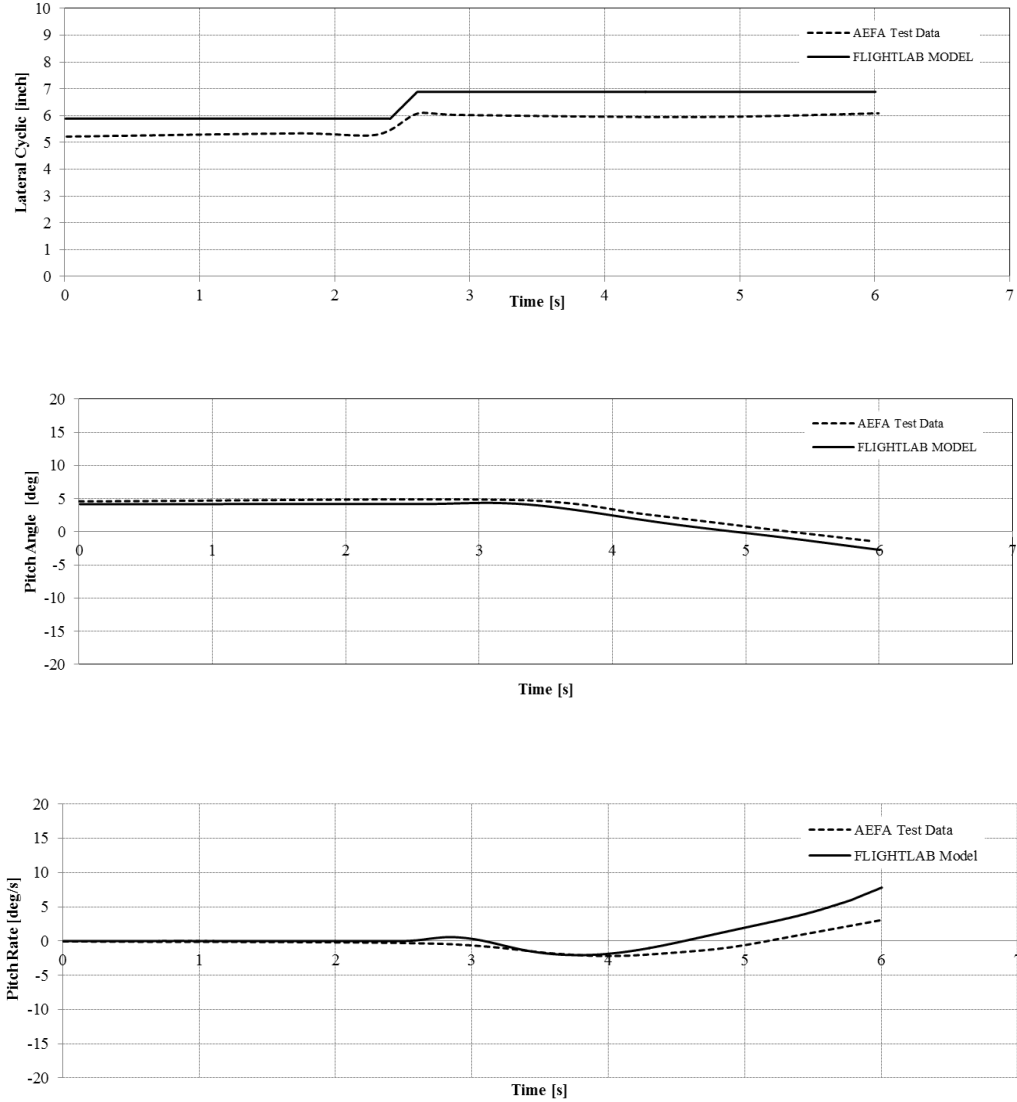


Figure A 2 Comparison of test data and simulation model response to 1 inch Right Cyclic Input At Hover

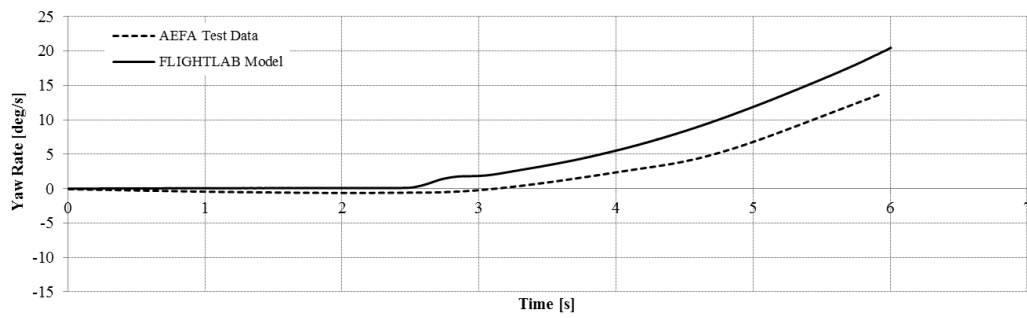
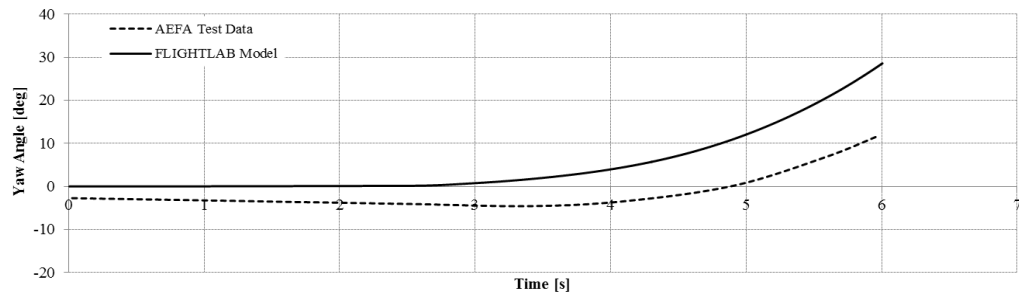
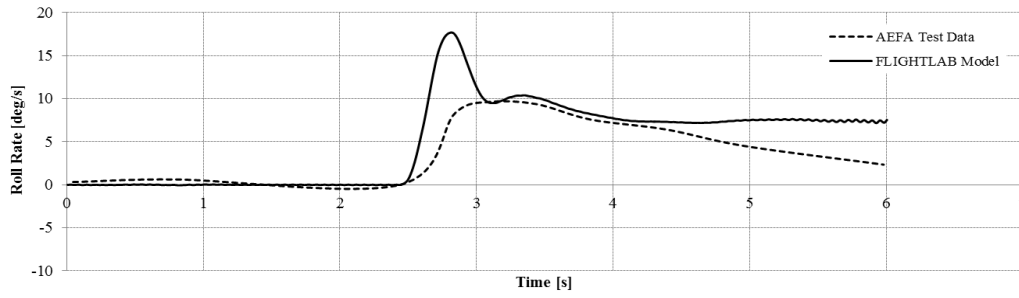
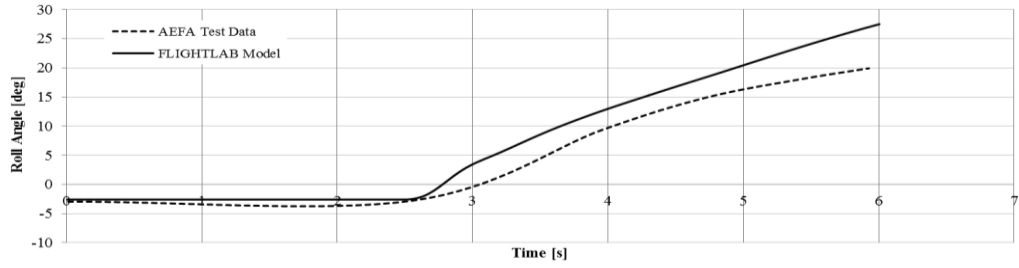


Figure A 2 (continued)

A.3 Response to 1 inch Up Collective Input At Hover

The responses to collective stick increase at hover are also quite adequate in pitch and roll axis. However difference in the yaw rate tendency results in higher yaw angles compared to test data.

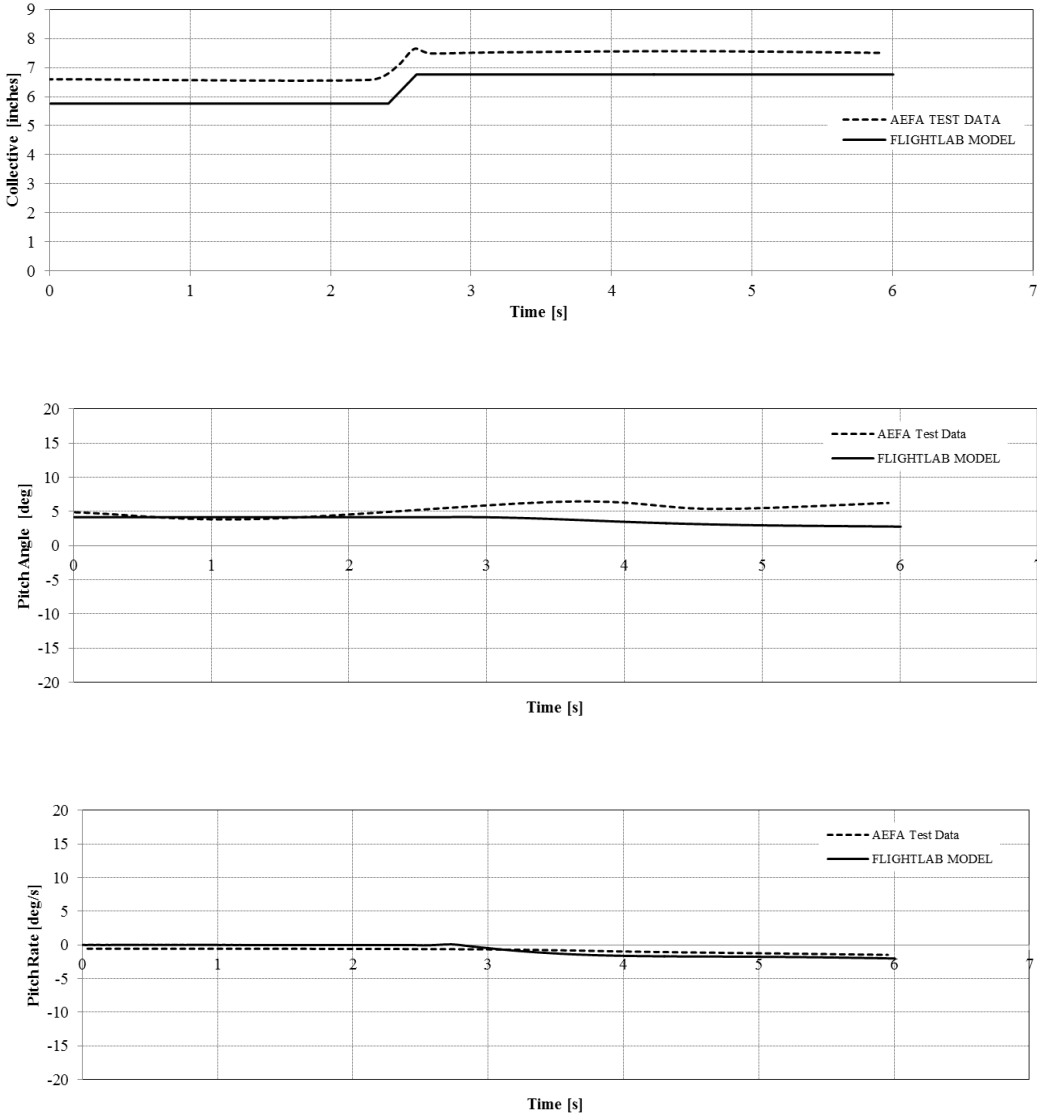


Figure A 3 Comparison of test data and simulation model response to 1 inch Up Collective Input At Hover

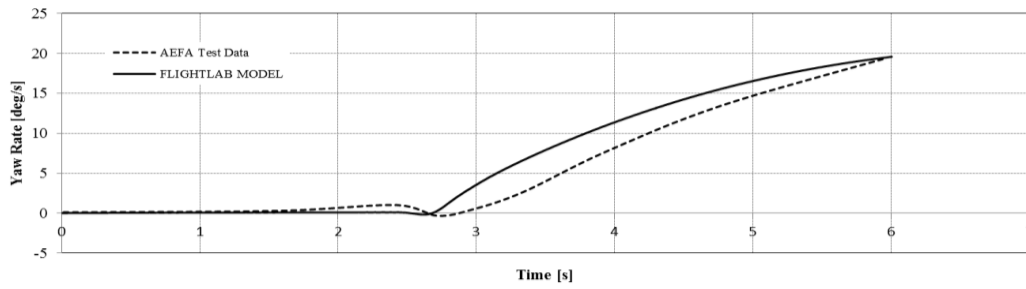
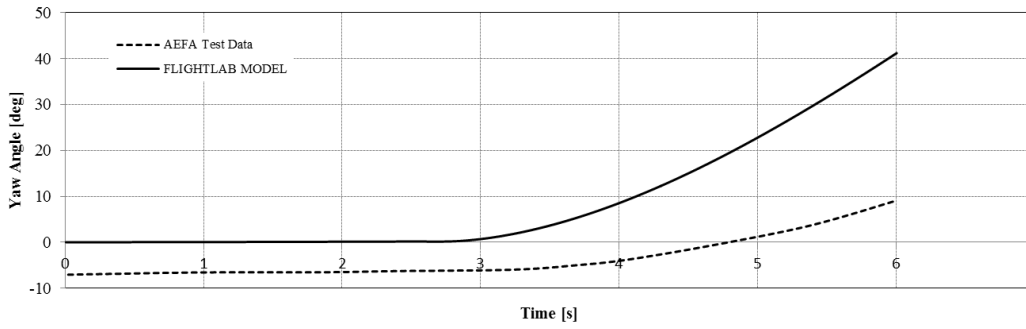
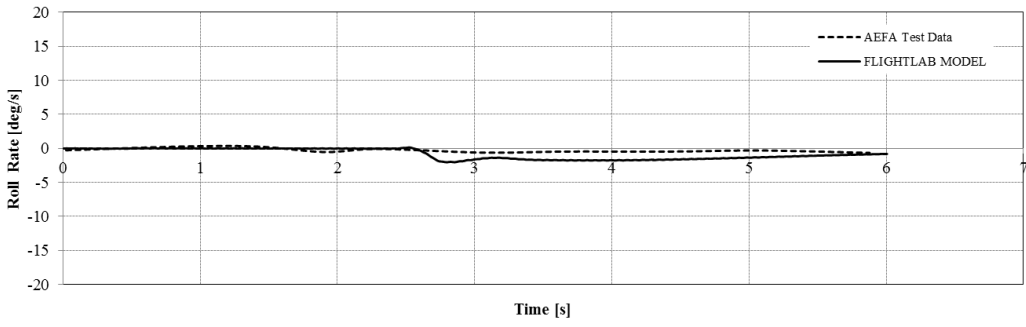
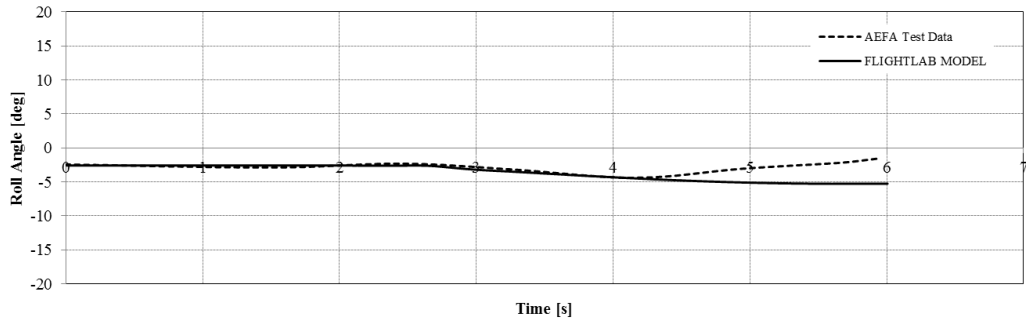


Figure A 3 (continued)

A.4 Response to 1 inch Left Pedal Input At Hover

Yaw and roll attitudes have quite good consistency with test data when left pedal input is applied to the simulation model. However the response results of pitch axis is not satisfactory since pitch angle increases in opposite directions.

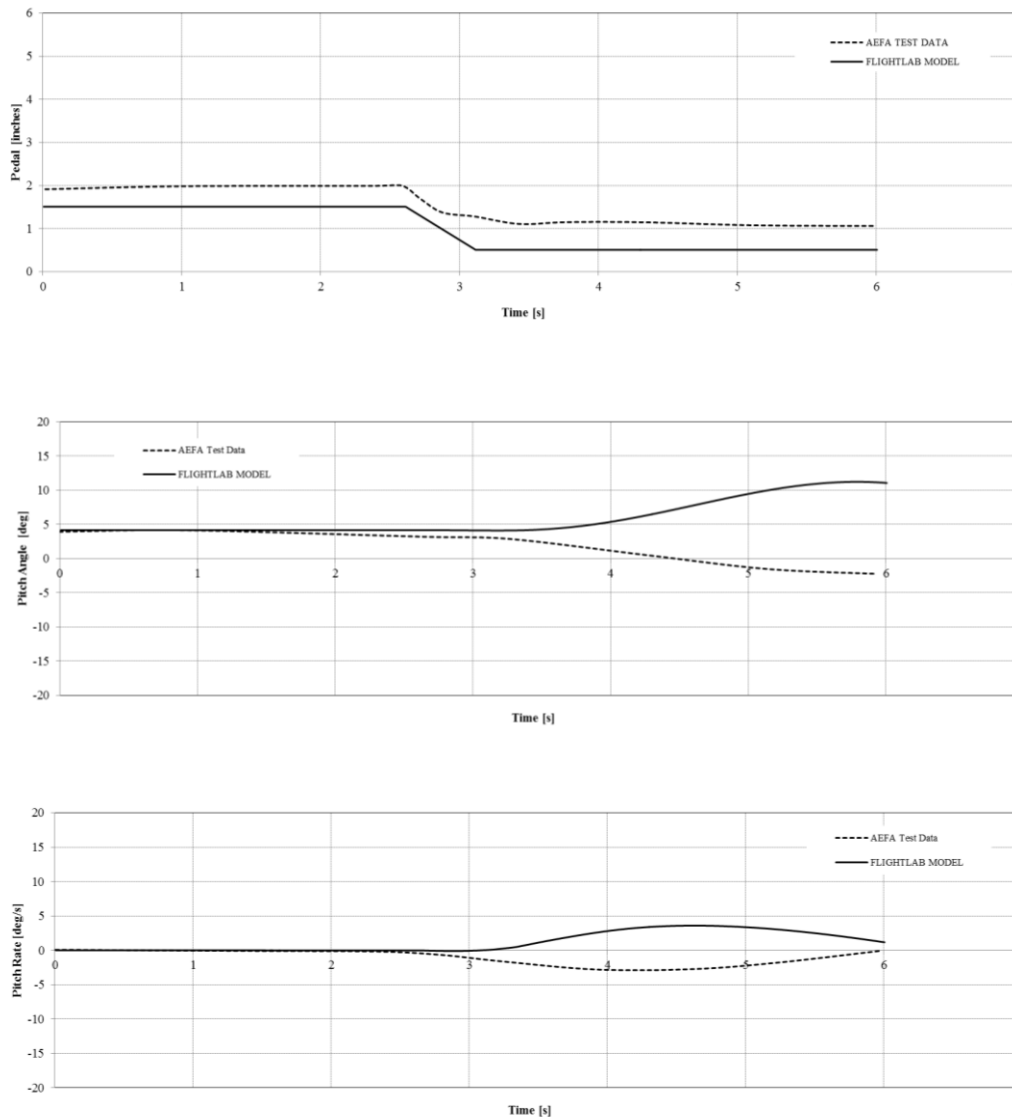


Figure A 4 Comparison of test data and simulation model response to 1 inch Left Pedal Input At Hover

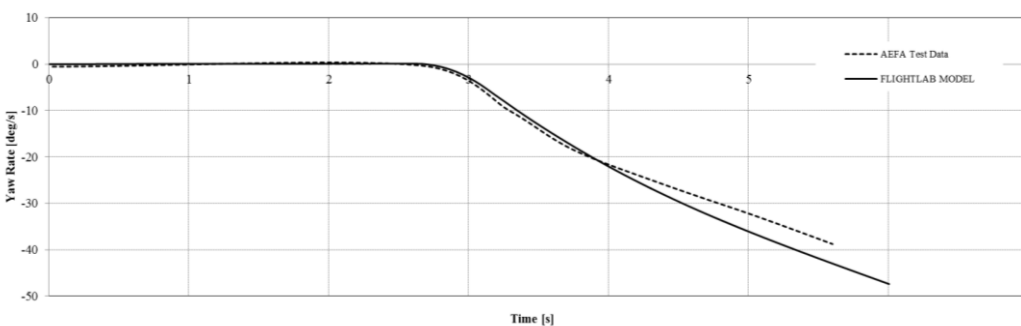
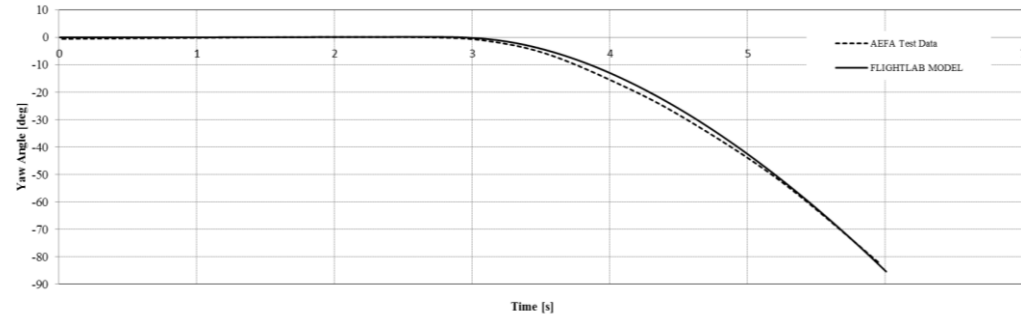
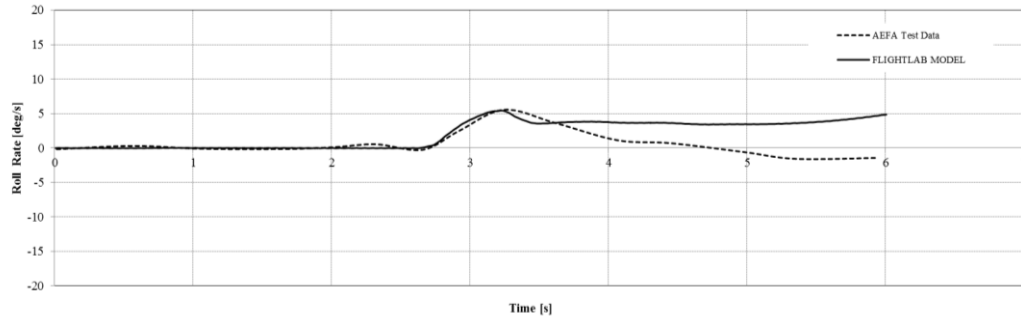
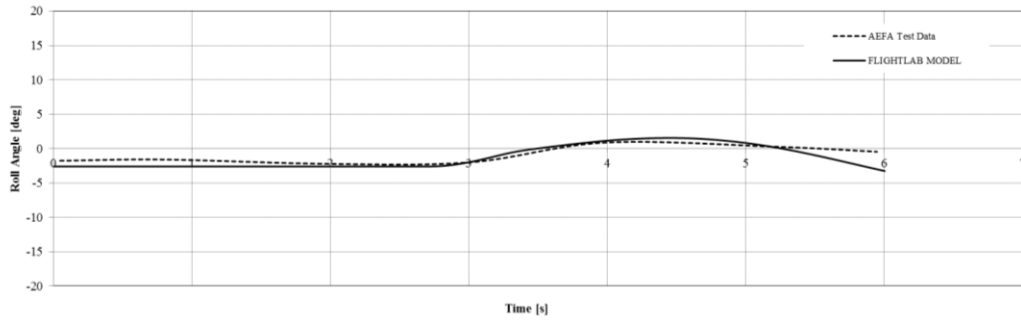


Figure A 4 (continued)

A.5 Response to 1 inch Aft Cyclic Input At 100 KTAS

As aft cyclic input is given to the model at 100 knots forward flight, off-axis response is satisfactory. Unexpected variations in roll rate and small oscillations in yaw rate results are observed which may be encountered due to moment of inertia values used in the simulation models.

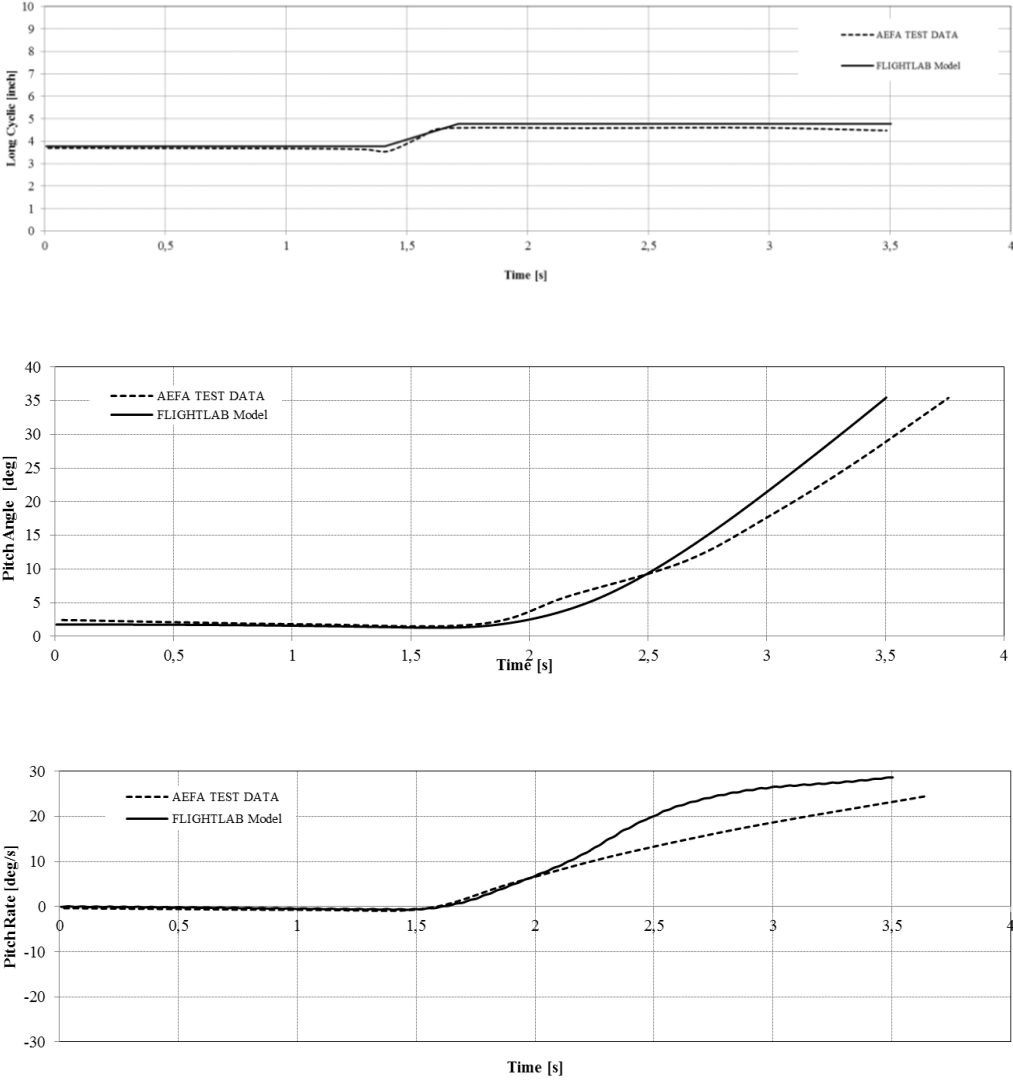


Figure A 5 Comparison of test data and simulation model response to 1 inch Aft Cyclic Input At 100 KTAS

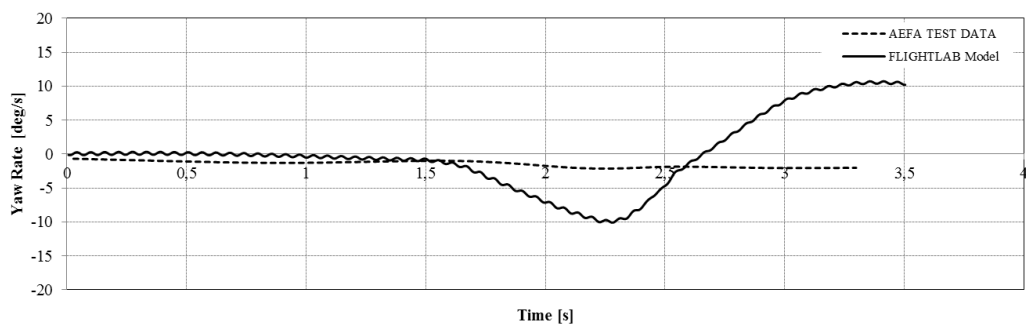
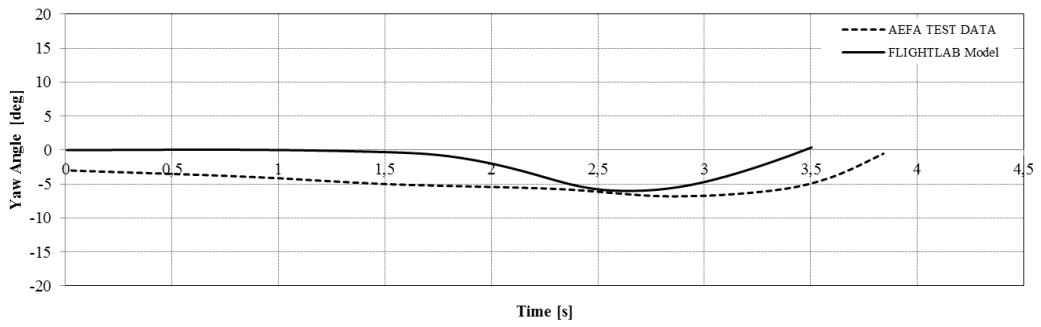
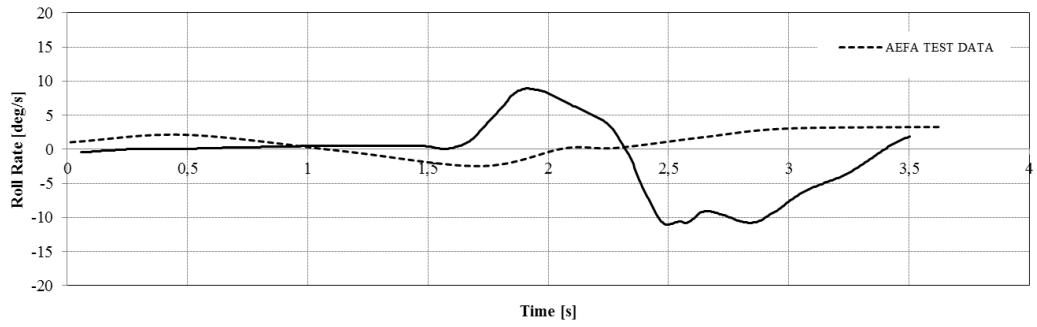
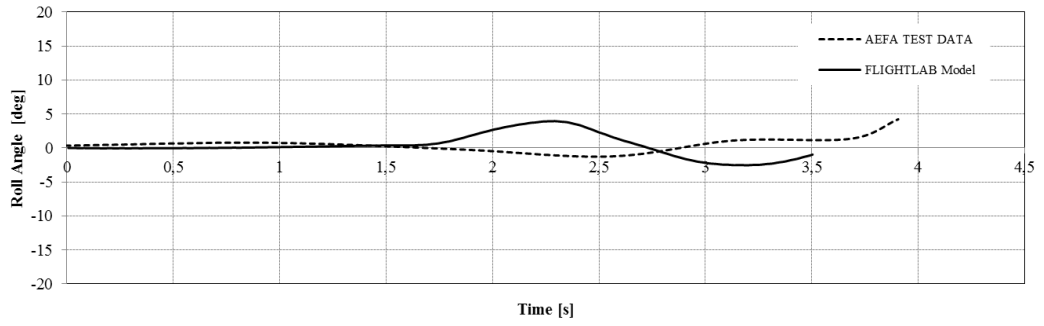


Figure A 5 (continued)

A.6 Response to 0.5 inch Up Collective Input At 100 kts

At 100 knots compensating coupling of pitch and roll response to collective input is stronger than the actual helicopter response. Yaw axis response are consistent with test data.

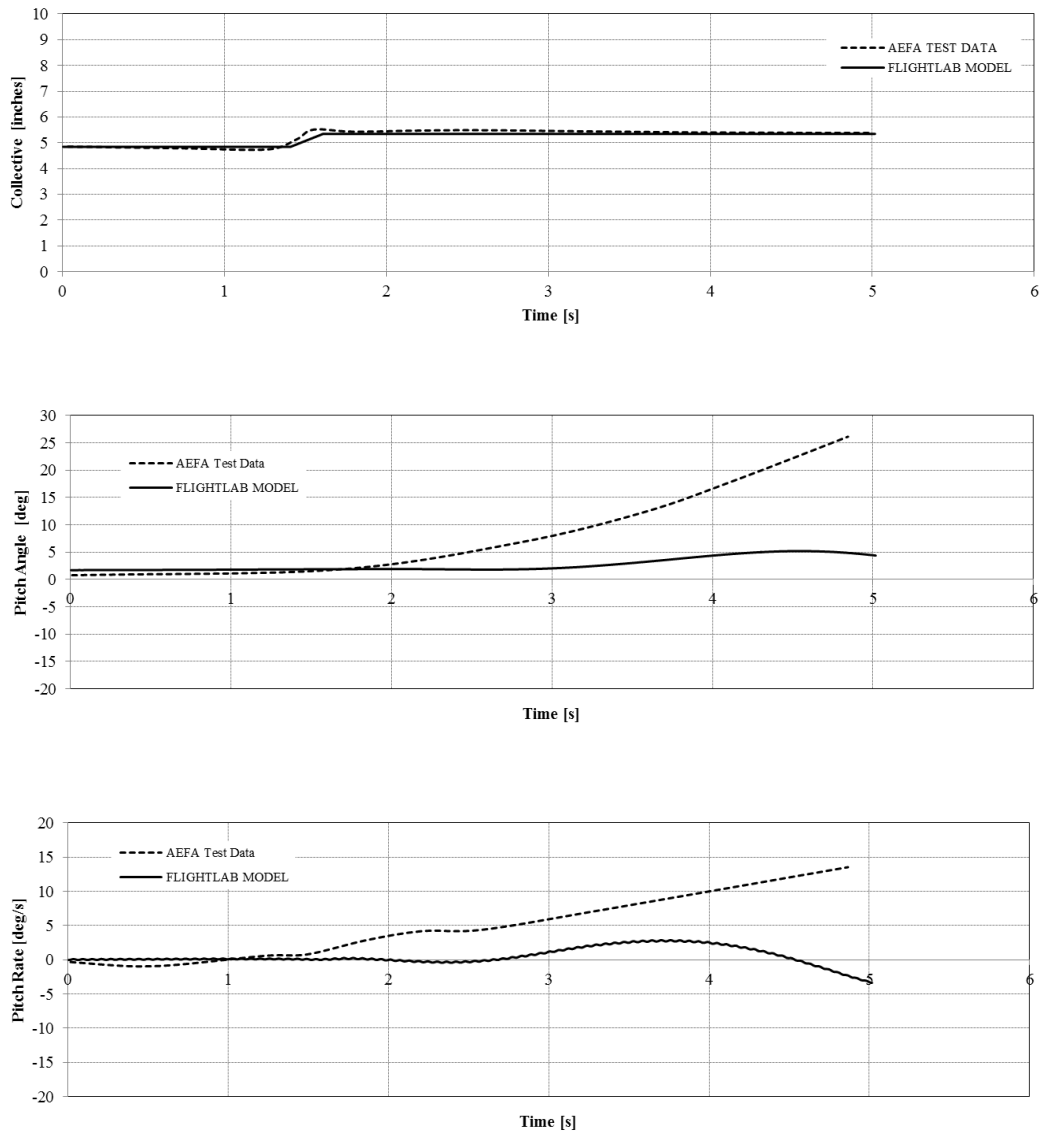


Figure A 6 Comparison of test data and simulation model response to 0.5 inch Up Collective Input At 100 kts

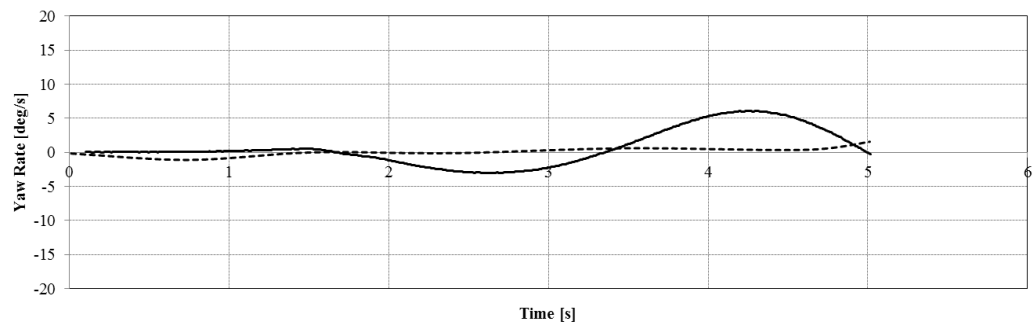
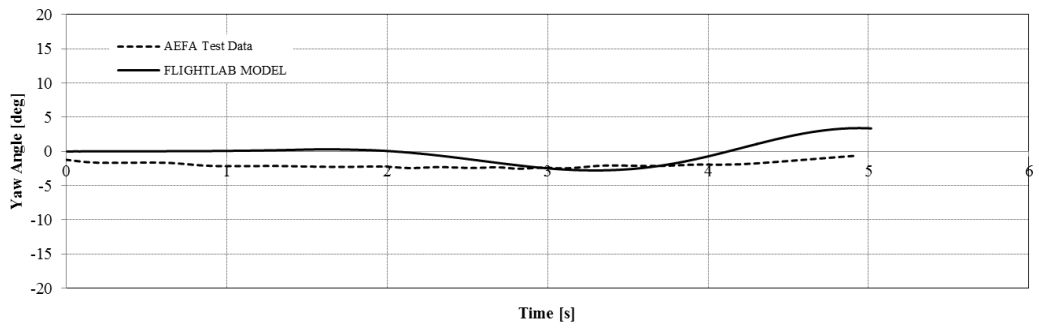
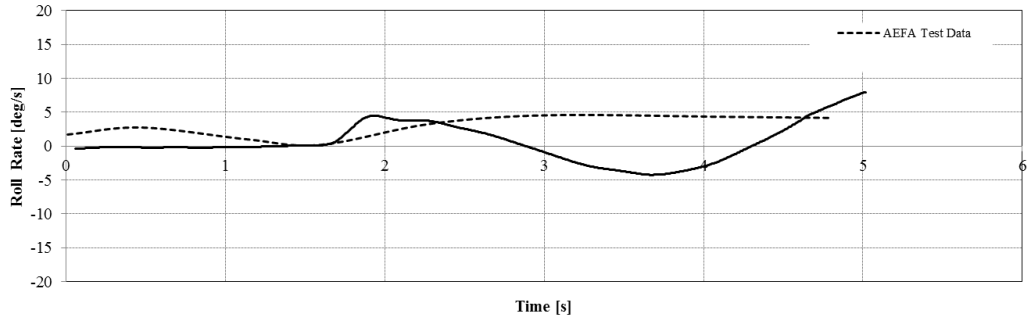
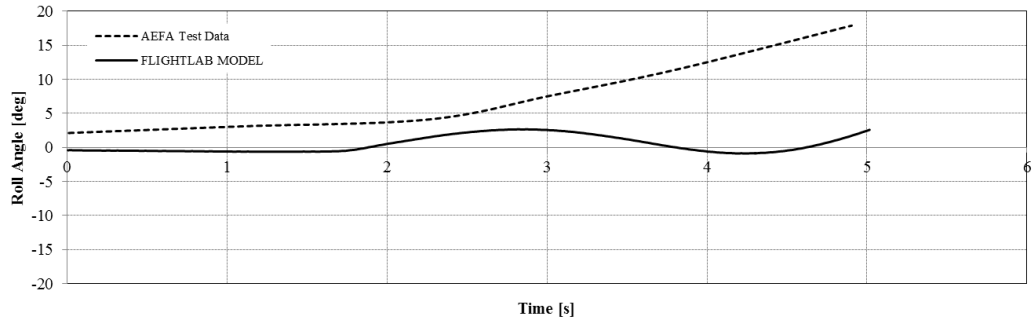


Figure A 6 (continued)

A.7 Response to 1 inch Right Pedal Input At 100 kts

Similar to collective input at 100 knots, there is a compensating coupling in pitch axis when pedal input is given at 100 knots forward flight. Simulation model predicts roll angle higher than the test values and good agreement is achieved in yaw axis response.

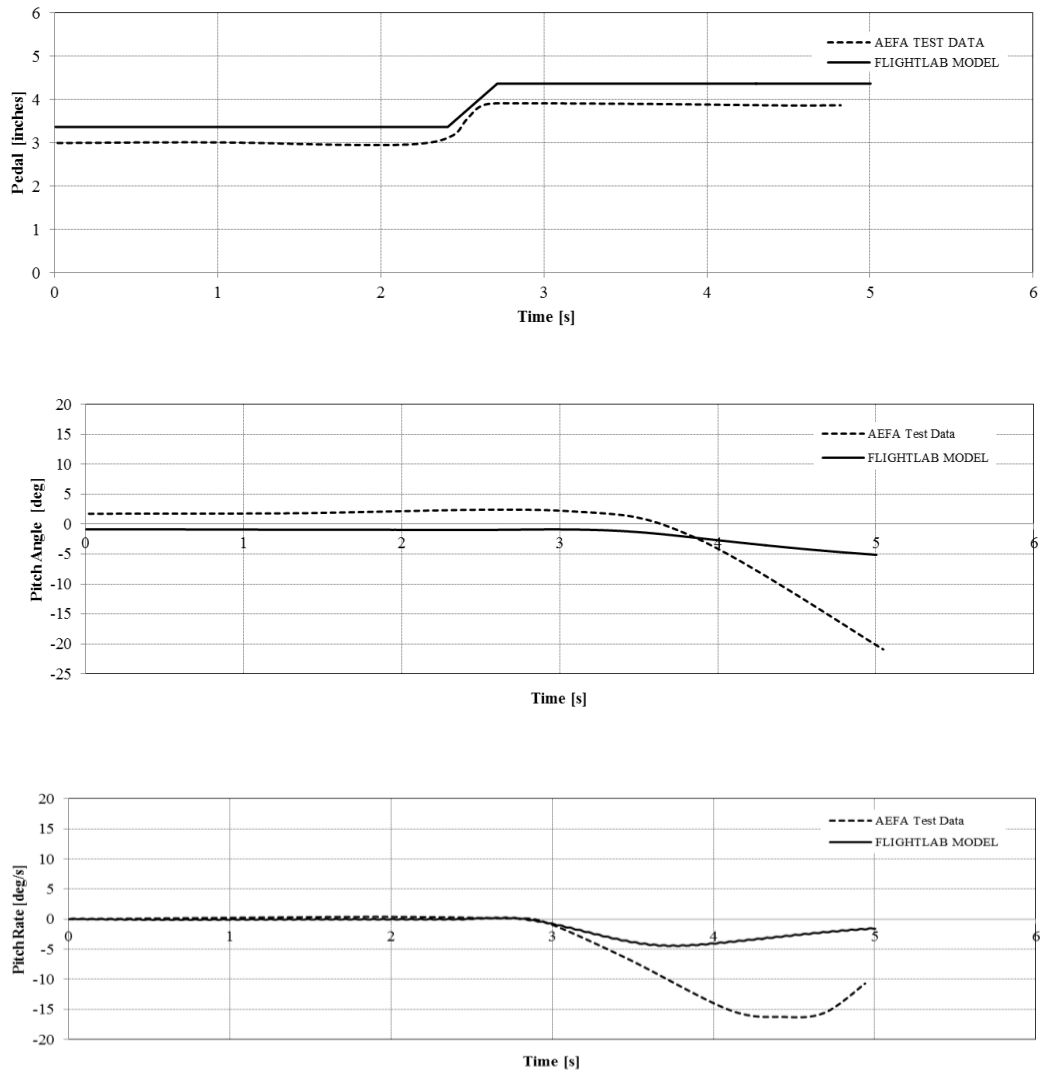


Figure A 7 Comparison of test data and simulation model response to 1 inch Right Pedal Input At 100 kts

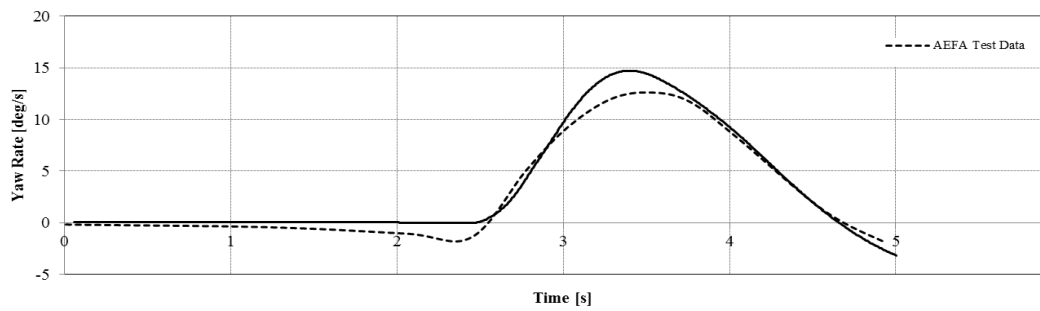
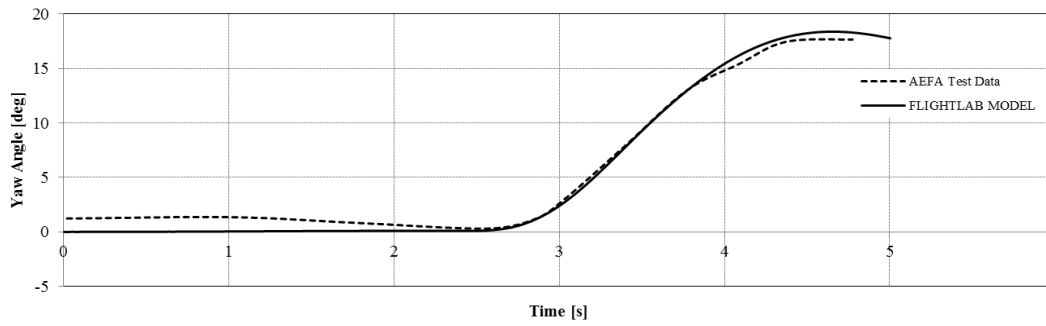
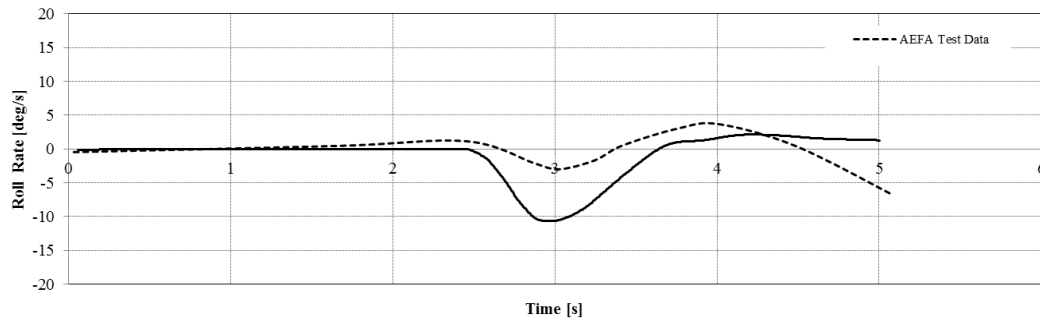
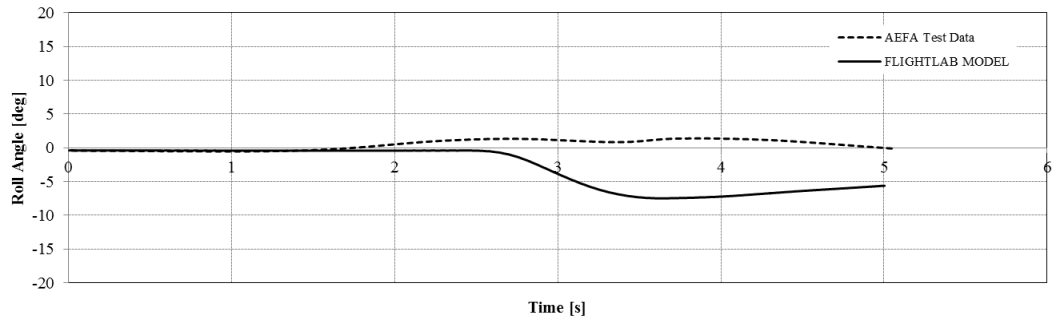


Figure A 7 (continued)

APPENDIX B

REVIEW OF FLIGHTLAB SOLUTION PROCESS

A review of modeling with FLIGHTLAB and solution methods for store separation simulation is made in this section. The detailed explanations are provided in FLIGHTLAB Theory Manual, [18].

B.1 Model Building Approach in FLIGHTLAB

A mathematical model in FLIGHTLAB is built by combination of kinematic (structural), aerodynamic, control and solution components. These components are assigned with data and connected to each other so that data can be transferred between components. Kinematic (structural) components have states and compute the forces acting at each node in the model. The positions, velocity and accelerations in structural frames are computed by kinematic components. In a similar way, the aerodynamic forces on the structural frame, inflow and interference are computed by aerodynamic components. Control components are used to model control system with gains, integrators, transfer functions, state space models etc... For the solution of the system states and propagating the model forward in time, solution components interact with other components.

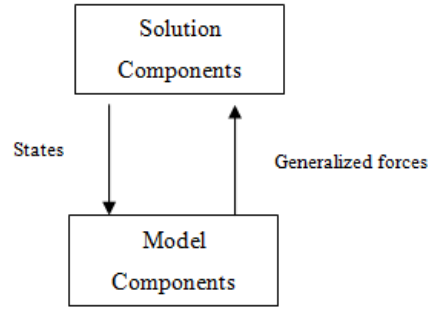


Figure B 1 Relationship between Solution and Model Components

B.2 Solution Process

Components are described with a set of nonlinear state equations. The imbalance between these nonlinear differential equations (Q) is calculated by solution components. The states that balance the nonlinear equations are calculated using Newton Raphson method by equating the generalized forces (Q) to zero.

$$Q = f(\ddot{x}, \dot{x}, x, u) = 0 \quad (8)$$

$$y = g(\ddot{x}, \dot{x}, x, u) \quad (9)$$

where u is the input to the component and y is the output from the components.

The Taylor Series expansion of Q around an initial condition is performed to estimate change in states and state derivatives. The iterative solution method is required because of nonlinear equations.

$$Q = Q_0(\ddot{x}_0, \dot{x}_0, x_0, u_0) + \frac{\partial Q}{\partial \ddot{x}} \delta \ddot{x} + \frac{\partial Q}{\partial \dot{x}} \delta \dot{x} + \frac{\partial Q}{\partial x} \delta x \quad (10)$$

$$\delta Q = Q_0 + M \delta \ddot{x} + C \delta \dot{x} + K \delta x = 0 \quad (11)$$

The parent-child relationship is described within the components. The parent frame of a component is the reference frame. The motion of the child frame is the sum of the motion of parent frame and motion of the child frame relative to the parent frame. Both parent and child frames have associated coordinate systems.

Solution methods of FLIGHTLAB consist of following steps:

- i. *Assemble* builds the set of nonlinear equations of the kinematic and aerodynamic components. The equations are linearized using perturbation methods.
- ii. *Genq* provides the pass of motion and force of structural and aerodynamic components.
- iii. *Solve* calculates a set of current states and derivatives that satisfies dynamic equilibrium of the model.
- iv. *Integrate* method integrates the states and propagates states forward to the next time step.

B.3 Modeling External Releasable Objects

External store is modeled with kinematic component which has motion and force methods. Motion methods compute the motion of child frame and current states of the system. Force methods calculate the loads produced by masses and aerodynamic components. The summation of the forces of child frames is transferred to the parent frame.

EXTOBJBAY kinematic class component is used to provide an interface for external store model. DOF6Q component models the six degree of freedom motion of external store as a free rigid body. In this method quaternions are utilized to calculate the orientation of the store. The derivatives of the quaternion are computed from the body axis rotational velocities and they are integrated to obtain orientation quaternion. Direction cosine matrix is calculated from the orientation quaternion.

The release of the store is initiated when trigger signal is set to one. The initial conditions of the released store are computed using the kinematic relations with motion of the parent frame.

$$r = r_{p/i}^i + T_{p/i}^T r_{c/p}^p \quad (12)$$

$$v = v_{p/i}^p + \omega_{p/i}^p \times r_{c/p}^p \quad (13)$$

$$a = a_{p/i}^p + \dot{\omega}_{p/i}^p \times r_{c/p}^p + \omega_{p/i}^p \times (\omega_{p/i}^p \times r_{c/p}^p) \quad (14)$$

where;

$r_{p/i}^i$ is the translational displacement vector of the parent frame with respect to the inertial frame expressed in the inertial coordinate system.

$T_{p/i}^T$ is the transformation matrix from inertial coordinate system to the parent coordinate system.

$r_{c/p}^p$ is the translational displacement vector of the child frame with respect to the parent frame expressed in the parent coordinate system.

$v_{p/i}^p$ is the translational velocity vector of the parent frame with respect to the inertial frame expressed in the parent coordinate system.

$\omega_{p/i}^p$ is the angular velocity vector of the parent frame with respect to the inertial frame expressed in the parent coordinate system.

$a_{p/i}^p$ is the translational acceleration vector of the parent frame with respect to the inertial frame expressed in the parent coordinate system.

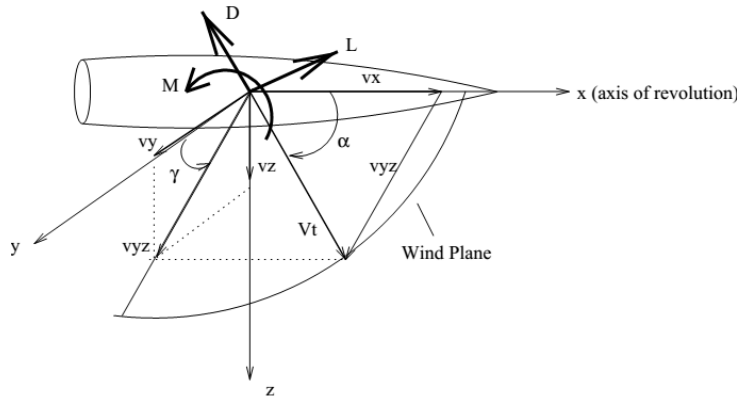


Figure B 2 Coordinate System of External Body, from Reference [18]

The airloads produced by the three dimensional aerodynamic body after separation is modeled with an aerodynamic component, AEBODYTAB3D. The airloads in the body axes are calculated as a function of angle of attack, side slip angle and Mach number. The coordinate system of the external body is shown in Figure B 2. The

aerodynamic force and moment coefficients of external stores are provided to the model by look-up table. The reference area and reference length utilized for the normalization of coefficients are also input to the mathematical model.

The air velocity is calculated as the vector sum of motion of the body frame, the induced velocity and the wind. Then the angle of attack and sideslip angle are computed as;

$$\alpha = \arctan\left(\frac{-v_z}{abs(v_x)}\right) \quad (15)$$

$$\beta = \arctan\left(\frac{-v_y}{sign(v_{xz}, -v_x)}\right) \quad (16)$$

$$\text{where } v_{xz} = \sqrt{v_x^2 + v_z^2} \quad (17)$$

Once the air velocity, angle of attack and sideslip angle are calculated, the aerodynamic force (C_{fx}, C_{fy}, C_{fz}) and moment (C_{mx}, C_{my}, C_{mz}) coefficients are computed from the aerodynamic database of the external store. The aerodynamic force and moments on the external store are obtained using reference area and reference length and the dynamic pressure which is considered by total air flow. The equations of motion for the external store are solved using the nonlinear dynamics solvers.

APPENDIX C

AERODYNAMIC DATABASE OF EXTERNAL FUEL TANK

For the jettison simulation of 230 gallon external tanks, the aerodynamic parameters are required as a function of angle of attack, sideslip angle and Mach number. Therefore, Missile Datcom tool is used to predict the aerodynamic force and moment coefficients of external tank. The coefficients are obtained at sideslip angle (β) and angle of attack (α) values given in Table C 1.

Table C 1 Variable List for Fuel Tank Aerodynamic Database Generation

Sideslip angle (β) [deg]	0, 5, 10, 15, 20, 30, 45, 60, 90, 105, 120, 135, 150, 180
Angle of attack (α) [deg]	0-90 (with 5° increments)
Reynolds Number	1.3 E+06
Mach number	0.05
Altitude	Sea Level (Density 1.225 kg/m ³ , 101325 Pa Air Pressure)
Reference Area [m ²]	0.159
Reference Length [m]	0.225

The aerodynamic coefficients obtained by Missile Datcom are transferred to the external tank body axis system (shown in Figure B 2) in order to be consistent with the required input format of the jettison simulation tool. Moreover, the force and moment coefficients for negative angle of attack and sideslip angles are derived from the original data assuming tank is symmetrical about xy and xz planes.

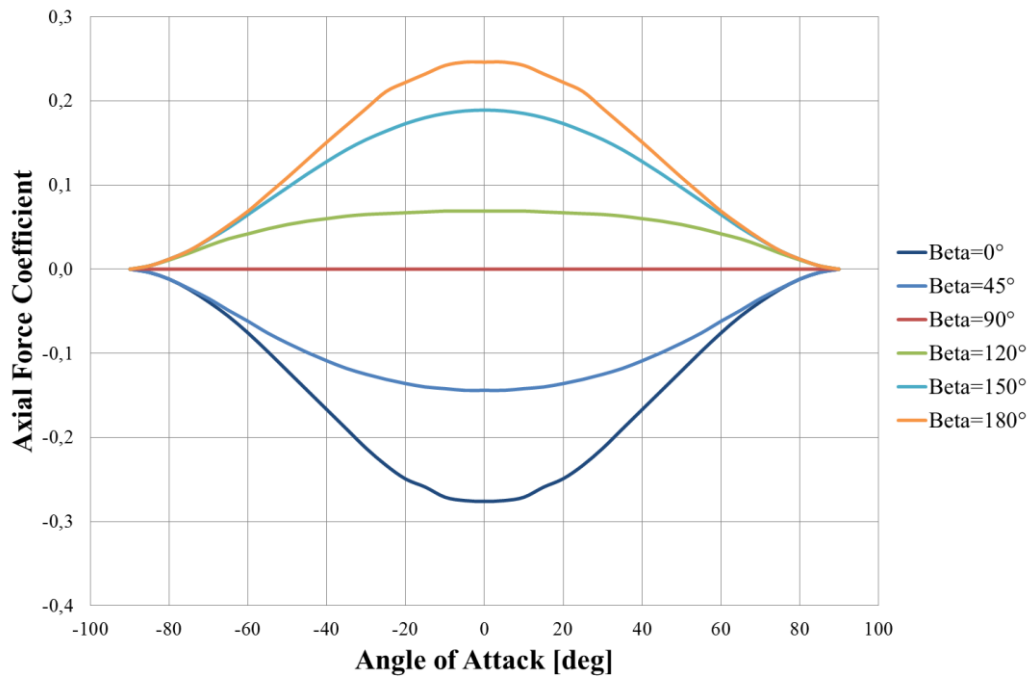


Figure C 1 Body Axis Axial Force Coefficient (CF_x) Variation

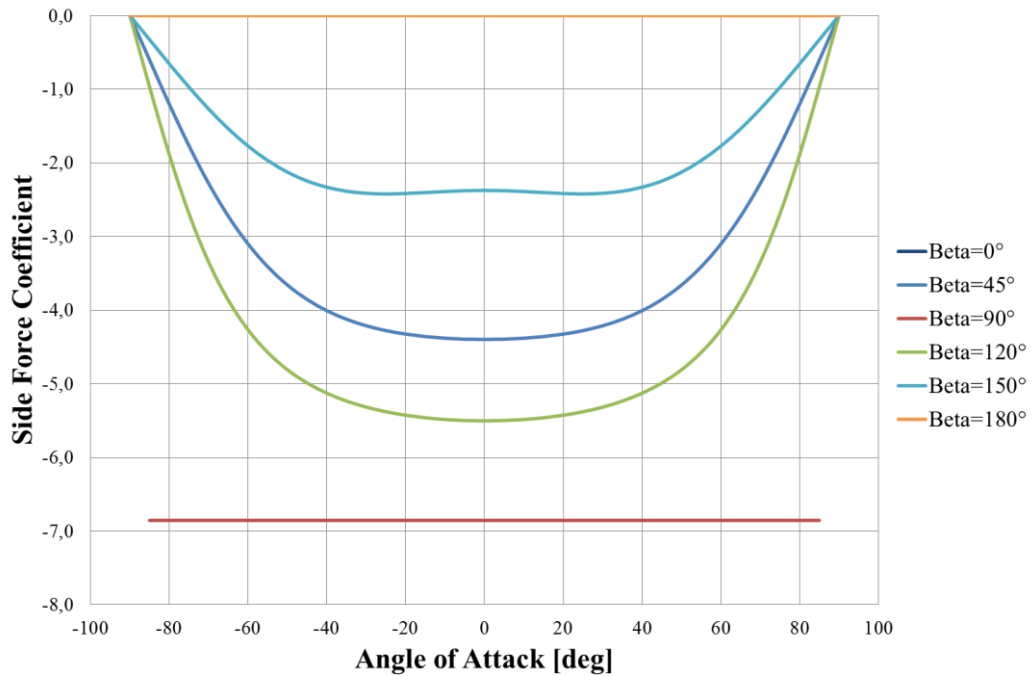


Figure C 2 Body Axis Side Force Coefficient (CF_y) Variation

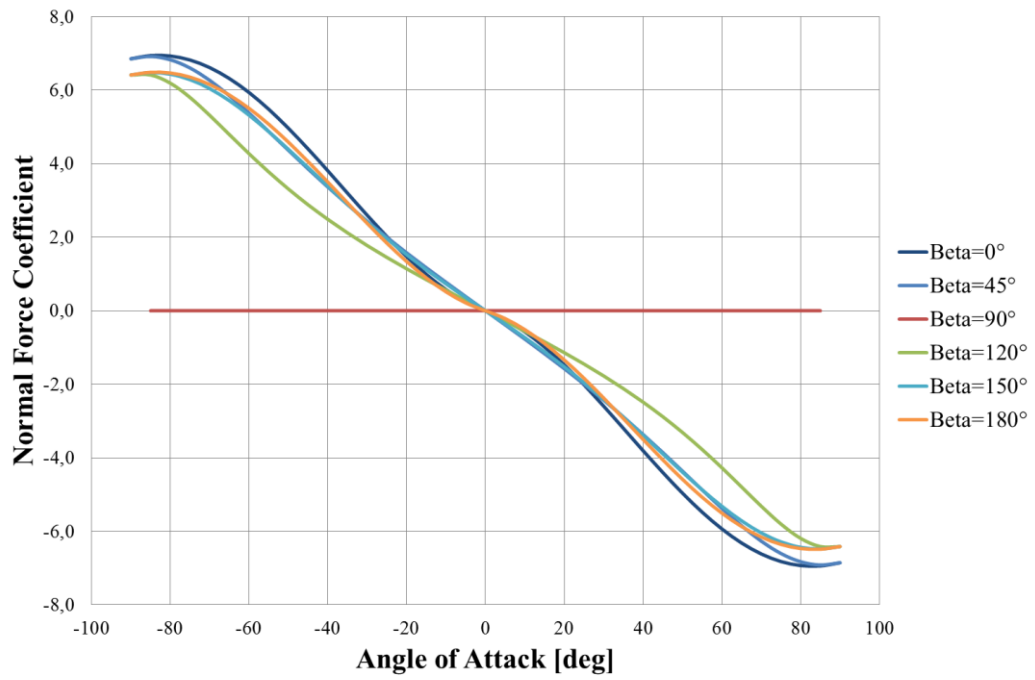


Figure C 3 Body Axis Normal Force Coefficient (CF_z) Variation

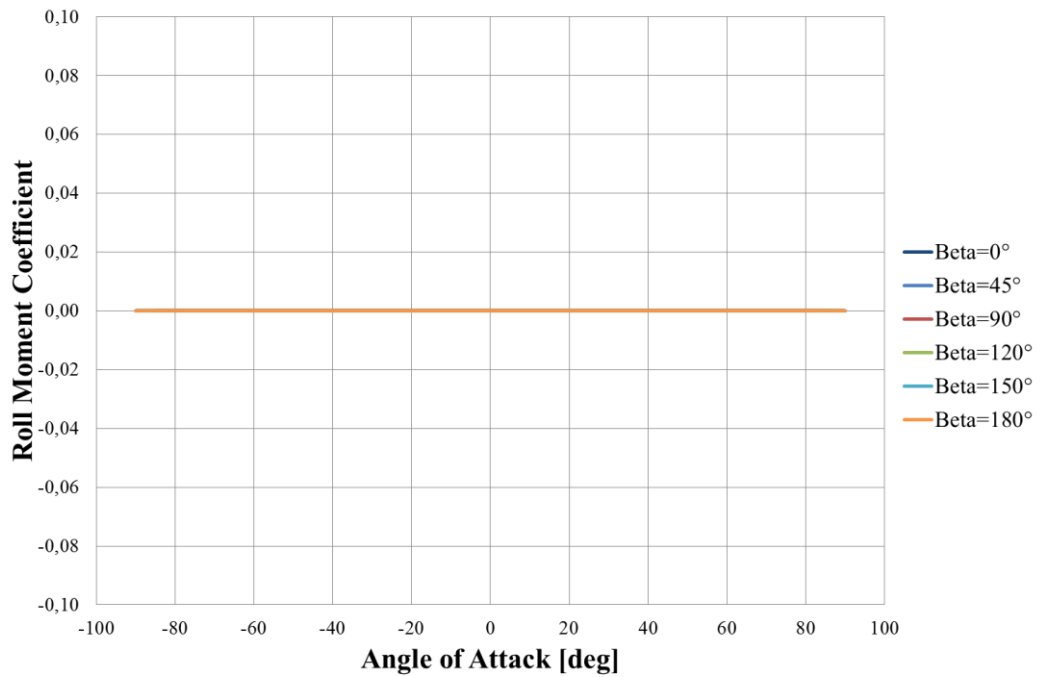


Figure C 4 Body Axis Rolling Moment Coefficient (CM_x) Variation

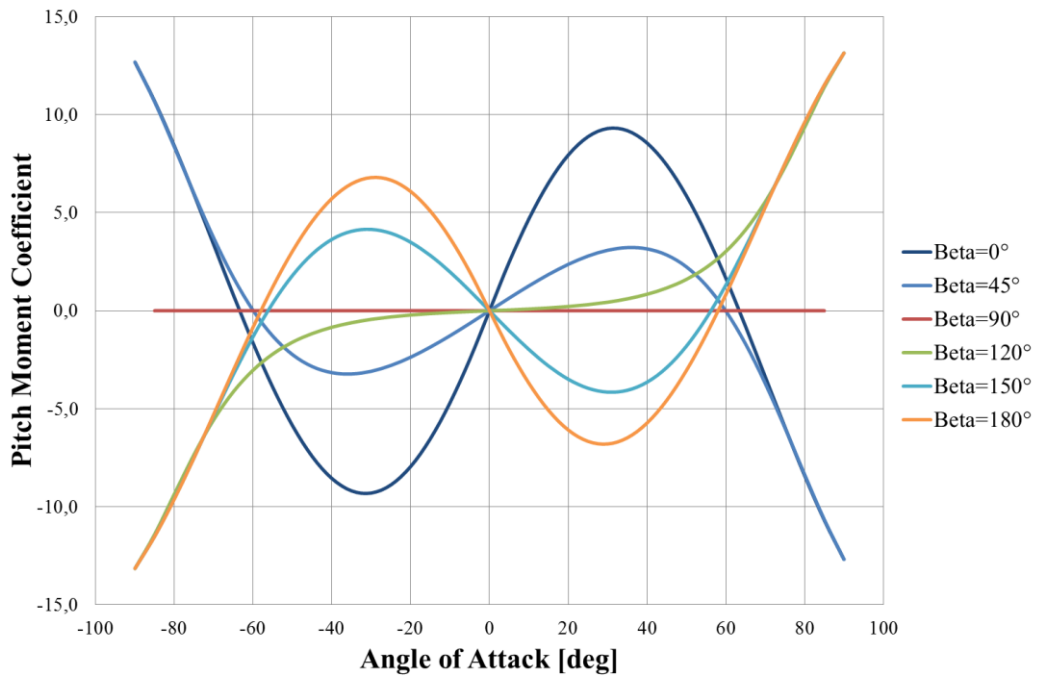


Figure C 5 Body Axis Pitching Moment Coefficient (CM_y) Variation

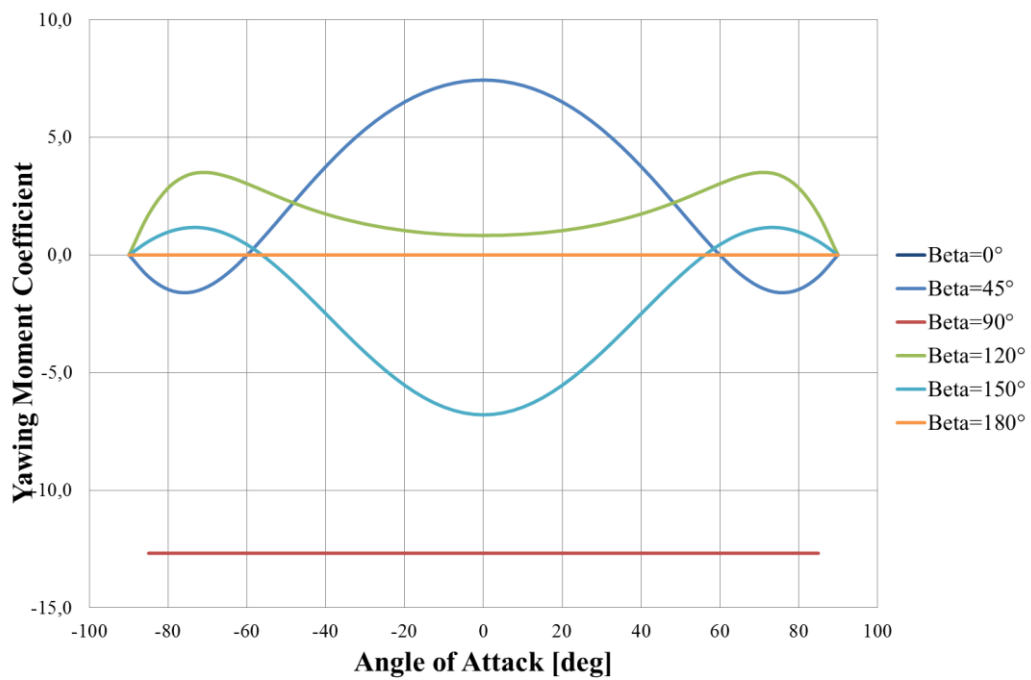


Figure C 6 Body Axis Yawing Moment Coefficient (CM_z) Variation